The bending elasticity of surfactant monolayers and bilayers

and its effect on

the swelling of free liquid films

Omslag:
detail van *De bouw van de toren van Babel* (1563),
Pieter Bruegel de Oude

Promotor:	dr J. Lyklema, hoogleraar in de fysische chemie, met bijzondere aandacht voor de grensvlak- en kolloïdchemie
Co-promotor:	dr ir J.M.H.M. Scheutjens, universitair hoofddocent bij de Vakgroep Fysische en Kolloïdchemie

P.A. Barneveld

The bending elasticity of surfactant monolayers and bilayers and its effect on the swelling of free liquid films

Proefschrift

ter verkrijging van de graad van doctor

in de landbouw- en milieuwetenschappen

op gezag van de rector magnificus,

dr H.C. van der Plas,

in het openbaar te verdedigen

op woensdag 12 juni 1991

des namiddags te twee uur in de Aula

van de Landbouwuniversiteit te Wageningen.

I

De Toren van Babel, die momenteel wordt herbouwd dankzij de sterk verbeterde informatie-overdracht, zal dit keer te gronde gaan zonder dat god op aarde hoeft te komen.

Genesis 11:1-9.

II

Vaak hebben duistere krachten hoge machten.

P.G. de Gennes, Scaling Concepts in Polymer Physics, Cornell University Press, Ithaca, New York, 1979.

III

In 1723 ruilde J.S. Bach (1685-1750) de functie van Capellmeister aan het hof van Cöthen in voor de functie van Cantor te Leipzig. Hij deed dat niet zozeer omdat zijn ware liefde bij de kerkmuziek lag, maar omdat de universiteitsstad Leipzig aanzienlijk betere ontplooiïngsmogelijkheden voor zijn kinderen bood.

H.T. David and A. Mendel, The Bach Reader, N.W. Norton & Company, New York.

IV

Het gebrek aan talent van de modale wetenschapper komt eerder aan het licht bij de sociale wetenschappen dan bij de natuurwetenschappen.

V

Discriminatie op grond van sexe of ras kan slechts verdwijnen als het denkpatroon van het individu dat van de soort gaat aannemen. Dit betekent dat menselijk denken twee niveau's hoger moet liggen dan nu gebruikelijk is.

VI

De natuurwetenschapper gelooft dat de werkelijkheid bepaald wordt door de zogenaamde fundamentele krachten. De gelovige gelooft dat god die fundamentele krachten geschapen heeft.

VII

De afnemende tolerantie bij het gebruik van cannabisprodukten heeft een adembenemende limiet.

J.H. van Epen, De drugs van de wereld, de wereld van de drugs, Samson Stafleu, Alphen aan den Rijn/Brussel, 1988.

VIII

In vrije vloeistoffilms gestabiliseerd door niet-ionogeen surfacant wordt de Helfrichrepulsie niet geëlimineerd door de grensvlakspanning.

Dit proefschrift.

IX

De waarde van de buigingselasticiteitsmoduli van bilagen die bestaan uit ionogene surfactants wordt gedomineerd door de dikte van de bilagen.

Dit proefschrift.

Stellingen behorende bij P.A. Barneveld, The Bending elasticity of surfactant monolayers and bilayers, Wageningen, 1991.

CONTENTS

---

* Chapter 3 has been published in Colloids & Surfaces, 52 (1991) 107, in coauthorship with J.M.H.M. Scheutjens and J. Lyklema.

CHAPTER 1

Introduction

General

Sedimentation and creaming are phenomena that may occur in unstable dispersions. Large particles, dispersed in a liquid, sediment if their density exceeds that of the liquid. Creaming occurs if the particle density is smaller than that of the liquid. The rate of these processes depends on the difference in specific gravity, the size of the particles and the viscosity of the system.

These two are often exploited in practice; for instance, the process of churning to obtain butter and buttermilk, in wine making to dispose of grape pulp and dead yeast, and as a step in water purification.

Sedimentation and creaming are not always desired. Often a stable and apparently homogeneous non-settling suspension is required, as in paints, ink, lubricating oil and fruit juices. The capacity for keeping particles in suspension frequently results from added polymers. If adsorbed onto particles, polymers are able to prevent coagulation and to reduce the sedimentation or creaming velocity significantly, by inducing *structure* to the system. In rare cases the suspension

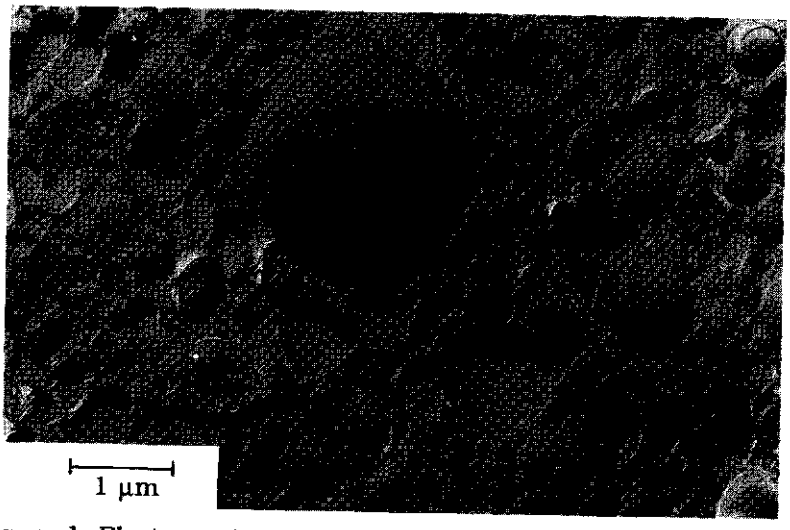

Figure 1. Electron micrograph of a lamellar dispersion, containing 12.3% Na-Dodecyl Benzene Sulfonate (NaDobs), 3.1% $C_{<13.6>}E_{<7>}$ (Ukanil 43), 23.1% NaI, (w/w) and water. (after ref. 2).

itself has an intrinsic structure. Examples include a number of liquid detergents which are structured by the presence of surfactant aggregates. As the motivation for the present study arose from problems in understanding the properties of such liquid detergents, these systems will be discussed in more detail.

Structure of liquid detergents

Basically, commercial surfactant-structured liquid detergents contain 10-15% anionic and nonionic surfactant (the *actives*), about 50% water and a large amount of electrolyte consisting of builder and buffer salts. Builder salts are added in order to bind any calcium from tap water. The limited solubility of the builder salts and the phase separation of the actives require a liquid structure to prevent sedi-

mentation. When the anionic and nonionic surfactants are mixed in the right proportion, the above-mentioned composition creates a lamellar liquid crystalline structure in the detergent. The structure of the resulting lamellar dispersion, as observed by electron spectroscopy, is shown in figure 1. The actives form lamellar droplets arranged in alternating active bilayers and water layers, the whole structure reminiscent of the arrangement of scales in an onion.

Whether stable dispersions are formed can be read from the stability diagram of the system. Figure 2 gives such a diagram for the

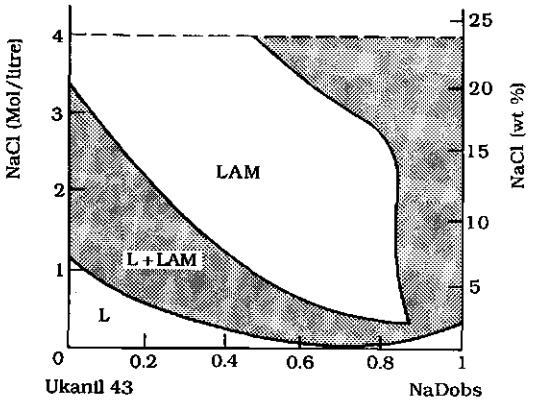

Figure 2. Stability diagram for the system NaDobs, Ukanil 43 and brine (after ref. 10).

system Na-Dodecyl Benzene Sulfonate (NaDobs) (anionic), $C_{<13.6>}E_{<7>}$ (Ukanil 43) (nonionic) and NaCl in water. Conductivity measurements can be used to obtain the volume fraction of lamellar droplets, φ_{lam}, in the system [1, 2]. It appears that stable dispersions are obtained if φ_{lam} exceeds 0.6 [2]. This value suggests a dense packing of spheres. As the average volume fraction of the active is only 0.2, the multilayer vesicles must contain large quantities of aqueous solu-

tion to be space-filling. The hydrocarbon part of the active bilayer has a thickness of about 2.0 nm, as judged from molecular dimensions. The water layer thickness between the active shells is then estimated to be between 5 and 10 nm [2]. Combined with an average lamellar droplet size of diameter c. 0.5 μm, this indicates that the typical number of layers in a droplet is 25. All evidence suggests that we are dealing with spontaneously formed systems (equilibrium systems). It is inferred that the equilibrium structure is determined by a balance of forces.

Extreme swelling

The water layer thickness is the result of several interactions between the bilayers in the droplet. The main attraction is due to the Van der Waals force, which arises from the fact that in the layered structure of the droplet regions with different Hamaker constants are present. At the repulsive side, there are electrical double layer and steric interactions originating from the anionic and nonionic surfactants, respectively. All these interactions decrease when the water layer becomes thicker. The thickness of the water layer suggests that a long distance force is present. As the concentration of electrolytes is quite high (in the order of kmole/m^3, see figure 2), the double layer is effectively screened and consequently, electrical double layer repulsion is negligible.

As the nonionic surfactant head groups are relatively large, steric repulsion should be considered. The sum of the contour lengths of

two $C_{<13.6>}E_{<11>}$ (Ukanil 87) head group chains is about 8 nm, which is about the same as the observed thickness of the water layer. However, the head groups are not fully stretched, so that the head group layer is actually much thinner. The extension of the head groups depends on the quality of the solvent, which in turn is affected by the nature and concentration of the electrolyte involved.

For the detergent composition 16.9% NaDobs and 3.8% Ukanil 87, figure 3a shows the dependency of the water layer thickness d_w in lamellar droplets on the electrolyte concentration for NaBr, NaCl

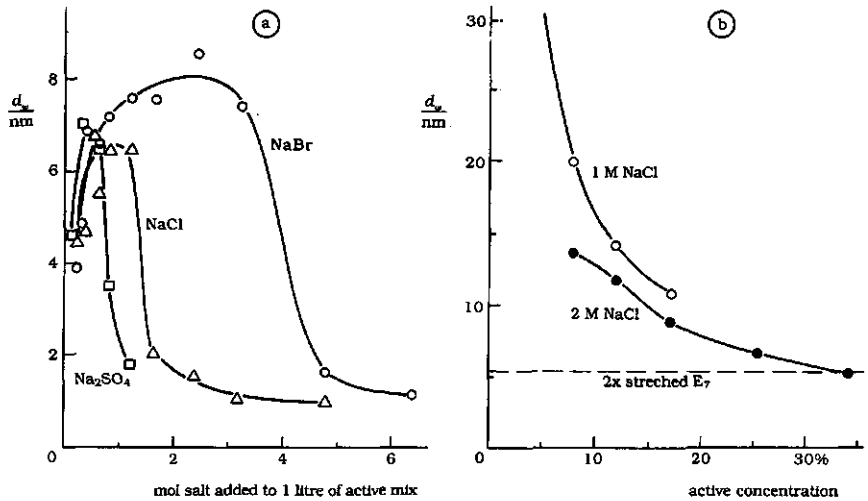

Figure 3. (a) Water layer thickness in the lamellar droplets, d_w, as a function of the NaBr, NaCl and Na_2SO_4 concentration, respectively. The basic mixture consists of 16.9% NaDobs and 3.8% Ukanil 87. The stability range is indicated (after ref. 6).

(b) Water layer thickness in lamellar droplets, d_w, as a function of surfactant concentration at two different NaCl concentrations (1 and 2 kmole/m^3). The surfactants are NaDobs and Synperonic A7 in the mole ratio 7/3.

and Na_2SO_4. Unlike NaCl and Na_2SO_4, NaBr, which is a salting-in electrolyte, increases the quality of the solvent which leads to

expansion of the head group chains. This promotes thick water layers and hence stable dispersions. For the two other salts a much smaller stable area is measured because shrinking of the ethylene oxide chain reduces d_w and hence φ_{lam}. This is done more effectively by Na_2SO_4 than by NaCl because it is a stronger salting-out agent [3, 4, 5]. The increase in d_w at relatively low electrolyte concentrations is not understood.

Figure 3b illustrates the dependence of d_w on the active concentration. The actual actives are a mixture of NaDobs and the nonionic $C_{<12>}E_{<7>}$ (Synperonic A7), in the mole ratio 7/3. Small amounts of surfactants can lead to very high values of d_w, depending on electrolyte concentration. This *extreme swelling* can lead to a water layer thickness up to 30 nm or more [6]. This phenomenon has no obvious explanation, since head group repulsions are not likely to have an impact over 5-10 nm.

A possible candidate for an additional repulsive force originates from thermal surfactant layer undulations. When the amplitude of these undulations is in the order of the bilayer to bilayer distance, steric repulsion is enhanced. The amplitude depends on the rigidity of the layer, hence this is an important, though somewhat elusive quantity.

Liquid films

Similar swelling in high salt concentrations has been observed in free liquid films [7]. Free thin liquid films are ideal model systems for swelling studies. A thin liquid film or soap film consists of a water layer which is stabilized by a surfactant. The surfactant is adsorbed on the liquid air interfaces with the tails in air and the head groups in the water. The film is in contact with bulk solution. Figure 4 illus

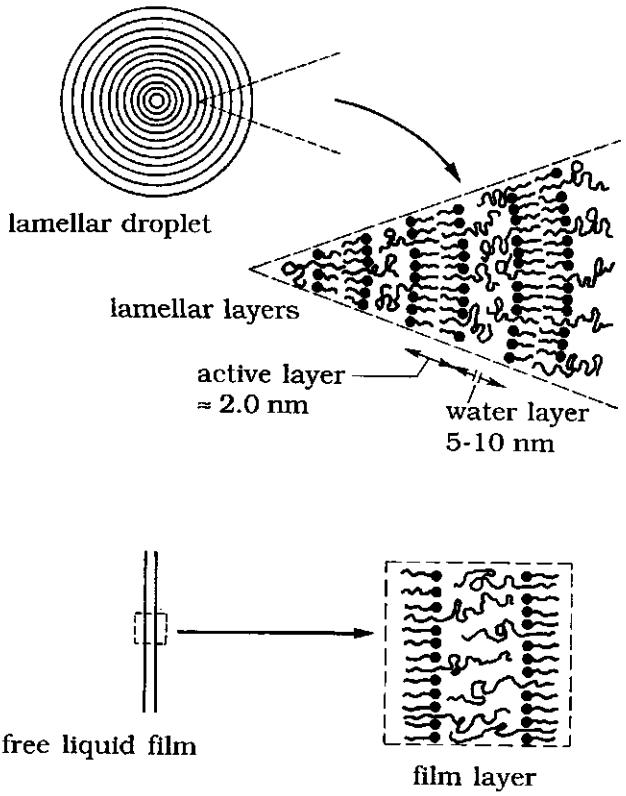

Figure 4. Schematic representation of a lamellar droplet and a thin liquid film.

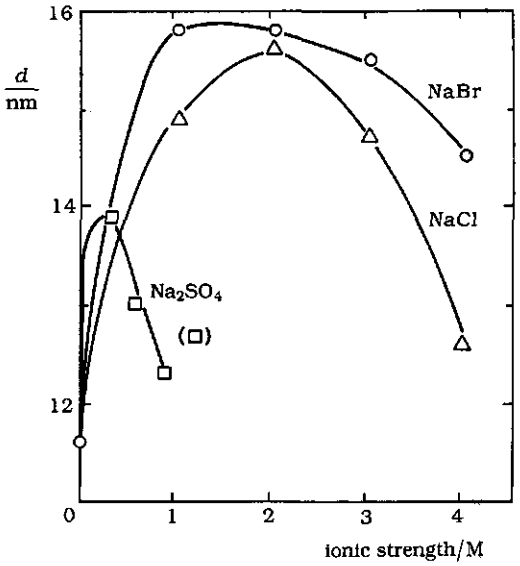

Figure 5.Thickness of equilibrium films stabilized by Synperonic NPE 1800 as a function of electrolyte concentration (after ref. 7).

trates the resemblance between a layer in a lamellar droplet and a vertical thin film. The fact that the resemblance is not only structural is shown in figure 5, where the thickness of thin liquid films stabilized by the nonionic surfactant Synperonic NPE 1800, is given as a function of electrolyte concentration. The dependency is strikingly similar to that in figure 3a. This similarity suggests a common physical background. In view of the discussion given so far, interpretation in terms of the usual double layer and steric interaction theories is not sufficient and hence a more thorough consideration of the forces involved is required.

Aims and outline of the thesis

One of the aims of the present thesis was to carry out an experimental study to obtain more information about the unexpected behaviour in free liquid films of nonionic surfactants. Another major aim was to compute rigidities of surfactant monolayers and bilayers which are needed to estimate the undulation repulsion in the films [8]. Undulation repulsion was anticipated to contribute to the unexpected behaviour of both lamellar suspensions and free liquid films.

In chapter 2, the solubility of poly (ethylene oxide) in water as a function of temperature is considered. This is a relevant polymer because the head groups of the nonionic surfactant used in this study consist of ethylene oxide units. The link between temperature and electrolyte concentration is that they both affect the degree of hydration of the ethylene oxide chain. Using a Flory-Huggins approach the solubility gap in the phase diagram can be calculated.

Chapter 3 describes an experimental study which investigates whether electrostatic repulsion in thin liquid films can explain the increase in film thickness at relatively low electrolyte concentrations (up to about 1 M) as reported in figure 5. This was not shown to be the case. It is suggested that undulations of the surfactant layer provide an additional long range repulsive force.

Chapter 4 deals with the bending elasticity parameters of interfaces which determine the amplitude of undulating surfactant layers and hence the undulation repulsion. Extending the self-consistent field theory of Scheutjens and Fleer [9], bending elasticity parame-

ters are calculated for a number of systems. In this chapter, only nonionic systems are considered.

Chapter 5 is devoted to ionic systems. Bending elasticity parameters are calculated and compared with available analytical solutions.

Chapter 6 provides strong experimental evidence supporting the idea that undulation repulsion is important in thin liquid films. Experimental data of liquid films stabilized by mixtures of nonionic surfactant and n-alcohols are interpreted using calculated bending elasticity parameters. On the basis of chapter 4 it is argued that electrolytes increase the elasticity of the surfactant layers in the film, thereby promoting undulations and hence, a thicker water layer.

References

1 D. A. G. Bruggeman, Am. Physics, 24 (1935) 636.

2 J. C. Van de Pas, Tenside Surf. Det., (1991) Accepted.

3 W. A. P. Luck, Topics in Current Chem., 64 (1976) 113.

4 M. J. Schick, J. Colloid Sci., 17 (1962) 801.

5 H. Scott, Colloids Surfaces, 11 (1984) 51.

6 J. C. Van de Pas, Personal Communication (1990).

7 T. v. d. Boomgaard and J. Lyklema, Langmuir, 5 (1989) 245.

8 W. Helfrich, Z. Naturforsch., 33a (1978) 305.

9 J. M. H. M. Scheutjens and G. J. Fleer, J. Phys. Chem., 83 (1979) 1619.

10 A. Jurgens, Tenside Surf. Det., 26 (1989) 222.

CHAPTER 2

A Simple Model for Upper and Lower Critical Solution Temperatures in Poly(ethylene oxide) Solutions

Abstract

Upper and lower critical solution temperatures (i.e., solubility gaps) are calculated for solutions of poly(ethylene oxide) (PEO) in water. The behaviour of PEO in water is relevant PEO constitutes the head groups of the nonionic surfactants. The model used is a simple extension of the well-known Flory-Huggins theory for linear homopolymers, in that the PEO molecule is considered as a copolymer with alternating polar and non-polar segments. The effect of temperature is incorporated by letting the Flory-Huggins χ-parameters decrease with increasing temperature. Upper and lower critical temperatures are calculated as a function of the degree of polymerization of the PEO. The results are compared with experimental data. In addition, upper and lower critical temperatures are calculated as a function of the non-polar fraction in the polymer. With this model, the insolubility of poly(propylene oxide) is recovered. However, the insolubility of poly(methylene oxide) is not reproduced.

Introduction

Phase separation is observed in many solutions when temperature is decreased. Some polymer systems also show phase separation when the temperature is increased. The temperature at which this

happens is called the upper consolute temperature or the lower critical solution temperature (LCT). Further, above the LCT, the system may become miscible again at the upper critical solution temperature (UCT).

Formally, two phases of different composition can coexist when in both phases the molecules have the same chemical potential. This may be best explained on the basis of figure 1, where for two differ

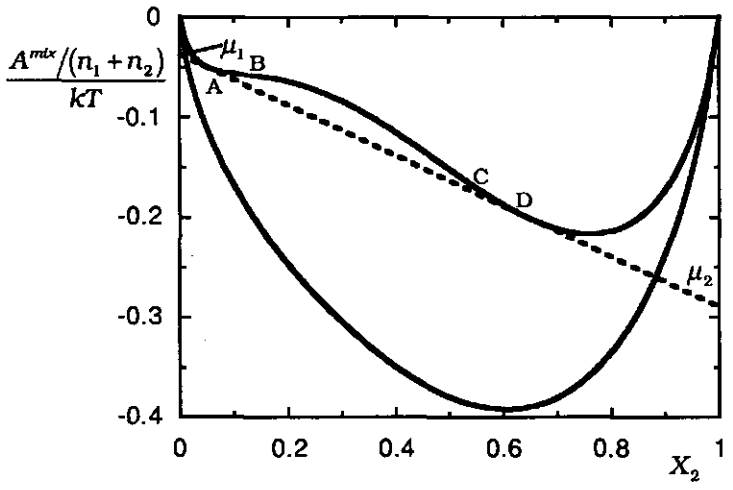

Figure 1. Schematic representation of the Helmholtz energy of mixing $A^{mix}/(n_1+n_2)$ as a function of the mole fraction of polymer, X_2, for two principal cases. The upper full curve represents a partially miscible system, the lower full curve a completely miscible system. The dashed curve joins points of equal chemical potential.

ent situations the molecular Helmholtz energy of mixing solvent (component 1) and polymer (component 2), $A^{mix}/(n_1+n_2)$, is given schematically as a function of the mole fraction of polymer, X_2. The

lower full curve represents the situation where the system is completely miscible. In this case, the chemical potentials of the constituent polymers, which are the intercepts of the tangent of the curve, are decreased for both components when they are mixed. For the upper full curve, however, there are two compositions, denoted by A and D, in which the solvent and polymer have the same chemical potentials (see the dashed curve). These are called the binodal points. Outside the binodals, the system is completely miscible, but between the binodals the system can gain Helmholtz energy by separating into two phases, one with polymer composition A and one with D. Compositions between A and B, in figure 1, and between C and D are meta-stable. The inflection points, B and C, are called spinodal points.

A change in, for example, the temperature affects the shapes of the curves in figure 1. The upper full curve, which represents a partially miscible system, may change into the lower full curve, i.e., a completely miscible system and vice versa. The point where the system is just completely miscible over the entire composition range is the critical point and occurs when points A-D of the dashed curve coincide. Mathematically, at this critical point:

$$\frac{\partial \mu_1}{\partial X_2} = 0 \qquad \text{and} \quad \frac{\partial^2 \mu_1}{\partial X_2^2} = 0 \tag{1}$$

In order to predict the critical points, one needs a model to obtain an expression for the chemical potentials of the components involved.

When it comes to explaining the solubility gap of poly(ethylene oxide) (PEO) solutions, the importance of chain hydration is recognized by several authors [1, 2]. In their view the occurrence of a lower critical solution temperature is due to a diminished PEO hydration at higher temperatures. We shall show here that this idea are in nice agreement with Flory-Huggins theory for polymer solutions [3] if PEO is considered as a copolymer, i.e., a polymer with distinct nonpolar (ethylene) and polar (oxide) regions. To do so, we first briefly review some required elements of the Flory-Huggins theory, then we discuss the parameters and we conclude with a section on results and discussion.

Flory-Huggins Theory of Polymer Solutions

We start with homopolymers and show that there is only one critical point. The extension of the theory to copolymers reveals that the phase diagram of copolymers may have two or more critical points.

Homopolymers

The system under consideration consists of polymer chains of r segments and a monomeric solvent. Polymer and solvent are distributed over a lattice in such a way that each lattice site is filled with either a polymer segment or a solvent molecule. The molecular entropy of mixing is [3]:

$$S^{mix} = -k(n_1 \ln \varphi_1 + n_2 \ln \varphi_2) \qquad (2)$$

where n is the number of molecules and φ is the volume fraction. The subscripts 1 and 2 represent solvent and polymer, respectively.

The interaction enthalpy between segments and solvent molecules is calculated in a mean field approximation:

$$H^{mix} = kT\chi n_1 \varphi_2 \tag{3}$$

where χ is the well-known Flory-Huggins interaction parameter.

From the mixing entropy and enthalpy, the chemical potentials can be derived:

$$\begin{cases} (\mu_1 - \mu_1^*)/kT = \ln(1-\varphi_2) + (1-1/r)\varphi_2 + \chi\varphi_2^2 \\ (\mu_2 - \mu_2^*)/kT = \ln\varphi_2 - (r-1)(1-\varphi_2) + r\chi(1-\varphi_2)^2 \end{cases} \tag{4}$$

Here, μ_i^* is the chemical potential of components i in the pure (amorphous) state.

From the conditions for the critical point, eqn (1), we obtain for the value of the χ-parameter at the critical temperature, χ^{cr}:

$$\chi^{cr} = \tfrac{1}{2}\left(1 + r^{-\frac{1}{2}}\right)^2 \tag{5}$$

A system with $\chi > \chi^{cr}$ can separate into two phases, provided that the composition is in the biphasic region, i.e., between the binodals.

Now we consider the temperature dependence of the interaction parameter χ around its critical temperature T^{cr}. In the simple case

that χ is purely enthalpic, χ is proportional to T^{-1}. However, let us assume that, more generally, χ scales as:

$$\chi = \chi^0 \left(\frac{T^0}{T} \right)^{\zeta^0} \qquad (\zeta^0 > 0) \tag{6}$$

where $\chi^0 = \chi(T^0)$ is its value at a given temperature T^0 not too far from T^{cr}. In this equation, ζ allows for deviations from ideality (if $\zeta \neq 1$), which may arise from free volume effects and/or specific interactions. The most important property of this equation is that, when the temperature is increased, the *absolute* value of χ is always decreased. This should be so, because enthalpic interactions invariably decrease with increasing temperatures. With the help of eqn (5), the critical temperature can be obtained from:

$$T^{cr} = T^0 \left(\chi^0 / \chi^{cr} \right)^{\frac{1}{\zeta}} \tag{7}$$

This expression accounts for only one critical solution temperature, since there is only one χ involved. This χ should be positive in order to be meaningful. Negative χ-parameters do not lead to any phase separation.

For PEO/water systems it is more appropriate to consider PEO as a copolymer, since the polymer has hydrophobic as well as hydrophilic (hydration) interactions with the solvent. We discuss the implications for the Flory-Huggins theory in the next section.

Copolymers

Here, we deal with the case of a copolymer, consisting of two different types of segments, *C* and *O*, and monomeric solvent *W*. Each segment *C* represents either a $-CH_2-$ or $-CH_3$ group and each *O* segment stands either for an -O- or -OH group. A PEO chain can thus be represented as $O-(C-C-O)_x$, where x is the degree of polymerization. This representation is rather suggestive. The Flory-Huggins theory assumes a random mixing of segments, hence the order of segment types in the chain is irrelevant. The equations for the mixing entropy (eqn 2) and the mixing enthalpy (eqn 3) remain the same but in eqn (3) the interaction parameter between polymer and solvent is now an average of three χ-parameters:

$$\chi = f_C\chi_{CW} + (1-f_C)\chi_{WO} - f_C(1-f_C)\chi_{CO} \qquad (8)$$

where f_C is the fraction of *C* segments in the chain (which is $2x/(3x+1)$ for PEO/x). The parameter χ_{CW} represents the interaction between CH_2 and water. The value for this parameter at room temperature is higher than the critical value, since water and alkanes do not mix. The parameter χ_{WO} represents interactions between water and the oxygen atoms of the polymer. It is likely that χ_{WO} is dominated by hydrogen bridges. This value is probably considerably below the critical value. The interactions between polar and nonpolar regions in the polymer are represented by χ_{CO}, which value is expected to be close to χ_{CW}, since in both cases only Van der Waals interactions are involved.

Let us assume that for any of the interaction parameters the temperature dependence may be written as in eqn (6):

$$\chi_{xy} = \chi^0_{xy}\left(\frac{T^0}{T}\right)^{\zeta^0_{xy}} \qquad (\zeta^0_{xy} > 0) \tag{9}$$

where x and y may be either C, O, or W. The critical temperature can be obtained from:

$$f_C\chi^0_{CW}\left(\frac{T^0}{T}\right)^{\zeta^0_{CW}} + (1-f_C)\chi^0_{WO}\left(\frac{T^0}{T}\right)^{\zeta^0_{WO}} - f_C(1-f_C)\chi^0_{CO}\left(\frac{T^0}{T}\right)^{\zeta^0_{CO}} = \tfrac{1}{2}\left(1+r^{-\frac{1}{2}}\right)^2 \tag{10}$$

This equation in T can have more than one solution, depending on χ and ζ. If applied to PEO, we expect two solutions which correspond to the LTC and UTC. At very low temperatures a third solution may be also expected.

Methods and Parameters

There are three χ and three ζ parameters. We assume that the interactions between W and C are equal to those between O and C, which leaves us with four parameters. The two χ parameters are derived from the solubility of alkanes in water and from c.m.c. data of ethylene oxide nonionic surfactant. At room temperature (300 K) they are $\chi_{CW} = \chi_{CO} = 2.0$ and $\chi_{WO} = -1.6$ [4]. When the temperature is increased, the polymer becomes better soluble because of a decrease in χ_{CW} and χ_{CO}, but at the same time less soluble because χ_{WO}

becomes less negative (cf. eqn 9). The parameters ζ are chosen such that the calculated critical solution temperatures of PEO/50 (440K and 500K, respectively [5]) are in agreement with experiment, yielding: $\zeta_{cw} = \zeta_{co} = 0.552$ and $\zeta_{wo} = 3.82$, respectively. A value less than one indicates that interactions are not purely enthalpic, whereas the high value of ζ_{wo} illustrates the sensitivity of H-bonding on temperature. The values given are used throughout this study.

The volume fractions at the binodals are obtained numerically from $\mu_i^{\alpha} = \mu_i^{\beta}$, where α and β represent the two phases and i refers to either the polymer or the solvent.

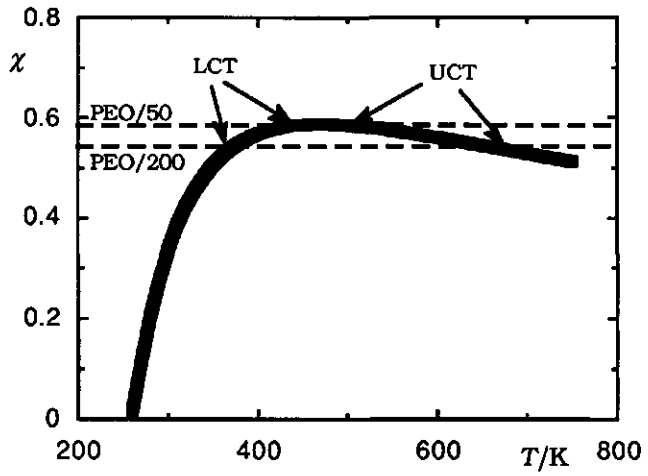

Figure 2. The effective Flory-Huggins parameter χ for PEO in water as a function of temperature. The degree of polymerization has no significant influence on the position of the line. The upper and lower dashed lines are the critical χ values for PEO/50 ($r = 151$) and PEO/200 ($r = 601$), respectively. The resulting critical temperatures are indicated by the arrows.

Results and Discussion

In figure 2 the χ-parameter of PEO, from eqn (8) and (9), is plotted as a function of the temperature. The polymer length enters χ through $f_C = 2x/(3x+1)$, where x is the degree of polymerization (for PEO, $r = 3x+1$). This influence of the polymer length is so small that it is covered by the width of the full line. At very low temperatures, the negative contributions of χ^0_{wo} and χ^0_{co} (see eqn 8) dominate so that χ is very low. However, the large value of ζ_{wo} leads to reduction of the influence of χ^0_{wo} at higher temperatures. Around 450 K the curve has a maximum which is higher than the critical χ value for chains longer than about 48 EO units. The critical χ parameters for PEO/50 ($\chi^{cr} = 0.585$) and PEO/200 ($\chi^{cr} = 0.542$) are indicated by dashed lines and the critical temperatures are indicated by arrows. Between the critical temperatures the polymer solutions show a miscibility gap, since χ is beyond its critical value. At high temperatures the effective χ parameter decreases since all χ values diminish with increasing temperature.

Figure 3 presents solubility gaps for aqueous PEO solutions for three different degrees of polymerization, $x = 50$, 100 and 200. Although the calculated binodals differ from experimentally obtained binodals (the triangles in figure 3) [5], the shapes of the curves do agree with experiment. High molecular weight polymers show a larger gap, because the critical χ for these polymers is lower (cf. eqn 5).

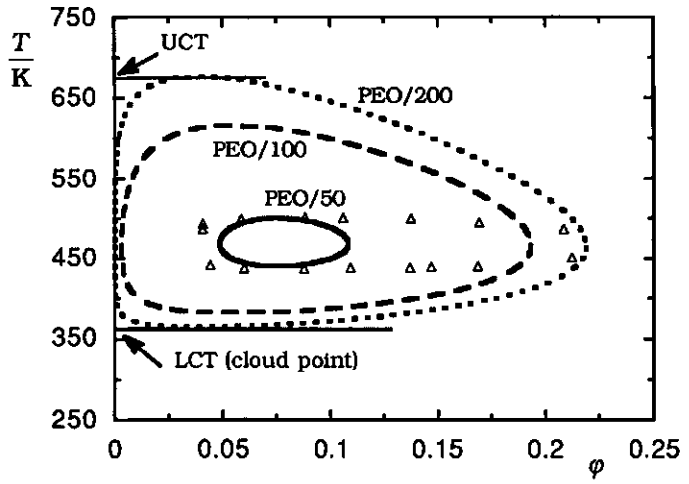

Figure 3. Calculated solubility gaps for aqueous PEO solutions. The three curves correspond to 50, 100 and 200 EO units per molecule (indicated).
The triangles correspond to the data for PEO/48, experimentally obtained by Saeki et al. [5].

In figure 4 the upper and lower critical solution temperatures are plotted as a function of the degree of polymerization of the PEO. Below 48 EO units, no critical temperatures are found, which agrees with experiment [5].

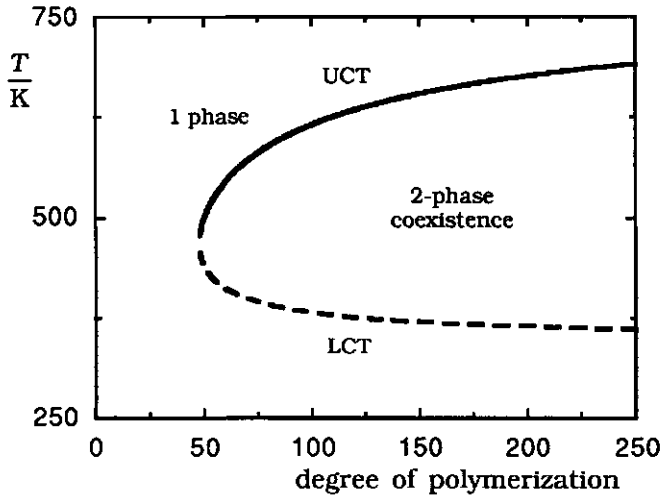

Figure 4. Upper and lower critical solution temperatures of aqueous PEO solutions as a function of the degree of polymerization.

Figure 5 illustrates, for two different chain lengths of polymers, the effect of chain composition. Upper and lower critical solution temperatures are plotted as a function of the fraction of C segments in the chain (full and dashed curve, respectively) . The UCT is stronger dependent on molecular weight then the LCT (cf. figure 2).

A fraction of C segments of 2/3 corresponds to poly(ethylene oxide) (PEO) and a fraction of 3/4 to poly(propylene oxide) (PPO). As may be concluded from figure 5, PPO is not miscible with water, since the lower critical solution temperature lies below the freezing point of water. Indeed, PPO is insoluble in water.

Poly(methylene) oxide, PMO, which has a C fraction of 1/2, does not mix with water either although figure 5 gives the impression that

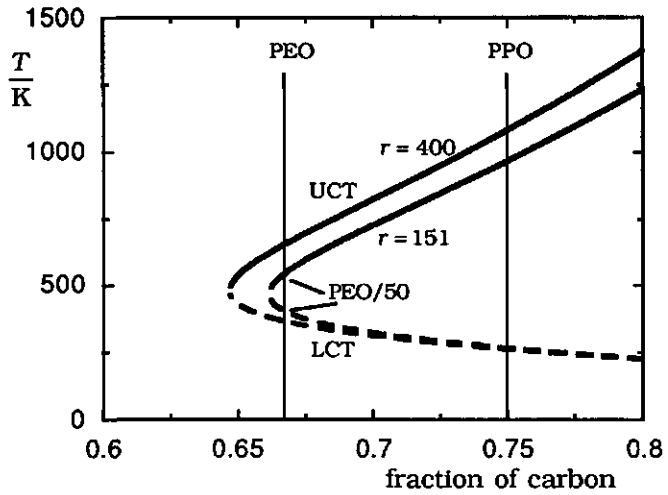

Figure 5 Upper and lower critical solution temperatures of aqueous polymer solutions as a function of the fraction of carbon in the polymer. The curves correspond to polymer chains of 151 and 400 segments. The LCT and UCT of PEO/50 (r = 151) are indicated.

it would. However, the oxygen atoms in PMO cannot be hydrated to the same extent as those in PEO and PPO, because the low fraction of carbon in PMO results in too much steric hindrance for adsorbed water molecules. This means that in the case of PMO, χ_{wo} must be less negative, or even positive, so that the polymer is not soluble in water.

Conclusion

We have shown that the miscibility gap of aqueous PEO solutions can be quantitatively described by the Flory-Huggins theory provided

the polymer is considered as a copolymer with O and CH_2 segments. With one set of independently obtained χ parameters and two scaling parameters, the phase diagram of PEO in water can be constructed. Using the same parameters, the insolubility of PPO in water is predicted. The insolubility of PMO in water is explained by steric hindrance of hydration.

References

1 R. E. Goldstein, J. Chem. Phys., 80 (1984) 5340.

2 D. J. Mitchell, G. J. T. Tiddy, L. Waring, T. Bostock and M. P. McDonald, Chem. Soc. Faraday Trans. 1, 79 (1983) 975.

3 Flory, Principles of Polymer Chemistry, Cornell University Press, Ithaca, NY, 1953.

4 P. A. Barneveld, This thesis, Ch. 4 (1991)

5 S. Saeki, N. Kuwahara, M. Nakata and M. Kaneko, Polymer, 17 (1976) 685.

CHAPTER 3

Ionic Features in Free Liquid Films of Non-Ionics[*]

Abstract

The thickness of thin liquid films stabilized by hepta-ethylene-glycol mono n-dodecyl ether ($C_{12}E_7$) is measured as a function of NaCl concentration. This thickness passes through a maximum at around 1 M, similar to what has been found with other non-ionic surfactants. The maximum is much less pronounced in films stabilized by a mixture of $C_{12}E_7$ and sodium dodecyl sulfate (SDS) or cetyl trimethyl ammonium chloride (CTAC) and there is an enhanced thickness at lower NaCl concentration in these films. We have extended the self-consistent field lattice theory of Böhmer et al. for the adsorption of polyelectrolytes to liquid films stabilized by a mixture of non-ionic and ionic surfactants. This theory accounts for the presence of electric fields and for the excluded volumes of surfactant segments and ions. For mixed films, the enhanced thickness at low salt concentration can indeed be explained by electrostatic repulsion. When the thickness of the mixed film is corrected for this repulsion the result of pure $C_{12}E_7$ films is retrieved, re-establishing the effect of electrolytes on non-ionic surfactants. For non-ionic films in the absence of ionic surfactants, the maximum at high salt concentration cannot be explained by the model. We suggest an explanation for this maximum in terms of contributions of monolayer fluctuations leading to an additional repulsion which depends on the salt concentration.

---

[*] Published previously in Colloids & Surfaces, 52 (1991) 107, in coauthorship with J.M.H.M. Scheutjens and J. Lyklema.

Introduction

The influence of electrolytes on micelles and thin films stabilized by ionic surfactants is well-established. A substantial proportion of this interaction fits well into classical double layer pictures (Gouy-Stern). On the other hand, the corresponding effects on micelles and thin films made of non-ionic surfactants is more subtle and perhaps more specific. Because of the absence of charges on the surfactant molecules, major screening features are unlikely to occur. Consequently, no pronounced electrolyte concentration dependence is anticipated on such parameters as the c.m.c. or the film thickness. In the last decades, a few number of papers have appeared reporting on experiments with nonionic surfactants in the presence of electrolytes [1, 2, 3, 4, 5, 6]. In these papers the attention was focussed mainly on the effect of *low* electrolyte concentrations and on the influence of the surfactant concentration. Due to the poor definition of the materials used, results were hard to interprete. However, recent experiments at relatively high salt concentrations has shown that such electrolyte influences do exist, that they are no minor features and that they exhibit some trends that so far defied interpretation. In the present paper we intend to contribute to the understanding of this interesting problem by presenting and comparing data on the thickness of free non-ionic films in the presence of electrolytes and discussing some suggestions for interpretations.

Regarding the subject matter, a recent publication is a paper by Van den Boomgaard and Lyklema [7] who measured the film

thickness of free liquid films stabilized by Synperonic NPE-1800 as a function of the concentration of NaCl, NaBr and Na_2SO_4. (Synperonic NPE-1800 is a heterodisperse commercial non-ionic surfactant of which the systematic name is $C_9PhP_{<13>}E_{<26>}$ in Clunie and Ingram's code (except the Ph for phenyl) [8]. Here, C, P and E stand for the moieties of the (branched) hydrocarbon tail, P for propylene and E for ethylene, respectively.) In all three cases, the film thickness passed through a maximum. The curve for NaCl is reproduced in figure 1 for comparison purposes. The maximum is situated at about 2 M NaCl. For NaBr and Na_2SO_4 the maxima are found at 1.5 and 0.4 M, respectively. Indications for such maxima can also be found in a

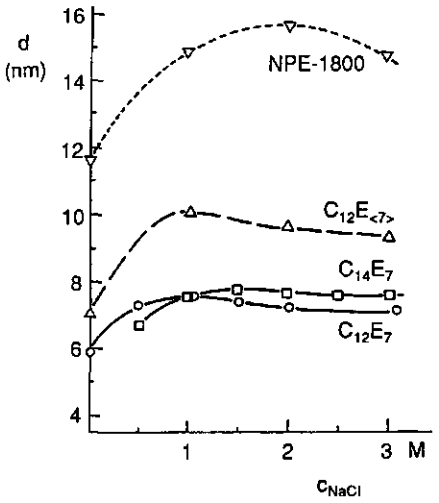

Figure 1. Thickness of free aqueous films, stabilized by homodisperse $C_{12}E_7$, $C_{14}E_7$ (c = 0.4 mM) and by heterodisperse $C_{12}E_{<7>}$ (c = 0.2 mM, dashed curve). Dotted curve: heterodisperse $C_9PhP_{<13>}E_{<26>}$ according to ref. [7].

study by Müller et al. [9] for non-ionics of the $C_{12}E_x$ type, although these experiments are subject to more scatter than ours.

Apparently, there is some evidence for salt-induced maxima in non-ionic films. The first purpose of the present paper was to verify whether this feature is also observed with better defined surfactants.

Theoretical interpretation is the accompanying issue. No simple obvious picture presents itself immediately. First, the salt concentrations where the maxima are observed are far above the coagulation concentrations of the pertaining electrolytes for hydrophobic sols. Hence, the observations are not likely linked to double layer features. Of course, it is well-known that electrolytes do affect the cloud points of poly(ethylene oxides) and EO surfactants. See for instance Durham's conclusions [10] which did not have to be materially modified by more recent work. The trend is that electrolytes reduce the quality of water as a solvent for the poly(ethylene oxide), but this trend cannot be responsible for a maximum. In this paper, we shall also devote some attention to mechanistic interpretations.

Experimental

Most experiments have been done with 98% pure $C_{12}E_7$, purchased from Nikko Chemicals (Japan), a few additional ones with $C_{14}E_7$ and with Synperonic A_7, a commercial heterodisperse non-ionic ex. ICI (England) with average composition $C_{12}E_{<7>}$ and probably containing some carbonic acid. All other chemicals were at least

of P.A. quality. Water was purified by filtration through a Millipore Milli RD60 combined with a Super Q system. All chemicals were used as received.

Methods

The apparatus to measure film thicknesses has been described in some detail before [7]. Basically, the equivalent solution thickness d_{eq} is obtained from laser light reflection under well-controlled conditions. The reproducibility is better than 0.1 nm.

The equivalent solution thickness is computed as if the film consisted entirely of homogeneous bulk solution. In reality this is of course not the case and corrections have to be applied for the differing refractivity of the various layers. Van den Boomgaard and Lyklema estimated the correction to be -2.85 nm for Synperonic NPE-1800. We have calculated the film thickness d as follows. According to Frankel and Mysels [11]

$$d = d_{eq} + 2\sum_{i} d_i (n_{eq}^2 - n_i^2) / (n_{eq}^2 - 1) \qquad (1)$$

The factor 2 accounts for the fact that there are two monolayers in the film. Each surfactant monolayer leads to two corrections in the film thickness. These corrections depend on the corresponding layer thickness d_i and refractive index n_i of the apolar tails and of the polar head groups of the surfactant layer, respectively. The

Surfactant	c_{NaCl} (or c_{DMF}) (M)	d_{eq} (nm)	δ (nm)	d (nm)
$C_{12}E_7$	0	7.40	−1.45	5.95
	0.50	8.70	−1.37	7.33
	1.06	8.85	−1.29	7.56
	1.52	8.60	−1.22	7.38
	2.01	8.45	−1.14	7.31
	3.10	8.22	−1.00	7.22
	1.3 (DMF)	7.19	−1.34	5.85
	2.6 (DMF)	6.71	−1.23	5.48
$C_{14}E_7$	0.5	8.17	−1.42	6.75
	1.0	8.85	−1.34	7.51
	1.5	9.02	−1.26	7.76
	2.0	8.85	−1.18	7.67
	2.5	8.75	−1.10	7.65
	3.0	8.70	−1.03	7.67
$C_{12}E_7$/SDS (1-1)	0.25	9.01	−0.88	8.13
	0.50	7.79	−0.86	6.93
	1.00	7.79	−0.81	6.98
	1.50	7.69	−0.75	6.94
	2.00	7.55	−0.70	6.85
	2.50	7.45	−0.66	6.79
	3.00	7.35	−0.61	6.74
$C_{12}E_7$/CTAC (1-1)	0.25	8.31	−0.94	7.37
	0.50	7.31	−0.92	6.39
	1.00	7.53	−0.86	6.67
	1.50	7.78	−0.80	6.98
	2.00	7.75	−0.75	7.00
	2.50	7.68	−0.70	6.98
	3.00	7.57	−0.65	6.92

Table I. Measured equivalent solution thickness d_{eq}, applied correction δ and resulting film thickness d.

equivalent layer thickness is essentially the adsorbed amount in volume per surface area. As the surface area per molecule is mainly determined by the alkane tail and is close to 0.5 nm^2, the adsorption is around 3.3 $\mu mole/m^2$. In combination with a volume of 15 cm^3/mole per CH_2 or O segment we arrive at d_i = 0.6 nm for the C_{12} tails and d_i = 1.09 nm for the E_7 head groups. No corrections are

made for ionic head groups. It is assumed that the composition of surfactants in the monolayer is the same as in the bulk solution. For example, in a 1 - 1 mixture of $C_{12}E_7$ and SDS we use d_i = 0.6 nm for the tails and d_i = 0.545 nm for the head groups. The refractivities are $n_w = 1.3325 + 0.01\ c_{NaCl}$ or $n_w = 1.3325 + 0.0055\ c_{DMF}$, n_C = 1.42 and n_E = 1.47. Table I is a compilation of the results for d_{eq} and the applied corrections.

Gibbs elasticity measurements were along the lines of work by Crilly and Earnshaw [12].

Results and Discussion

Maxima in thin films

Figure 1 presents film thicknesses as a function of c_{NaCl} for $C_{12}E_7$, $C_{14}E_7$ and $C_{12}E_{<7>}$. Again, curves with maxima are observed. The absolute values of the thicknesses are much lower than for NPE-1800, which is at least in part due to the lower molecular weight of our surfactants. In our previous work it was found that the surfactants adsorb like three-dimensional coils (rather than like cylinders), the thickness scaling with the inverse cube of the ethylene oxide length [7]. This picture is in agreement with the adsorption of these surfactants at solid-liquid interfaces [13]. That $C_{12}E_{<7>}$ gives thicker films than $C_{12}E_7$ over the range of salt concentrations may be due to the heterodispersity of the sample: a few relatively long surfactants may adsorb preferentially. However, the maximum for homodisperse

samples shows that heterodispersity is not responsible for the maximum itself. The maxima for $C_{12}E_7$ and $C_{12}E_{<7>}$ are situated around c_{NaCl} = 1 M, i.e., lower than for $C_{14}E_7$ and Synperonic NPE-1800. A value for $C_{14}E_7$ without salt could not be established due to slow drainage and subsequent rupture of the film.

Regarding the position of the maximum, we may report on other but related measurements in which also an extreme is found as a function of salt concentration. Many years ago, Ivanov derived the molecular area a_0 of homodisperse $C_{12}E_{18}$ from γ - log c measurements at different salt concentrations [14]. He found a maximum around 1.6 M for KCl. This result was confirmed by Bersma for $C_{12}E_{<7>}$ and $C_{12}E_7$ in solutions of NaCl [15], where the maximum was found at 1 M. Hence, not only is the position of the maximum well-established, it may also be concluded that apparently upon NaCl (or KCl) addition the surfactant molecule first expands and later compresses. However, we have now some evidence that expansion in the direction perpendicular to the film may actually not occur: we will arrive at an alternative explanation below. Note that a maximum in the surface area per molecule is equivalent to a minimum in the adsorption of surfactant. If this would have been taken into account in the corrections in Table I the maximum in film thickness would have been more pronounced by about 0.15 nm.

Compression of the surfactant molecule beyond the maximum is readily accounted for by the decreasing solvency power of the water, but the ascending branch poses more problems. One could imagine that of the electrolyte ions one species is selectively absorbed by the surfactant, giving rise to an electrical double layer which leads to

some expansion. This possibility may not be immediately dismissed on the ground that the electrolyte concentrations are so high that double layer features should already be suppressed; the spatial distribution of the created charged sites should be considered in some detail. In this connection, it may be recalled that also in the case of adsorbed polyelectrolytes, where three-dimensional distributions of charges occur, salt effects persisting up to the molarity range have been predicted [16] and verified experimentally [17].

Effects of additives

Figure 2 presents the influence of dimethylformamide (DMF) on d. This substance reduces the solvent quality of the water [18] but is unable to charge the surfactants. Only the descending branch is retrieved.

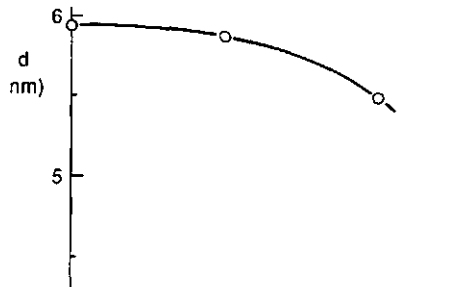

Figure 2. Thickness of free aqueous films, stabilized by homodisperse $C_{12}E_7$ (c = 0.4 mM) as a function of the concentration of N,N dimethylformamide.

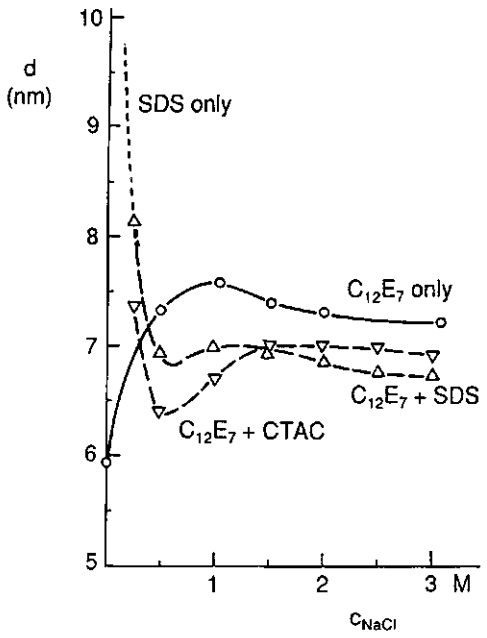

Figure 3. Thickness of free aqueous films, stabilized by equimolar (0.4 mM + 0.4 mM) mixtures of homodisperse $C_{12}E_7$ and sodium dodecyl sulfate (SDS) or cetyl trimethyl ammonium chloride (CTAC) at 25 °C (dashed curves). The thickness of films stabilized by pure SDS, according to ref. [19], is also given (dotted curve).

Figure 3 illustrates the consequences of intentionally charging the surfactant layer by adding equimolar amounts of SDS or CTAC. It is seen that for the high salt concentration range ($c_{NaCl} \gtrsim 2$ M) this has little consequence. The maximum persists, although it is less defined and shifted to higher concentration. Most conspicuously, there is, both for the cationic and the anionic additive, a strong increase at low c_{salt}. This part of the curve compares well with the same for films stabilized by SDS only [19] (see dotted curve in figure 3). Hence, it is concluded that the mixed films behave as a superpo-

sition of classical ionic at low c_{salt} to purely non-ionic at high c_{salt} with a transition zone, in which interaction between the two takes place.

Regarding the occurrence of the maximum the last experiment only confirms that the double layer interaction due to more or less flat layers of charged groups is unable to explain it, because such double layers are already fully screened around 1 M electrolyte. The question then poses itself whether an interpretation may be found in a model in which the spatial distribution of the charges is explicitly accounted for, i.e., a picture in which the surfactant acquires polyelectrolyte character due to preferential uptake of ions from the electrolyte.

Such a theory has been originated by Van der Schee et al. [16, 20] and was recently extended by Böhmer et al. [21]. In theses papers, homopolyelectrolytes were considered but in the present case we are dealing with copolyelectrolytes. We outline the principle below.

Self-consistent field theory for free liquid films

In our department we have initiated [22] and further developed [23] a statistical thermodynamical self-consistent field type of theory to describe the equilibrium conformation of lipids and other non-ionic surfactants in bilayer membranes, vesicles and micelles. A basic feature of this theory is its *ab initio* character in that no preassigned positions of head- or tail groups have to be assumed. The final situation is exclusively determined by the solution properties of the

molecules, as expressed in nearest neighbour interaction energies between head groups, tail segments and solvent molecules and molecular parameters such as its composition, chain branching, gauche - trans isomerism, etc.

The air-film interfaces are simulated in the theory by considering air (vacuum) and free volume in the film as an apolar monomeric component (holes). The size of the holes in the film is of the order of the size of the water molecules. The theory is based on a lattice model. Hence we assume that holes, water molecules, ions and surfactant segments have the same size as a lattice site. In order to account for electrostatic interactions we have introduced the method of Böhmer et al. [21] into the membrane model.

For the case of planar symmetry a volume fraction profile in the z-direction normal to the plane of the film, $\phi_x(z)$, is present for each type of group or segment x (segment, solvent, ...). For ions and water the volume fraction profile is given by the Boltzmann factor $\exp\{-u_x(z)/kT\}$ multiplied by their volume fraction in the bulk solution ϕ_x^b. The local potential energy $u_x(z)$ of species x includes all types of interactions at location z with respect to the bulk solution and will be specified below.

A chain molecule experiences a potential energy which depends on the spatial position of each of its segments, i.e., on its conformation c. We assume that the potential energy u^c of conformation c is the sum of the potential energies $u_x(z)$ of the segments. Thus, if $r_x^c(z)$ segments of type x are in lattice layer z, the potential energy of conformation c is given by

$$u^c = \sum_x \sum_z r_x^c(z) u_x(z) \qquad (2)$$

The probability of conformation c is proportional to the Boltzmann factor of u^c and from the conformation distribution the volume fraction profile of segments x of molecules i is readily computed as

$$\varphi_{ix}(z) = C_i \sum_c r_{ix}^c(z) \exp(-u^c / kT) \qquad (3)$$

where C_i is a normalization constant which is either deduced from the total amount of molecules i in the system or from the volume fraction in the bulk solution where $u^c = 0$. Note that equation (3) applies to monomers like water and ions as well.

The potential energy profiles $u_x(z)$ determine the concentration profiles subject to a number of boundary conditions. Firstly, the packing constraint requires that for all z the sum of the volume fractions is unity:

$$\sum_x \varphi_x(z) = 1 \qquad (4)$$

Secondly, neutrality demands that the net charge in the system is zero. The charge distribution is directly coupled with the volume fraction profile of the ions and charged segments. Generally, if the valency of segment x is denoted by v_x and the charges are assumed to be located on planes parallel to the surface, the plane charge in layer z is given by

$$\sigma(z) = \sum_x e v_x \varphi_x(z) / a_s \qquad (5)$$

where e is the elementary charge and a_s the cross-sectional area of a lattice site. With this in mind, the second boundary condition becomes

$$\sum_z \sigma(z) = 0 \qquad (6)$$

Finely, the volume fraction profiles should be consistent with the preassumed potential energy profiles:

$$u_x(z) = u'(z) + kT \sum_y \chi_{xy} \left(< \varphi_y(z) > - \varphi_y^b \right) + e v_x \psi(z) \qquad (7)$$

In equation (7) the interactions in the bulk solution are subtracted so that the bulk solution is the reference point for $u_x(z)$. The first term on the right hand side represents the steric interaction energy and is the same for any segment and solvent type (u' replaces -kT ln(1-ϕ) in a Langmuir type of approach). By adjusting u'(z) condition (4) can always be met. The second term accounts for the contact energies of segment x with its nearest neighbours. The interaction parameters are of the Flory-Huggins type and the number of contacts with segment type y is supposed to be proportional with its volume fraction in the neighbouring lattice sites:

$$< \varphi_y(z) >= \lambda_1 \varphi_y(z-\ell) + \lambda_0 \varphi_y(z) + \lambda_1 \varphi_y(z+\ell) \qquad (8)$$

Here, λ_1 is the fraction of neighbouring sites in each of the adjacent layers and λ_0 is fraction in layer z. The thickness of a lattice layer is l.

The last term in equation (7) is the electrostatic energy of segment x. This term is also completely determined by the volume fraction profiles. We assume that the dielectric permittivity is a linear combination of the permittivities of the components:

$$\varepsilon(z) = \sum_x \varepsilon_x \varphi_x(z) \qquad (9)$$

In our model, the volume fractions are constant within each lattice layer, i.e., in lattice layer z $\phi_x(z)$ is supposed constant from $(z - \ell/2)$ to $(z + \ell/2)$. Hence, the volume fraction and the permittivity profile are step functions. The electric field strength is also a step function, like in a multilayer capacitor, changing abruptly at positions z by $\sigma(z)/\varepsilon(z)$ because of the plane charge and at positions $(z + \ell/2)$ due to the change in ε. The electrostatic potential profile is then obtained by incremental integration of the field strength:

$$\psi(z+\ell) - \psi(z) = \frac{-\ell}{2}\left(\frac{1}{\varepsilon(z+\ell/4)} + \frac{1}{\varepsilon(z+3\ell/4)}\right)\sum_{z'=-\infty}^{z}\sigma(z') \qquad (10)$$

At $z = -\infty$, $\Psi(z+\ell) = \Psi(z)$.

Equations (3), (4), (5) and (7) form a set of simultaneous equations which have to be solved numerically. Details are given in ref. [21].

Salt effects in films

Volume fraction profiles of a monolayer at an air-water interface

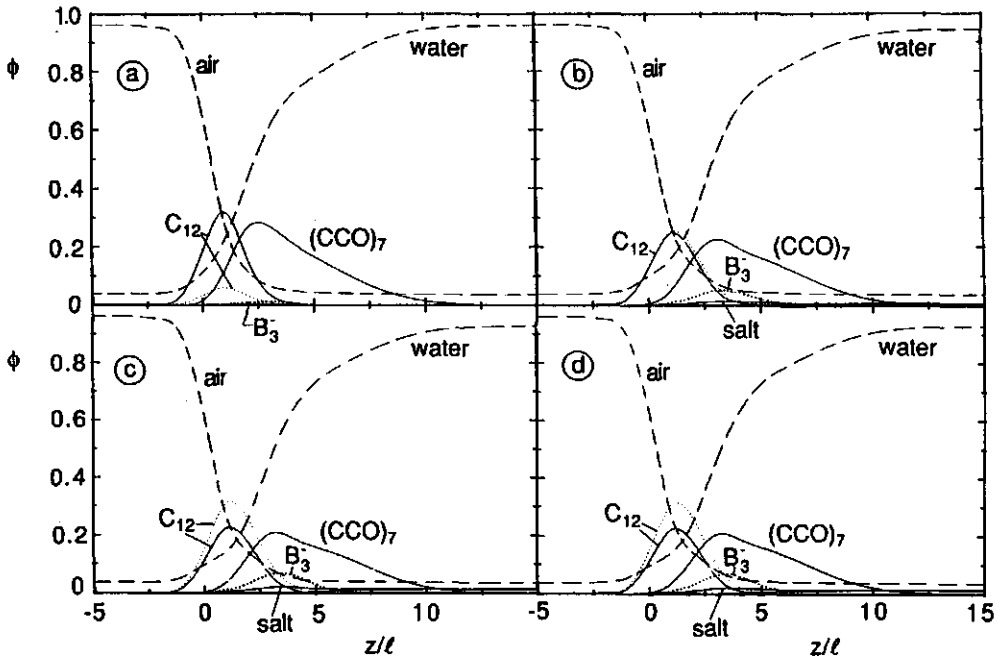

Figure 4. Theoretical segment density profiles of the monolayers of mixed surfactants in the films of figure 3 at four different salt concentrations: a) 0.01 M, b) 0.5 M, c) 1 M and d) 2 M. The interaction parameters between air (A), water (W), alkane groups (C) and oxide groups (O) are: χ_{AW} = 3.5, χ_{AC} =1.6, χ_{CW} = 2, χ_{OW} = -1.6. Ions are treated as water, except for their electrostatic interactions. The relative dielectric permittivities are 1 for air, 5 for C and 80 for water and ions. The solution volume fraction of the non-ionic surfactant $C_{12}(OCC)_7$ is 5.45 10^{-4} and of the anionic surfactant $C_{12}B_3$ is 2.56 10^{-4}. The thickness ℓ of the lattice layers in the hexagonal lattice is 0.3 nm.

as in figure 3. The nonionic surfactant $C_{12}E_7$ is modeled as chains with segment order $C_{12}(OCC)_7O$ and the anionic (SDS) as $C_{12}B_3^-$ and Na^+. In this way the size of the head group of the anionic is three times that of a CH_2. The monolayer consists of non-ionics and ionics adsorbed from a solution of equimolar composition, i.e., with volume fraction $5.45\ 10^{-4}$ of non-ionic and $2.56\ 10^{-4}$ of an ionic surfactant. The NaCl concentrations in figures 4a-d are 0.01, 0.5, 1 and 2 M, respectively.

Interaction parameters were estimated as follows. The air-water (A-W) interface develops spontaneously because of a strong net repulsion between holes and water molecules. Hence, χ_{AW} must be high and positive. We set $\chi_{AW} = 3.5$. (there is no interaction between holes and molecules but the Flory-Huggins χ-parameters refer to the mixing energies and thus the mutual attraction between water molecules in pure water is the reference state, i.e., $\chi_{WW} = 0$.) The value for χ_{AW} determines the volume fraction of water in air as well as the free volume in water. Both volume fractions are the same in our case (about 0.033) because of the equal sizes of holes and water molecules. More precise values can be obtained by fitting vapour pressure data and the compressibility of water, but this is irrelevant for the present purpose. The solubility of alkanes in water [24] and the vapour pressure of pure alkanes are needed for an estimation of the interactions with alkanes. We have used $\chi_{CW} = 2$ and $\chi_{CA} = 1.6$. The oxide groups (O) in the non-ionic surfactant is considered to form hydrogen bridges with water so that a negative χ-parameter is

anticipated: $\chi_{ow} = -1.6$. Ions are treated the same as water, except for their electrostatic interactions.

The volume fraction profiles are qualitatively the same for all salt concentrations. Apart from water all concentrations in air are extremely low. The position of the head groups of the surfactants shows a large fluctuation: the monolayer has a rough surface. The extent of the head groups of the non-ionics is nearly independent of the salt concentration. Their volume fractions vanish around $z = 11\ell$ at any salt concentration. It is inferred that electrolytes do not substantially affect the steric component of the interaction. The thickness of a film is apparently not much affected by steric interactions.

Differences do occur in the surfactant composition of the monolayer. In 0.01 M salt (figure 4a) the monolayer consists mainly of non-ionic surfactant, in 0.5 M (figure 4b) the amounts of ionic and non-ionic surfactant are about the same and in higher salt concentrations (figures 4c and 4d) the ionic surfactant dominates. The adsorption of ionic surfactant is easier when the charged head groups are screened by salt ions. Even in very high salt concentrations the electrostatic effect is still operative. This is more clearly shown in figure 5, where the electrostatic potential profiles are given for the four situations in figure 4. At low c_{salt}, the extension of the double layer decreases strongly with increasing salt concentration but above 0.5 M this decrease is partly counteracted by the enhanced adsorption of ionic surfactant. The same trend is observed in the magnitude of the (negative) electrostatic potential. However, the

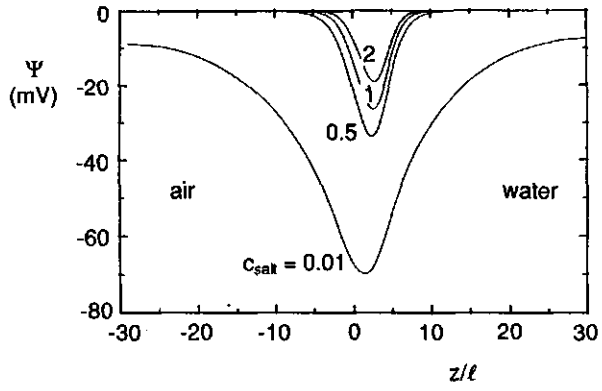

Figure 5. Electrostatic potential profiles of the monolayers in figure 4.

increase in adsorption is not enough to compensate the screening of the surface charge. This is in accordance with the experimental observation in figure 3 that electrostatic effects are negligible beyond 0.1 M salt. The preferential adsorption could affect the corrections in Table I and the curves in figure 3. At low salt concentration, where nonionic surfactant is preferentially adsorbed, the film may be about 0.5 nm thinner than indicated, whereas at high salt concentration the film thickness may actually be around 0.2 nm thicker. However, this has no effect on the conclusion. Note that in figure 5 the electrostatic potential profile is not symmetrical because the solubility of the surfactants and ions is different in the two phases. There is a small potential drop over the monolayer.

An advantage of the present model in comparison with Gouy-Chapman models is that ion binding can be simulated. For example, a negative χ-parameter for the interaction between Na and O would simulate adsorption of sodium ions on the non-ionic head groups,

charging the surfactant. However, we did not find any extra repulsion in the film when such a negative χ-parameter was introduced. Instead, the same ions adsorb on both monolayers and this bridging effect leads to some extra attraction.

Consequently, an increase in the thickness of liquid films with salt concentration can neither be expected from steric interactions alone, nor from double layer repulsion, even if salt ions charge the non-ionic surfactants by strongly adsorbing on their head groups.

Contributions owing to undulations

As an alternative we have been considering an interpretation of the maximum in terms of the salt-influence on the thermal undulations. As proposed by Helfrich [25], thermal fluctuations may lead to repulsion between a pair of tension-free interacting lipid bilayers. Undulations are more pronounced when the bilayers are more flexible. As a liquid film consists of two interacting flexible monolayers, undulations in these monolayers may also affect their interaction and thus the thickness of the film. Although the surface tension opposes undulations, monolayers are thinner and hence more flexible than bilayers. If the salt-maximum of the film thickness were due to Helfrich-type undulations only, the flexibility should pass through a maximum as a function of c_{salt}. As the decrease in film thickness at high salt concentration may be caused by a decrease in solvent quality, it would be sufficient for the interpretation of the maximum if the flexibility would increase with salt concentration.

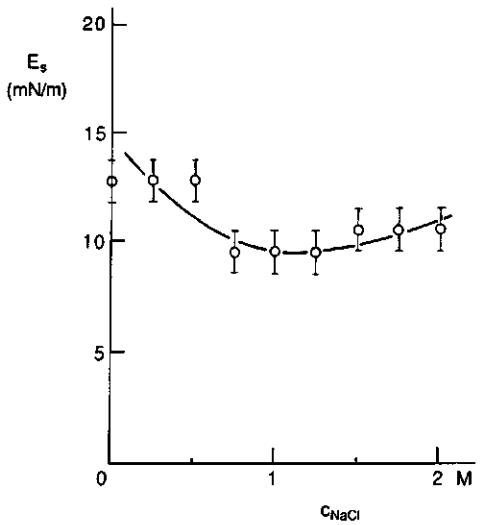

Figure 6. Gibbs elasticity of a monolayer of $C_{12}E_7$ measured at 25 °C by photon correlation spectroscopy as a function of the NaCl concentration.

It is not too farfetched to expect that this approach has some promise. First, we recall the fact that a_0 passes through a maximum coinciding with the maximum in the film thickness. As theory predicts that the flexibility increases with a_0 [26], the combination of these observations could well explain the maximum as function of c_{salt}.

A second argument is based upon the elasticity of a $C_{12}E_7$ monolayer as measured by photon correlation spectroscopy which passes through a minimum at the same salt concentration (figure 6), or at least increases with salt concentration below 1 M. Although the relation between this parameter and the bending energy is not yet quantitatively established, it is possible that some correlation exists [27]. A minimum in the elasticity implies a greater susceptibility of the layer to area changes, i.e., suggesting a greater flexibility.

Conclusion

It is well-established that liquid films stabilized by non-ionic surfactants can exhibit a maximum thickness with salt concentration which for (1-1) electrolytes is situated around 1 M. The decrease in thickness beyond the maximum may be due to a solvent quality effect, possibly augmented by a weak change in the electric double layer. However, the increase of the thickness below the maximum is not easy to explain. We have strong experimental and theoretical evidence that electrostatic interactions are unlikely to play a role. We suggest that thermal undulations may be responsible for the observed trends. This would be the case if the flexibility of the interacting monolayers increases with salt concentration. It is known that the surface area of some non-ionics on air-water interfaces shows a maximum around 1 M of salt and the existence of a direct relation between surface area per molecule and flexibility of the monolayer is supported by theory. More quantitative calculations are in progress to verify the suggested relations between film thickness, thermal undulations and salt concentration.

References

1 E. M. Duyvis and J. T. G. Overbeek, Conference Proceedings Koninkl. Nederl. Akademie van Wetenschappen: Physical Chemistry, Amsterdam, 1962.

2 D. Exerowa and A. Scheludko, Conference Proceedings International Congress on Surface Activity, Brussels, Belgium, 1964.

3 D. Exerowa, Kolloid. Z., 232 (1969) 703.

4 D. Exerowa, M. Zacharieva, R. Cohen and D. Platikanov, Colloid & Polymer Sci., 257 (1979) 1089.

5 M. Paluch, Pol. J. Chem., 54 (1980) 1827.

6 T. Kolarov, R. Cohen and D. Exerowa, Colloids and Surfaces, 42 (1989) 49.

7 T. v. d. Boomgaard and J. Lyklema, Langmuir, 5 (1989) 245.

8 J. S. Clunie and B. T. Ingram, in G. D. Parfitt and C. H. Rochester (Ed.), Adsorption from Solution at the Solid-Liquid Interface, Acad. Press, London, New York 1983, p. 105.

9 H.-J. Müller, G. Kretzschmar and R. Holzbauer, Abh. Akad. Wiss. DDR, Abt. Math., Naturwiss., Tech., 1N (1987) 331.

10 K. Durham, in K. Durham (Ed.), Surface Activity and Detergency, MacMillan, London 1961, p. 1.

11 S. P. Frankel and K. J. Mysels, J. Appl. Phys., 37 (1966) 3725.

12 J. F. Crilly and J. C. Earnshaw, Biophys. J., 41 (1983) 197.

13 T. v. d. Boomgaard, T. F. Tadros and J. Lyklema, J. Colloid interface Sci., 116 (1987) 8.

14 I. Ivanov, L. Grigorov and T. Kolarov, Conference Proceedings International Conference on Colloid and Surface Science, Budapest, Hungary, 1975.

15 T. Bersma, (1985).

16 H. A. v. d. Schee and J. Lyklema, J. Phys. chem., 88 (1984) 6661.

17 B. C. Bonekamp, H. A. v. d. Schee and J. Lyklema, Croat. Chem. Acta, 56 (1983) 695.

18 W. J. M. Heuvelsland, Thesis, Amsterdam 1980.

19 J. Lyklema and K. J. Mysels, J. Am. Chem. Soc., 87 (1965) 2539.

20 J. Papenhuijzen, H. A. v. d. Schee and G. J. Fleer, J. Colloid Interface Sci., 104 (1985) 540.

21 M. R. Böhmer, O. A. Evers and J. M. H. M. Scheutjens, Macromolecules, 23 (1990) 2288.

22 F. A. M. Leermakers, J. M. H. M. Scheutjens and J. Lyklema, Biophys. Chem., 18 (1983) 353.

23 F. A. M. Leermakers and J. M. H. M. Scheutjens, J. Chem. Phys., 89 (1988) 3264.

24 C. Tanford, The hydrophobic effect: formation of micelles and biological membranes, John Wiley, New Y ork, 1973.

25 W. Helfrich, Z. Naturforsch., 33a (1978) 305.

26 I. Szleifer, D. Kramer, A. Ben-Shaul, D. Roux and W. M. Gelbart, Phys. Rev. Lett., 60 (1988) 1966.

27 M. M. Kozlov, S. L. Leikin and V. S. Markin, J. Chem. Soc., Faraday Trans. 2., 85 (1989) 277.

CHAPTER 4

Bending Moduli and Spontaneous Curvature I. Bilayers and Monolayers of Pure and Mixed Nonionic Surfactants

Abstract

The mean and Gaußian bending elasticity moduli of monolayers and bilayers of nonionic surfactants are computed from the solution properties of the surfactant, without adjustable parameters. To that end, the grand potential Ω (the grand canonical characteristic function) is calculated as a function of the surface curvature using a modification of the the self-consistent field lattice model of Scheutjens and Fleer. The interfaces are formed by self-assembling of the surfactants. It is found that with increasing tail length of the surfactant the bending modulus k_c of a bilayer rises linearly, whereas the Gaußian bending modulus $\bar{k}_c$ shows a maximum. The addition of short linear alcohols considerably decreases k_c and $\bar{k}_c$, whereas the presence of long chain alcohols can increase the rigidity of the bilayer. The spontaneous curvature of a monolayer at an oil-water interface strongly depends on the concentration of the surfactant.

Introduction

The curvature of an interface can be characterized by the mean curvature $J = c_1 + c_2$ and the Gaußian curvature $K = c_1 c_2$. Here, c_1 and c_2 are the principal curvatures. For example, the surface of a cylinder of radius R is characterized by $c_1 = 1/R$ and $c_2 = 0$, whereas that of a

sphere of radius R has curvatures $c_1 = c_2 = 1/R$. With the process of bending, two rather well-known bending elasticity moduli are associated: the mean bending modulus k_c and the Gaußian bending modulus $\bar{k}_c$. An interface also has a preferred or *spontaneous* mean curvature J_{sp} and *spontaneous* Gaußian curvature K_{sp}. It is believed that in microemulsions J_{sp} largely determines which type of emulsion is formed (O/W or W/O) [1]. For symmetrical interfaces, J_{sp} is zero. Obviously, k_c, $\bar{k}_c$, J_{sp} and K_{sp} depend on the nature of the interface.

The parameter k_c is important because it determines the amplitude of thermal undulations of surfactant layers [2]. A small value for k_c leads to large fluctuations. By observing undulations, using for instance ellipsometry or X-ray scattering, k_c can in principle be measured [3, 4, 5]. When two surfactant layers approach each other, undulations are restricted, which leads to repulsion between these layers. As was shown by Helfrich, this repulsion is proportional to k_c^{-1} [2].

An emulsion droplet, as we define it here, consists of a condensed phase α which is immersed in a condensed (bulk) phase β. The two phases do not mix and the interface is usually stabilized by a surfactant monolayer. The pressure in the emulsion droplet differs from that in the bulk phase due to the interfacial tension γ in combination with the (mean) curvature J. The Laplace pressure drop $p^\alpha - p^\beta$ over the interface is given by:

$$p^\alpha - p^\beta = \gamma_t J_t \qquad (1)$$

The superscripts α and β denote the phases and the subscript t

refers to the surface of tension, which can be used to define the position m of the interface. Obviously, $p^{\alpha} - p^{\beta}$ is independent of any assumption about the position of the interface. Eqn (1) is valid *only at* the surface of tension, the general equation being $p^{\alpha} - p^{\beta} = \chi J + \partial\gamma/\partial m$, where the derivative corrects for an imaginary displacement of the dividing interface and vanishes at the surface of tension. Another important parameter that does not depend on the actual choice of the dividing interface, is the grand potential Ω (grand canonical characteristic function), for which one can write:

$$\Omega = -p^{\alpha}V^{\alpha} - p^{\beta}V^{\beta} + \gamma A_s \tag{2}$$

where V^{α} is the volume of phase α, V^{β} that of phase β and A_s the area of the interface. Obviously, γ, V^{α}, V^{β} and A_s are simultaneously defined by position of the dividing interface. When eqn (1) and (2) are combined, the curvature and interfacial tension *at the surface of tension* can be expressed in terms of $p^{\alpha} - p^{\beta}$ and $\Omega + p^{\beta}V$, where V is the total volume $V^{\alpha} + V^{\beta}$. Generally, $\Omega + p^{\beta}V = -\left(p^{\alpha} - p^{\beta}\right)\left(V_t^{\alpha} - A_t/J_t\right)$. For instance, for a cylinder, $\Omega + p^{\beta}V = \left(p^{\alpha} - p^{\beta}\right)\pi h/J_t^2$, where h is the length of the cylinder and for a sphere $\Omega + p^{\beta}V = \left(p^{\alpha} - p^{\beta}\right)(16\pi/3)/J_t^3$. Hence,

$$\begin{cases} J_t^2 = \pi h\left(p^{\alpha} - p^{\beta}\right)/\left(\Omega + p^{\beta}V\right) & \text{(cylinder)} \\ J_t^3 = \dfrac{16\pi}{3}\left(p^{\alpha} - p^{\beta}\right)/\left(\Omega + p^{\beta}V\right) & \text{(sphere)} \end{cases} \tag{3}$$

and, in combination with eqn (1),

$$\gamma_t = \begin{cases} (\pi h)^{-1} J_t \left(\Omega + p^\beta V\right) & \text{(cylinder)} \\ \dfrac{3}{16\pi} J_t^2 \left(\Omega + p^\beta V\right) & \text{(sphere)} \end{cases} \tag{4}$$

An important difference between emulsion droplets and vesicles is that vesicles lack an oil phase. Let us consider the situation that the phases inside and outside the interface are aqueous. In order to achieve a stable surfactant layer, the surfactant molecules need to self-aggregate into (at least) bilayers. Because of the identity of phases α and β, there is no Laplace pressure drop across the bilayer; any pressure occurs only at nonequilibrium and would be annihilated by leakage of solution through the bilayer (for emulsions the permeability of the monolayer cannot release all pressure since the solubility of oil in water is limited). Note that, according to eqn (3) and (4), the property $p^\alpha = p^\beta$ implies $J_t = 0$, i.e., the (formal) area of the interface is infinite and $\gamma_t = 0$.

For an emulsion droplet the surface of tension of the monolayer can be used to define the surface area: its position is virtually the same as that of the centre of the monolayer. For determining the surface area of a vesicle the surface of tension is inappropriate since it is infinite. A practical choice is to take the mass centre of the bilayer as the position of the interface. The interfacial tension γ is then computed from the corresponding surface area A_s in combination with eqn (2) as

$$\gamma = \frac{\Omega + p^{\beta}V}{A_s} \qquad (p^{\alpha} = p^{\beta}) \tag{5}$$

The dependency of γ on the curvature parameters J and K can be used to formulate k_c, $\bar{k}_c$, J_{sp} and K_{sp}. The interfacial tension contains information on these parameters because enlarging the interface at constant curvature means bending the interface. In this paper, the interfacial tension of mono- and bilayers is computed using a modification of the self-consistent field (SCF) lattice theory of Scheutjens and Fleer [6]. The bending elasticity moduli of surfactant monolayers and bilayers are obtained, without any adjustable parameters, from the solution properties of the surfactant. The surfactants are models of nonionics of the poly(oxyethylene) type ($C_nH_{2n+1}(OC_2H_4)_mOH$, abbreviated as C_nE_m). Linear alcohols ($C_nH_{2n+1}OH$, denoted by C_nOH) are chosen as the cosurfactants. Whenever appropriate, the oil phase consists of n-alkanes (C_nH_{2n+2}, written as C_n).

This paper is organized as follows. First a general thermodynamic analysis is given to relate the curvature elasticity parameters to the interfacial tensions of curved interfaces. Then a statistical thermodynamical model is presented to calculate the interfacial tensions for mixed monolayers and bilayers. Following a discussion of the methods used, the paper is completed by a section on results and conclusions.

Bending elasticity parameters

The change of energy, dU, of a system during a reversible process can be expressed as

$$dU = TdS - p^{\alpha}dV^{\alpha} - p^{\beta}dV^{\beta} + \sum_i \mu_i dn_i + \gamma dA_s + A_s C_1 dJ + A_s C_2 dK \qquad (6)$$

The coefficients C_1 (dimensions of force) and C_2 (dimensions of energy) are known as the first and second moment, respectively. The second moment is also known as $\bar{k}_c$, the Gaußian bending modulus. This expression is generally valid for systems with curved interfaces in the absence of external fields. The grand potential Ω, is defined by $\Omega = U - TS - \sum_i n_i \mu_i$. Therefore:

$$d\Omega = -SdT - p^{\alpha}dV^{\alpha} - p^{\beta}dV^{\beta} - \sum_i n_i d\mu_i + \gamma dA_s + A_s C_1 dJ + A_s C_2 dK \qquad (7)$$

Note that integrating this equation yields eqn (2).

The contribution of the interface to $d\Omega$, called $d\Omega^s$, is defined by:

$$d\Omega^s = -S^s dT - \sum_i n_i^s d\mu_i + \gamma dA_s + A_s C_1 dJ + A_s C_2 dK \qquad (8)$$

As the integrated form of $d\Omega^s$ is γA_s, we arrive at an equation analogue of the Gibbs-Duhem relation [7]:

$$d\gamma = -s^s dT - \sum_i \Gamma_i d\mu_i + C_1 dJ + C_2 dK \qquad (9)$$

In this equation, s^s is the interfacial entropy per unit area and Γ_i is the amount of component i adsorbed. From eqn (9) it follows directly that:

$$C_1 = \left(\frac{\partial \gamma}{\partial J}\right)_{T,\{\mu_i\},K} \qquad C_2 = \left(\frac{\partial \gamma}{\partial K}\right)_{T,\{\mu_i\},J} \tag{10}$$

At constant T and $\{\mu_i\}$ the interfacial tension, $\gamma(J,K)$, is just a function of mean and Gaußian curvatures, so that we may expand this quantity in terms of J and K around any point. Obvious choices for such a point are the unbended state, where $J = K = 0$ and the spontaneous state, where $\left(\frac{\partial \gamma}{\partial J}\right)_K = \left(\frac{\partial \gamma}{\partial K}\right)_J = 0$. Expansion up to second order around the unbended state yields:

$$\gamma(J,K) - \gamma(0,0) = C_1(0,0)J + C_2(0,0)K + \tfrac{1}{2}E_{JJ}J^2 + \tfrac{1}{2}E_{KK}K^2 + E_{JK}JK \tag{11}$$

In this equation, the coefficients C_1 and C_2 are defined by eqn (10), whereas the elasticity moduli E_{JJ}, E_{KK} and E_{JK} are defined by:

$$E_{JJ} = \left(\frac{\partial C_1}{\partial J}\right)_K \qquad E_{KK} = \left(\frac{\partial C_2}{\partial K}\right)_J \qquad E_{JK} = \left(\frac{\partial C_1}{\partial K}\right)_J = \left(\frac{\partial C_2}{\partial J}\right)_K \tag{12}$$

The coefficients $C_1(0,0)$ and $C_2(0,0)$ in eqn (11) can be related to the state of minimal interfacial tension, i.e., to the spontaneous curvatures J_{sp} and K_{sp}:

$$\begin{cases} C_1(0,0) = -E_{JJ}J_{sp} - E_{JK}K_{sp} \\ C_2(0,0) = -E_{KK}K_{sp} - E_{JK}J_{sp} \end{cases} \tag{13}$$

For interfaces that are thin as compared to the reciprocal curvatures, terms proportional to K^2 and JK may be omitted in eqn (11). This yields:

$$\gamma(J,K) - \gamma(0,0) = \tfrac{1}{2}k_c J^2 - k_c J_{sp} J + \bar{k}_c K \qquad \text{(thin interfaces)} \tag{14}$$

Here have equated E_{JJ} to the mean bending modulus k_c and $C_2(0,0)$ to the Gaußian bending modulus $\bar{k}_c$. Again, the spontaneous mean curvature J_{sp} is deduced from the criterion $\left(\frac{\partial \gamma}{\partial J}\right)_K = 0$. In this way, Helfrich's equation [8] is recovered.

The elasticity moduli can be formulated in terms of the dependence of γ on curvature by considering different geometries of interfaces. For a cylindrical interface ($K = 0$) eqn (14) reduces to:

$$\gamma(J,0) - \gamma(0,0) = \tfrac{1}{2}k_c J^2 - k_c J_{sp} J \qquad \text{(thin interfaces)} \tag{15}$$

and for a spherical interface ($K = J^2/4$):

$$\gamma(J,\tfrac{1}{4}J^2) - \gamma(0,0) = \tfrac{1}{2}\left(k_c + \tfrac{1}{2}\bar{k}_c\right)J^2 - k_c J_{sp} J \qquad \text{(thin interfaces)} \tag{16}$$

The combination of eqn (15) and (16) allows us to obtain k_c and $\bar{k}_c$ unambiguously if $\gamma(J,0)$ and $\gamma(J,\frac{1}{4}J^2)$ are known. Moreover J_{sp} can also be calculated.

In the next section a lattice model is described which enables us to calculate the interfacial tension of curved monolayers and bilayers from molecular interaction parameters.

Self-consistent Field Lattice Theory

Lattice

In order to evaluate the conformation distribution of the molecules in an aggregate (vesicle, emulsion droplet, bilayer), the number of representative conformations must be limited. A common way to achieve this is to divide the molecule into chain segments, which can be placed on a lattice. A subsequent reduction of complexity is to allow for inhomogeneities in only one dimension, z, normal to the interface of the aggregate. This leads to lattice layers parallel to the interface in which the volume fraction of segments is constant. A consequence of this approach is that aggregates are unable to seek their optimum geometry by themselves, i.e., the geometry of the aggregate is imposed by the symmetry of the lattice. The lattice has M layers, numbered from $z=\ell$ to $z=M\ell$, where ℓ is the thickness of a layer. Conventionally, the first layer (from $z=0$ to $z=\ell$) is in the centre of the aggregate (phase α) and the last layer (from $z=(M-1)\ell$ to $z=M\ell$) is so far in phase β, that bulk properties have been reached.

The volume of a lattice layer is denoted by $L(z)$ and varies with z in the case of a curved lattice. In this study, we deal with planar, cylin-

drical and spherical lattices. At $z = M\ell$ a reflecting boundary condition is applied. For planar lattices this is also done at $z = 0$.

The area $A_s(z)$ and the volume $V(z)$ of a lattice up to and including layer z are given by:

$$A_s(z) = \begin{cases} L/\ell & \text{planar} \\ 2\pi hz & \text{cylindrical} \\ 4\pi z^2 & \text{spherical} \end{cases} \qquad (17)$$

and

$$V(z) = \begin{cases} Lz/\ell & \text{planar} \\ \pi hz^2 & \text{cylindrical} \\ \frac{4}{3}\pi z^3 & \text{spherical} \end{cases} \qquad (18)$$

respectively, where h is the length of the cylinder. The volume $L(z)$ is then given by

$$L(z) = V(z) - V(z - \ell) \qquad (19)$$

We consider a homodisperse multicomponent system of linear chains of r_i segments, where i denotes the component. Each component is a sample of (chain) molecules characterized by a given sequence of segment types $x = A,B,C,....$ The solvent molecules W are monomers ($r = 1$). We consider the case that each segment occupies just one lattice site.

A random walk, representing a chain, gives rise to an a priori probability $\lambda_{z'-z}$ for a step from layer z to an adjoining layer z'. This parameter is defined by the geometry of the lattice. For a planar hexagonal lattice the following set of parameters hold:

$$\lambda_{-\ell} = \frac{3}{12}, \qquad \lambda_0 = \frac{6}{12}, \qquad \lambda_{+\ell} = \frac{3}{12}, \qquad \lambda_{|z'-z|>\ell} = 0 \tag{20}$$

For a curved lattice the a priory probabilities are functions of z. The numerical values can easily be computed from the planar (bulk solution) probabilities at $z \to \infty$ [9]:

$$\begin{aligned}
\lambda_{-\ell}(z) &= \frac{\ell A_s(z-\ell)}{L(z)}\lambda_{-\ell}(\infty), \\
\lambda_{+\ell}(z) &= \frac{\ell A_s(z)}{L(z)}\lambda_{+\ell}(\infty), \\
\lambda_0(z) &= 1-\lambda_{-\ell}(z)-\lambda_{+\ell}(z)
\end{aligned} \tag{21}$$

Note that the number of different steps from z to $z+1$ equals that from $z+1$ to z, so that no chain segments are lost or generated: $L(z)\lambda_{+\ell}(z) = L(z+\ell)\lambda_{-\ell}(z+\ell)$.

Chain statistics

Chain segments as well as free monomers are subject to interactions with surrounding segments. Each type of segment x is assigned a potential energy $u_x(z)$ relative to the bulk solution. A segment weighting factor $G_x(z)$ can be defined as [10]

$$G_x(z) = \exp\{-u_x(z)/kT\} \tag{22}$$

As we neglect inhomogeneities within each layer z, the weighting factor $G_x(z)$ is a function of z only. The expression for $u_x(z)$ has been derived from statistical thermodynamics [10]:

$$u_x(z) = u'(z) + kT\sum_y \chi_{xy}\left(<\varphi_y(z)> - \varphi_y^\beta\right) \qquad (23)$$

The subscripts x and y refer to segment types A, B, C, ... in the system. In this expression $\varphi_y(z)$ is the volume fraction of segment y in layer z and φ_y^β is the corresponding volume fraction in bulk solution (phase β). The angular brackets indicate an averaging over nearest neighbours in three consecutive layers:

$$<\varphi(z)> = \lambda_{-\ell}(z)\varphi(z-\ell) + \lambda_0(z)\varphi(z) + \lambda_{+\ell}(z)\varphi(z+\ell) \qquad (24)$$

In eqn (23), χ_{xy} is the well-known Flory-Huggins parameter for the interaction between segments of type x and y [11].

The quantity $u'(z)$ in eqn (23), is a potential energy that accounts for the hard core interaction in layer z relative to that in bulk solution ($u'(M\ell) \equiv 0$). Values for this parameter are numerically obtained by adjusting $u'(z)$ so that $\sum_x \phi_x(z) = 1$ for all z.

The volume fractions $\varphi_x(z)$ of segments x and the volume fractions $\varphi_i(z)$ of chain i can easily be found once the so-called end segment distribution functions $G_i(z,s|1)$ are known. These functions describe the average weight of walks along chain i, starting at segment 1 in an arbitrary layer and finishing after s-1 steps at segment s in layer z.

The function $G_i(z,s|1)$ can be found from the segment weighting factor $G_i(z,s|s)$, which equals $G_x(z)$ if segment s is of type x, by the recurrence relation

$$G_i(z,s|1) = G_i(z,s|s) < G_i(z,s-1|1) > \tag{25}$$

Where the angular brackets denote averaging over neighbours, like in eqn (24).

To find the volume fraction profile $\varphi_i(z,s)$ of segments s in chains i of r_i segments, the end segment distribution functions of two subchains have to be considered. One subchain starts at segment 1 and ends at segment s, with end segment distribution function $G_i(z,s|1)$, the other starts at r and ends at s, with end segment distribution function $G_i(z,s|r)$:

$$\varphi_i(z,s) = C_i \frac{G_i(z,s|1)G_i(z,s|r)}{G_i(z,s|s)} \tag{26}$$

This equation accounts properly for the fact that segment s in chain i is connected to segment s-1 as well as to s+1. The division by $G_i(z,s|s)$ is needed to correct for double counting, since segment s occurs in both subchains.

The normalization factor C_i in eqn (26) can be related to the volume fraction φ_i^β in the bulk solution. Since in bulk solution all end segment distribution functions are unity, this factor is given by

$$C_i = \frac{\varphi_i^\beta}{r_i} \tag{27}$$

Alternatively, C_i can be expressed in terms of the total number n_i of chains in the system. The number of any segment s of chains i equals n_i, hence $\sum_z L(z)\varphi_i(z,s) = \sum_z L(z)\varphi_i(z,r_i) = n_i$. Summing both sides of eqn (26) over z with $s = r_i$ and weight $L(z)$:

$$C_i = \frac{n_i}{\sum_z L(z) G_i(z,r|1)} \tag{28}$$

At this point we are able to obtain all volume fractions of all segments for all components i. By proper summing one can obtain the volume fraction distribution of the complete chain, $\varphi_i(z)$ and the volume fractions of the various moieties (blocks) of the chain.

In conclusion, when we have a set of potential energies $u_x(z)$, we can calculate $G_x(z)$ from eqn (22) and the volume fraction distributions from eqn (25) through (28). In turn, $u_x(z)$ can be calculated from the volume fraction distributions with eqn (23). A numerical iteration procedure [10] is used to obtain a self-consistent solution under the condition $\sum_i \varphi_i(z) = 1$ for all z. The input parameters are the segment sequences of all the components, a set of χ-values and for all components either the bulk volume fraction φ_i^β or their total number of molecules n_i in the system.

Thermodynamic quantities

Expressions for the grand potential Ω and the chemical potential μ_i have been derived by Evers et al. [10] and Van Lent and Scheutjens [12].

$$\left(\Omega + p^{\beta}V\right)/kT = \sum_z L(z)\left\{-\sum_x \varphi_x(z)u_x(z)/kT - \sum_i \frac{\varphi_i(z)-\varphi_i^{\beta}}{r_i} + \tfrac{1}{2}\sum_x\sum_y \chi_{xy}\left[\varphi_x(z)\left(<\varphi_y(z)> - \varphi_y^{\beta}\right) - \varphi_x^{\beta}\left(\varphi_y(z)-\varphi_y^{\beta}\right)\right]\right\} \qquad (29)$$

The chemical potential μ_i can be written as

$$\left(\mu_i - \mu_i^{*}\right)/kT = \ln\varphi_i^{b} + 1 - r_i\sum_j \frac{\varphi_j^{b}}{r_j} + \tfrac{1}{2}r_i\sum_x\sum_y \chi_{xy}\left(\varphi_{xi}^{*} - \varphi_x^{b}\right)\left(\varphi_y^{b} - \varphi_{yi}^{*}\right) + r_i p^{b}/kT \qquad (30)$$

where the superscript * refers to the pure amorphous phase. The quantity φ_{xi}^{*} is the volume fraction of segments x in pure amorphous component i, which equals the fraction of x segments in the chain. The superscript b refers to phase α or β. As in equilibrium the chemical potential of any component i is the same everywhere, the Laplace pressure difference between the two phases follows from eqn (30) as:

$$\ell^3\left(p^{\alpha} - p^{\beta}\right)/kT = \frac{1}{r_i}\ln\left(\varphi_i^{\alpha}/\varphi_i^{\beta}\right) - \sum_j \frac{\varphi_j^{\alpha} - \varphi_j^{\beta}}{r_j} + \tfrac{1}{2}\sum_x\sum_y \chi_{xy}\left\{\varphi_{xi}^{*}\left(\varphi_y^{\alpha} - \varphi_y^{\beta}\right) - \varphi_x^{\alpha}\left(\varphi_y^{\alpha} - \varphi_{yi}^{*}\right) + \varphi_x^{\beta}\left(\varphi_y^{\beta} - \varphi_{yi}^{*}\right)\right\} \qquad (31)$$

In a lattice model with concentration gradients and segment interactions, the positioning of the lattice relative to the interface affects the Laplace pressure drop. In Appendix A a method is described to avoid this so-called lattice artefact.

Parameters and Methods

General

Poly(oxyethylene) nonionics C_nE_m are modelled as chains with segment sequence $C_n(OCC)_mO$. Linear alcohols are modelled as C_nO and alkanes as C_n. Water molecules are represented as single segments W. Thus, the segment types C, O and W stand for (a group of) atoms which occupy identical volumes. Note that we neither distinguish between -O- and -OH, nor between $-CH_2-$ and $-CH_3$. Moreover, the simplification is made that $-CH_2-$ groups in head groups are chemically equal to those in the tails.

The advantage of these simplifications is that only three interaction parameters are needed, i.e., χ_{cw}, χ_{ow} and χ_{co}. It is known that for these non-ionic surfactants the critical micellization concentration (c.m.c.) is decreased with increasing tail length and increased with increasing head group length. Every additional CH_2 in the tails decreases the CMC by about a factor of 3. Every additional EO group increases the CMC by 10% [13]. Moreover, it is assumed that $\chi_{cw} = \chi_{co}$ in order to restrict the number of parameters to two. This is not a serious restriction since the effects of the tail-head interac-

tions are very small [14]. Values for the remaining χ-parameters are obtained by fitting the dependence of the c.m.c. on the chain length [12]. This procedure yields the value 2.0 for χ_{cw} and χ_{co}. For χ_{ow} the value −1.6 is found, which reflects the strong hydration of the EO chain. These values are used throughout this study, except where stated otherwise. Strictly, the χ-parameters may depend on the volume fractions. This effect is completely disregarded here.

Leermakers and Scheutjens [9, 14] introduced a rotational isomeric state (RIS) scheme into the SCF theory. This scheme accounts for trans-gauche transitions in the chain and forbids back-folding of chain segments. For practical reasons this scheme is not used here. An hexagonal lattice, for which $\lambda_{-\ell}(\infty)=\lambda_{+\ell}(\infty)=3/12$, is used here throughout. Since the RIS scheme generates less flexible chains, we expect our predictions for k_c and $\bar{k}_c$ to be slight underestimations. The trends will be correct, however.

For bilayers our interest is focussed on k_c, on which the influence of chain length, χ-parameters and alcohols is studied. In the monolayer case, the interesting parameter is the spontaneous curvature J_{sp}, on which the effect of concentration and the EO length is analysed.

Bilayers

Cylindrical and spherical vesicles are calculated using the model outlined in the previous section. The normalization factor C_1 in eqn (26) is expressed in terms of the total amount of surfactant (eqn 28). Given a suitable estimate for $u_x(z)$, we iterate toward an volume fraction profile that is consistent with eqn (22)-(28). In figure 1a the

volume fraction profile of a spherical $C_{12}E_7$ vesicle is given. The curves refer to the C_{12}, E_7 and W volume fractions, as is indicated in the figure. The radius of the vesicle is about 20 lattice layers. Because of curvature, the bilayer is slightly asymmetrical. To obtain the interfacial tension γ from eqn (5), we need to define the curvature J of the vesicle, for which we take the reciprocal first moment of the excess surfactant volume fraction:

$$J = \begin{cases} \dfrac{\sum_z L(z)\left(\varphi_{C_nE_m}(z) - \varphi^{\beta}_{C_nE_m}\right)}{\sum_z zL(z)\left(\varphi_{C_nE_m}(z) - \varphi^{\beta}_{C_nE_m}\right)} & \text{(cylinder)} \\ 2\dfrac{\sum_z L(z)\left(\varphi_{C_nE_m}(z) - \varphi^{\beta}_{C_nE_m}\right)}{\sum_z zL(z)\left(\varphi_{C_nE_m}(z) - \varphi^{\beta}_{C_nE_m}\right)} & \text{(sphere)} \end{cases} \qquad (32)$$

Note that in figure 1a for all components the volume fractions in the interior and exterior of the vesicle are the same. This implies that

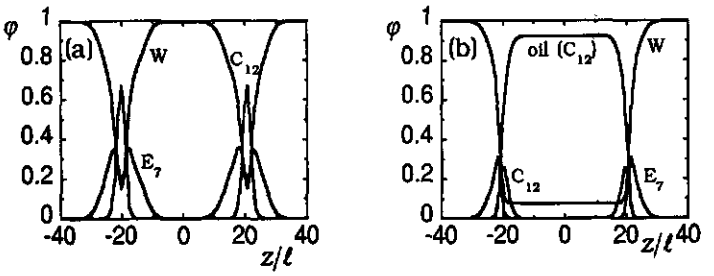

Figure 1. Volume fraction profiles of a spherical vesicle (a) and a spherical monolayer (b). The surfactant is $C_{12}E_7$ and the oil-phase is C_{12}. The number of surfactant molecules in the vesicle and the monolayer are 987 and 366, respectively. The parameters are $\chi_{cw} = \chi_{co} = 2.0$ and $\chi_{ow} = -1.6$.

there is no Laplace pressure drop over the membrane (cf. eqn 31).

Monolayers

In the case of monolayers, the normalization factor C_i in eqn (26) for the oil phase is calculated using the total amount of oil, which ensures the two-phase system to be stable. All other components (surfactant, cosurfactant) are normalized using their bulk solution volume fractions in eqn (27). Figure 1b shows a typical volume fraction profile of $C_{12}E_7$ adsorbed on a spherical oil-water interface, the oil being C_{12}. Again the position of the interface is needed to obtain the interfacial tension. We refer to appendix A for the calculation of γ.

Results and Discussion

I. *Bilayers*

We demonstrate how the bending moduli depend on the chain length of the surfactant, the interaction parameters and the fraction of alcohols in the bilayer. We start our survey by showing the validity of eqn (14). From the huge variety of geometries we selected the cylindrically and spherically shaped interfaces

Figure 2a shows for three different surfactants, $C_{12}E_4$, $C_{12}E_7$ and $C_{12}E_{10}$, the dependence of γ/J on the mean curvature J of cylindrical vesicles. Over a wide range straight lines are observed, which is in agreement with eqn (15). From the slopes k_c/kT values of 1.02,

0.94 and 0.78, respectively, are obtained. For large values of J (small vesicles), k_c is no longer constant because head group interactions in the centre of the vesicle start to develop, which affect γ. Not surprisingly, this effect is more pronounced for longer chain surfactants (see figure 2a). Extrapolation of the data in figure 2a to $J=0$ yields an abscissa of zero, which reflects the zero spontaneous curvature of bilayers. This is due to the symmetry of the flat bilayer [8].

Figure 2b shows, again for the surfactants $C_{12}E_4$, $C_{12}E_7$ and $C_{12}E_{10}$, the corresponding results for spherical vesicles. The curves are in agreement with eqn (16). The initial slope must be equal to $\frac{1}{2}\left(k_c+\frac{1}{2}\bar{k}_c\right)$. With k_c as obtained from the cylindrical vesicles, the values for $\bar{k}_c/kT$ are –1.99, –3.34 and –3.53, respectively.

Chain length

In figure 3 we analyze the effect of the tail and head group lengths on the two bending elasticity parameters of bilayers. These parameters have been obtained by the linearization method used in the

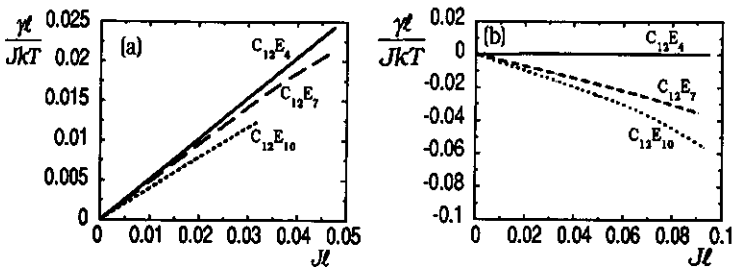

Figure 2. The quantity γ/J as a function of the mean curvature J for (a) cylindrical and (b) spherical vesicles. To obtain J and γ eqn (32) and (5) are used, respectively. The surfactants are $C_{12}E_4$, $C_{12}E_7$ and $C_{12}E_{10}$. The parameters are $\chi_{CW}=\chi_{CO}=2.0$ and $\chi_{OW}=-1.6$.

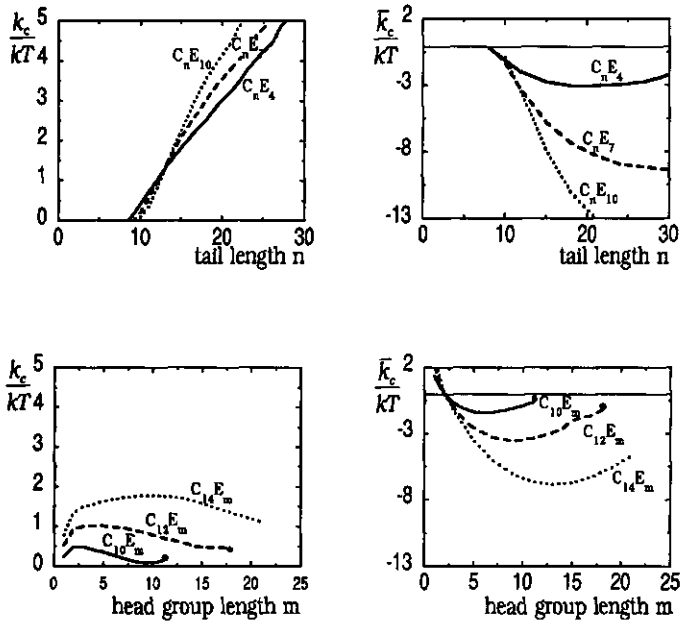

Figure 3. The mean bending modulus, k_c, (a,c) and the Gaußian bending modulus, $\bar{k}_c$, (b,d) as functions of the tail length (a,b) of the surfactants C_nE_4, C_nE_7 and C_nE_{10} and as functions of the head group length (c,d) of the surfactants $C_{10}E_n$, $C_{12}E_n$ and $C_{14}E_n$. The dots in (c) and (d) indicate the maximum head group length for stable membranes. The parameters are $\chi_{cw} = \chi_{co} = 2.0$ and $\chi_{ow} = -1.6$.

discussion of figure 2 above.

Surfactants with longer tails form thicker and more rigid membranes. This effect is shown in figure 3a, where the mean bending modulus, k_c, is plotted as a function of the tail length for three different head group lengths, E_4, E_7 and E_{10}. Essentially, almost straight lines are observed. Szleifer et al. [15] also observed a power-law behaviour, although they found a power of around two instead of one. Note that they assumed a fixed density of short

attached tails, whereas in our model the tails are not attached but part of surfactant molecules of which the density in the bilayer is established by equilibrium conditions. From figure 3a it is seen that, below a certain chain length, k_c vanishes. Below that chain length the hydrophobicity of the surfactant is so low that the membrane dissolves.

The curve for the Gaußian bending modulus, $\bar{k}_c$, shows for the E_4 surfactant a minimum at a tail length of about 20 carbon atoms (figure 3b). The curves for the other surfactants also suggest that a minimum may be present, although at a much higher tail length which is not attained in figure 3b. A decrease in $\bar{k}_c$ promotes saddle-splay configurations of the membrane, which for instance occur in cubic phases. In such an arrangement the energy is increased when either the head group length or the tail length is changed. This implies that there must exist an optimum head group / tail length ratio.

In figure 3c, k_c is plotted as a function of the number of EO units in the surfactant, for three different tail lengths, C_{10}, C_{12} and C_{14}. Two opposing effects are present. On the one hand, extra head group units thicken the membrane which hampers bending. On the other hand, the increasing solubility of the surfactant causes the bilayer to become thinner. At the head groups lengths indicated by the dots in figure 3c and 3d, the solubility of the surfactant is so high that beyond these points the membrane dissolves altogether. The Gaußian bending modulus as a function of the head group length, figure 3d, exhibits the same qualitative behaviour as the tail length dependence

of $\bar{k}_c$ (figure 3b), which underlines the argument for an optimum head group / tail length ratio there given.

Interaction parameters

The effects of χ_{cw}, χ_{co} and χ_{wo} on k_c and $\bar{k}_c$ are shown in figure 4.

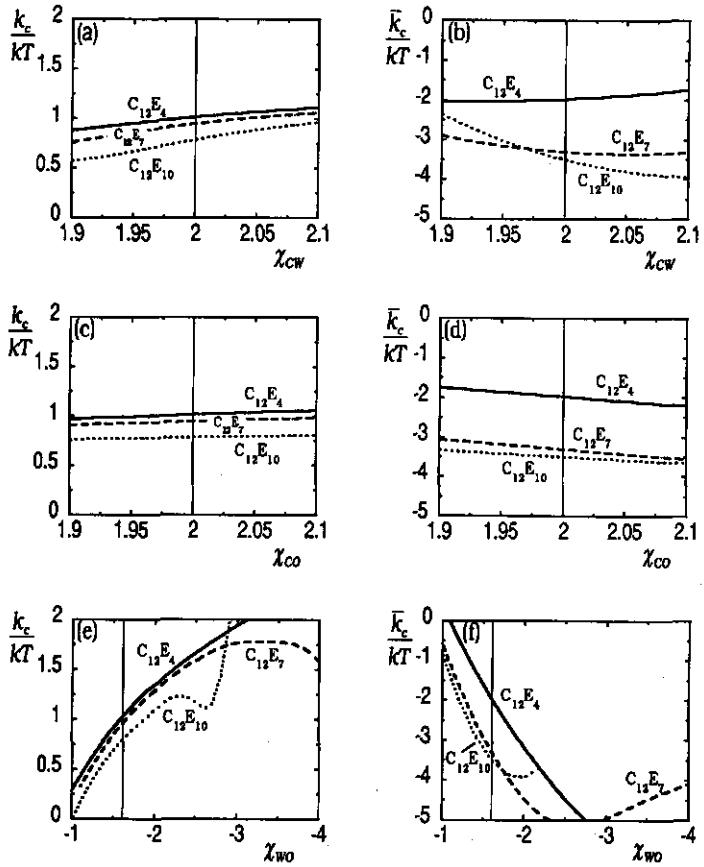

Figure 4. The influence of the interaction parameters χ_{cw} (a,b), χ_{co} (c,d) and χ_{wo} (e,f) on the mean bending modulus, k_c, (a,c,e) and on the Gaußian bending modulus, $\bar{k}_c$, (b,d,f). The standard parameters $\chi_{cw} = \chi_{co} = 2.0$ and $\chi_{ow} = -1.6$ are indicated as vertical lines.

The standard values of the χ parameters are indicated by vertical lines. A higher χ_{cw}, that is more hydrophobic chains, promotes phase separation as well as a denser packing, leading to an increased k_c (see figure 4a). For $\bar{k}_c$ again curves with a minimum are found (figure 4b).

The influence of χ_{co} (figure 4c and 4d) is essentially the same, although less pronounced. The general trend is in agreement with similar results for lipids, where the variation of tail - head group interactions has been investigated [14].

The effect of χ_{wo} on the bending moduli is a bit more complicated (figure 4e and 4f). A more negative χ_{wo} is equivalent to stronger hydration of the EO chains. Consequently the chains and hence the bilayer, become thicker, leading to a larger k_c. However, the chains become more soluble as well, thereby eventually decreasing k_c. For surfactants with longer head groups the resulting maximum is reached at lower χ_{wo} since they are more hydrophilic. For $C_{12}E_{10}$ a surprising effect is observed: k_c increases again at the right hand side of the (local) maximum. In this region the chains are so soluble that a high solution concentration of surfactant is needed for a stable equilibrium membrane. At such high concentrations multilayers start to develop, which explains the sharp increase of k_c. The effect of χ_{wo} on $\bar{k}_c$ is very much similar to the effect of increasing the head group length (compare figure 4f and 3d).

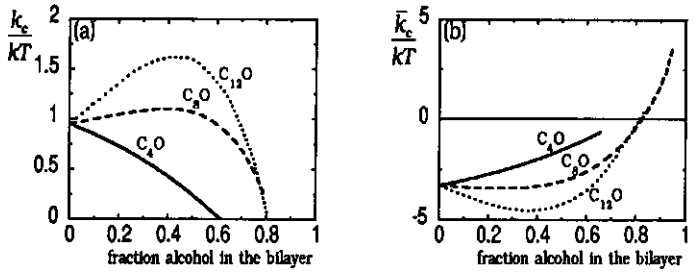

Figure 5. The influence of the fraction of three different alcohols (C_4O, C_8O and $C_{12}O$) in the bilayer on the mean bending modulus, k_c, (a) and on the Gaußian bending modulus, $\bar{k}_c$. (b). The surfactant studied is $C_{12}E_7$. The parameters are $\chi_{cw} = \chi_{co} = 2.0$ and $\chi_{ow} = -1.6$.

Mixed systems

The addition of short chain alcohols to membranes has a dramatic effect on the bending moduli. Depending on the chain length, the membrane becomes more stable or unstable. Some predictions by the present model are shown in figure 5.

In figure 5a values for k_c are presented which are obtained when n-alcohols are incorporated in a $C_{12}E_7$ bilayer. For the shortest alcohol, C_4O, k_c decreases as a function of the mole fraction of alcohol in the bilayer. A similar effect has been predicted by Szleifer et al. with mixtures of attached chains of 12 and 5 segments [15]. The reason is that the alcohol dilutes both the alkane and head group regions in the bilayer, which leads to a thinner bilayer. For the longer alcohols, C_8O and $C_{12}O$, k_c shows a maximum as a function of the mole fraction of alcohol. This can be explained as the result of two opposing effects: an increasing thickness of the tail region and the thinning of the head group region. In the absence of alcohol, lateral surfactant

head group interactions prevent the alkane region in the bilayer to reach its optimum density. When small amounts of a long chain alcohol is added, the head groups are diluted in the same manner as with short alcohols, but the alkane region becomes denser. This results in a thicker bilayer and hence in a higher k_c. Eventually, the optimum density of alkanes is reached so that the alkane region stops growing. As the head groups are still diluted, k_c decreases again. Negative values of k_c do not exist: at high alcohol fractions, the membrane breaks up into micelles.

The behaviour of $\bar{k}_c$, as shown in figure 5b, is qualitatively the same as that of k_c in figure 5a, but now with an opposite sign.

II. *Monolayers*

To obtain bending parameters for nonionic surfactant monolayers,

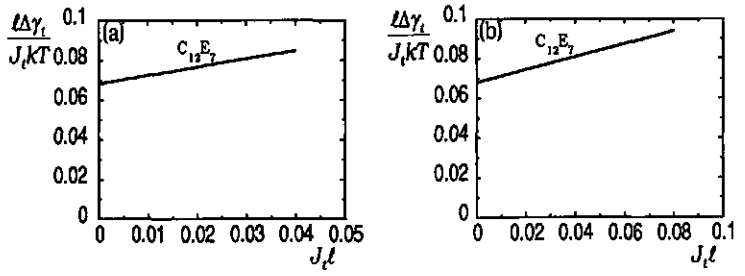

Figure 6. The quantity $(\gamma(J,K)-\gamma(0,0))/J$ *of an oil-water interface as a function of the mean curvature* J_t *at the surface of tension for (a) cylindrical monolayers and (b) spherical monolayers. To obtain* J *and* γ *eqn (3) and (4) are used, respectively. The surfactant is* $C_{12}E_7$ *at a constant surfactant volume fraction* $\varphi^{\beta}_{C_{12}E_7} = 10^{-4}$ *in the water phase (β). The oil phase (α) is* C_{12}*. The interaction parameters are* $\chi_{cw} = \chi_{co} = 2.0$ *and* $\chi_{ow} = -1.6$.

we analyze interfacial tensions of oil-water interfaces. The introduction of an oil phase adds more complexity to the system. Not only the type of oil must be chosen, the concentration of surfactant is now also a variable provided it remains below the c.m.c..

Here we discuss the influence of surfactant concentration and surfactant head group length on the bending elasticity parameters k_c and $\bar{k}_c$ and the spontaneous curvature J_{sp}. Throughout this section the oil phase is C_{12}.

We start by showing how we obtain the bending moduli. Figure 6a presents the dependence of $(\gamma(J_t,0)-\gamma(0,0))/J_t$ on the mean curvature, J_t, of a cylindrical $C_{12}E_7$ monolayer. The volume fraction of surfactant in the water phase, $\varphi^{\beta}_{C_{12}E_7}$, is 10^{-4}. As in figure 2a, a straight line is observed. From the slope a $\bar{k}_c/kT$ value of 0.82 is obtained. The intercept of the line is non-zero, which indicates a non-zero spontaneous curvature which in this case amounts to $J_{sp}\ell = -0.083$ (cf. eqn 15). Figure 6b shows the result for the corresponding spherical monolayer. In agreement with eqn 16, extrapolation of the curve to $J_t = 0$ reveals the same value of $k_c J_{sp}$ as in figure 6a. From the slope of the curve, with k_c as obtained from the cylindrical monolayer, a value of –0.35 is found for $\bar{k}_c/kT$ (cf. eqn 16).

Surfactant concentration

Figure 7 shows the effect of the solution volume fraction in the water phase, φ^{β}, of $C_{12}E_7$ on k_c (a), $\bar{k}_c$ (b) and J_{sp} (c). At very low surfactant volume fractions in the bulk (up to 10^{-7}), k_c is decreased by the surfactant, probably because the solubility of oil in the water

phase increases. Above 10^{-7}, the mean bending modulus increases because the monolayer grows thicker, which explains the concave shape of the curve.

Figure 7b illustrates that for this system the effect of solution volume fraction on $-\bar{k}_c$ is approximately similar as that on k_c.

Figure 7c shows that the spontaneous curvature of an oil-water interface at low surfactant concentrations is close to zero. As the bulk volume fraction rises, J_{sp} increases, which means that the preferred radius of the oil droplet becomes smaller. The sponta

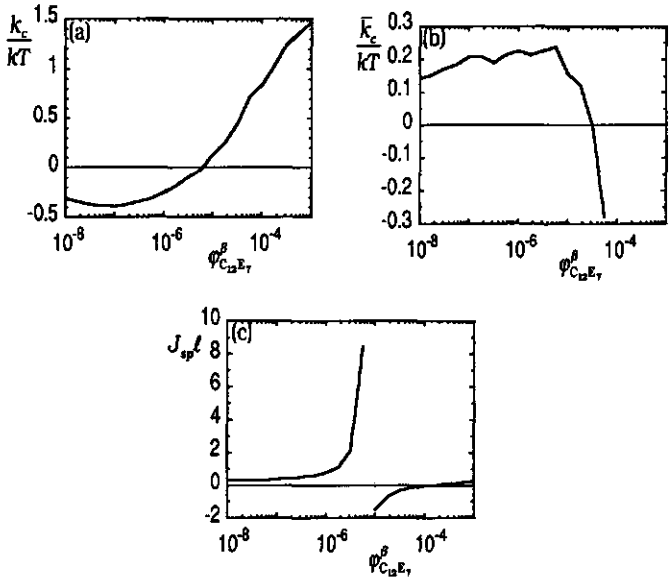

Figure 7. (a) The mean bending modulus, k_c, (b) the Gaußian bending modulus $\bar{k}_c$ and (c) the spontaneous curvature, J_{sp}, as functions of the concentration in the water phase, φ^{β}/r, of the surfactant $C_{12}E_7$. The oil phase is C_{12}. The interaction parameters are $\chi_{cw} = \chi_{co} = 2.0$ and $\chi_{ow} = -1.6$.

neous curvature increases asymptotically to infinite at about $\varphi^{\beta} = 8 \bullet 10^{-6}$, where the sign of J_{sp} changes, i.e., the radius passes through zero and becomes negative, indicating that inversion of the emulsion takes place. At still higher volume fractions, the oil/water interface tends to flatten and, due to strong lateral head group repulsions, at $\varphi^{\beta} \cong 2.2 \bullet 10^{-4}$ the spontaneous curvature changes sign again so that large oil droplets become the preferred structures. Hence, with increasing surfactant concentration, the following range of spontaneous situations is passed: initially there are oil in water droplets becoming smaller, then water in oil droplets growing larger and, eventually, again oil in water droplets of decreasing size.

Head group length

Figure 8 represents the effect of the head group length of $C_{12}E_m$ surfactants on k_c (a), $\bar{k}_c$ (b) and J_{sp} (c). To keep the surfactant concentration (i.e., the number of molecules per volume) in the water phase (β) constant, $\varphi^{\beta}_{C_{12}E_m}$ is fixed at $\left(r_{C_{12}E_m}/r_{C_{12}E_7}\right) \bullet 10^{-4}$. The oil phase is again C_{12}. From figure 8a we learn that the mean bending modulus is hardly affected by changing the head group chain length. The reason is that the thickness of the monolayer is fairly constant: the increase in surfactant length is compensated by a lower adsorption because of the better solubility of the surfactant. Figure 8b shows that the Gaußian bending modulus decreases with increasing head group length, eventually resulting in a destabilization of the droplets.

Figure 8c is interesting since it shows the effect of the head group

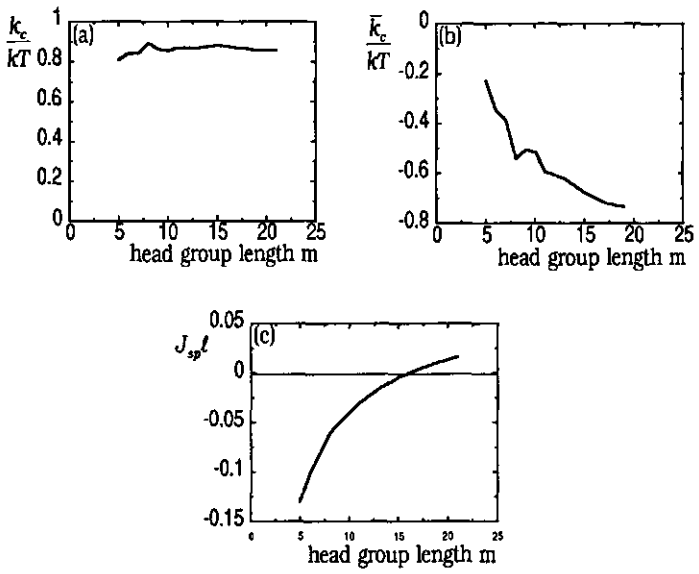

Figure 8. (a) The mean bending modulus, k_c, (b) the Gaußian bending modulus $\bar{k}_c$ and (c) the spontaneous curvature, J_{sp}, as functions of the head group length of the surfactants $C_{12}E_n$. The oil phase is C_{12}. The interaction parameters are $\chi_{cw} = \chi_{co} = 2.0$ and $\chi_{ow} = -1.6$. The volume fraction in the water phase (β) is $\left(r_{C_{12}E_m}/r_{C_{12}E_7}\right) \cdot 10^{-4}$.

length on the spontaneous curvature. As may be concluded from this figure, small head groups promote a water in oil emulsion ($J_{sp} < 0$). Increasing the head group length makes the spontaneous state more flat until at 16 EO units an oil in water emulsion is preferred ($J_{sp} > 0$). Qualitatively, this behaviour explains why the model of Ninham and Israelachvili, which is based on the assumption that the spontaneous curvature is determined by the relative dimensions of the head groups and tails works so well. Essentially, the reason is that the monolayer has a very constant thickness.

Conclusions

Using a self-consistent field lattice model, the curvature elasticity parameters of monolayers and tension-free bilayers of nonionic surfactants are calculated from solution properties of the molecules. The monolayers and bilayers are considered as equilibrium structures of self-assembling molecules. The model provides the grand potential as a function of the surface curvature. The mean bending modulus k_c is extracted from the surface part of the grand potential of cylindrically curved interfaces; the Gaußian bending modulus $\bar{k}_c$ is determined from data for spherical interfaces. The spontaneous curvature J_{sp} is obtained from cylindrical interfaces.

Results are presented for the nonionic surfactant class C_nE_m in water (W) and oil (C_{12}). Only three Flory-Huggins parameters are required, $\chi_{cw} = 2.0$, $\chi_{co} = 2.0$ and $\chi_{wo} = -1.6$. These parameters are obtained from the solubility of alkanes in water and the dependence of the CMC of C_nE_m on the n and m. The effect of varying the interaction parameters on the bending moduli is shown.

The mean bending modulus of bilayers is found to rise linearly with increasing tail length of the surfactant. A minimum length of 10 CH_2 units is necessary for a positive k_c. Shorter surfactants are not able to form stable bilayers. The Gaußian bending modulus $\bar{k}_c$ is negative and its value shows an optimum when plotted as a function of tail length or head group length of the surfactant.

The addition of linear alcohols has a dramatic effect on the bending moduli. Short alcohols increase the flexibility of the bilayer, whereas long alcohols lead to a higher rigidity.

The rigidity of a monolayer at an oil-water interface depends on the concentration of the surfactant. The spontaneous curvature of a $C_{12}E_7$ monolayer is predicted to promote the stability of emulsions at low and high surfactant concentrations and water in oil emulsions at intermediate concentrations.

Appendix A. Avoiding Artefacts Due To The Location Of The Lattice

Monolayers

The using of a lattice entails the possibility of a typical artefact This may be illustrated by considering an oil-water interface. The problem volume fraction profiles in figures A1a and A1b are shifted with

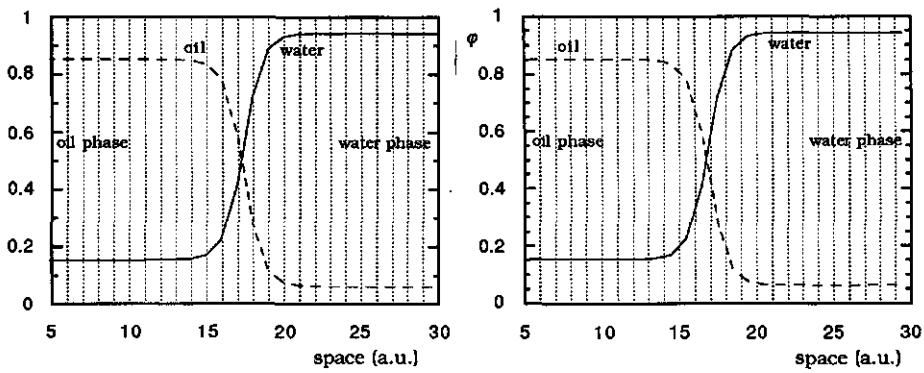

Figure A1 (a) Concentration profiles of an oil-water interface. (b) The same interface, but shifted half a lattice layer to the left. The discretization by the lattice affects slightly the form of the concentration profile and hence the grand potential.

respect to one another by half a lattice layer. Ideally, the volume fractions in the corresponding phases should be independent of the position of the lattice, because these are thermodynamic characteristics of the system (otherwise at least Kelvin's law should be applicable).

Due to the assumption of constant density within each lattice layer, a small shift Δm of the position of the lattice affects some quantities, including $u(z)$ nonlinearly (see eqn 23). The monolayer or bilayer may slightly contract or expand. As a result, when the lattice is shifted the surface free energy is modulated by a periodic deviation of wavelength ℓ. The monolayer or bilayer simultaneously tries to keep its optimal position with respect to the lattice. In other words, the lattice adds an extra surface tension $\gamma_{lattice}$ to the interface which causes a spurious pressure drop, $\Delta p_{lattice}$, over the interface:

$$\Delta p = \Delta p_{Laplace} + \Delta p_{lattice} = \gamma J + \partial \gamma_{lattice} / \partial m \tag{A6}$$

This, in turn, affects the apparent interfacial tension, via eqn (2) and, hence the bending moduli. Our goal is to provide a means to eliminate $\Delta p_{lattice}$. Equation (31) now becomes:

$$\ell^3 \left(\Delta p_{Laplace} + \Delta p_{Lattice}\right)/kT = \frac{1}{r_i}\ln\left(\varphi_i^{\alpha}/\varphi_i^{\beta}\right) - \sum_j \frac{\varphi_j^{\alpha} - \varphi_j^{\beta}}{r_j} + \tfrac{1}{2}\sum_x \sum_y \varphi_{xi}^{\bullet}\left(\varphi_y^{\alpha} - \varphi_y^{\beta}\right) - \varphi_x^{\alpha}\left(\varphi_y^{\alpha} - \varphi_{yi}^{\bullet}\right) + \varphi_x^{\beta}\left(\varphi_y^{\beta} - \varphi_{yi}^{\bullet}\right) \tag{A7}$$

With a preassigned value for the Laplace pressure, we shift the lattice position until $\Delta p_{lattice} = 0$, by changing the amount of oil in the

system. The preassigned value for $\Delta p_{Laplace}$ is determined by the desired curvature J_t. For a planar surface $\Delta p_{Laplace}$ is zero. The elimination of the pressure drop due to the lattice ensures a correct value for $\gamma(0,0)$, which is needed in eqn (14). Then, in curved systems, $\gamma(0,0)$ can be used to obtain the preassigned value for $\Delta p_{Laplace}$.

$$\Delta p_{Laplace} = \gamma_t J_t \cong \gamma(0,0) J_t \tag{A8}$$

Note that, after the elimination of the pressure drop due to the lattice, the curvature of the interface is close to the desired value of J_t, but not completely equal because the interfacial tension is a function of the curvature (which essentially is the basis for the existence of bending moduli).

Bilayers

As the bilayer is permeable to water, there is no Laplace pressure and an additional pressure due to the position of the permeable bilayer cannot build up. For this situation eqn (2) can be rewritten as:

$$\Omega = -p_{lattice} V^{\alpha+\beta} + \gamma A_s \tag{A9}$$

As there is no Laplace pressure, $\gamma_t J_t = 0$ and because of eqn (3) and (4), the curvature and the interfacial tension *at the surface of tension* are both zero. We then may apply the mechanical definition of the interfacial tension: $\gamma_t = -\int_z p_T(z) dz$, where p_T is the tangential component of the pressure tensor, which amounts to (cf. eqn (29)):

$$\gamma_t/kT = \sum_x \varphi_x(z) u_x(z)/kT + \sum_t \frac{\varphi_t(z) - \varphi_t^\beta}{r_t}$$
$$-\tfrac{1}{2}\sum_x \sum_y \chi_{xy}\left[\varphi_x(z)\left(<\varphi_y(z)> - \varphi_y^\beta\right) - \varphi_x^\beta\left(\varphi_y(z) - \varphi_y^\beta\right)\right] \qquad \text{(A10)}$$

In the calculations, the amount of surfactant is adjusted to fulfil $\gamma_t = 0$. This warrants $\Delta p_{lattice} = 0$ so that the grand potential Ω ($= \gamma A_s$, cf. eqn A9) can be obtained from eqn (29).

References

1 D. J. Mitchell and B. W. Ninham, J. Chem. Soc. Faraday Trans. 2, 77 (1981) 601.

2 W. Helfrich, Z. Naturforsch., 33a (1978) 305.

3 J. Meunier, J. Phys. Lett., 46 (1985) L-1005.

4 C. R. Safinya, D. Roux, G. S. Smith, S. K. Sinha, P. Dimon, N. A. Clark and A. M. Bellocq, Phys. Rev. Lett., 57 (1986) 2718.

5 P. Bassereau, J. Marignan and G. Porte, J. Phys., 48 (1987) 673.

6 J. M. H. M. Scheutjens and G. J. Fleer, J. Phys. Chem., 83 (1979) 1619.

7 C. E. Reid, Chemical Thermodynamics, McGraw-Hill Publishing Company, New York, 1990.

8 W. Helfrich, Z. Naturforsch., 28c (1973) 693.

9 F. A. M. Leermakers and J. M. H. M. Scheutjens, J. Phys. Chem., 93 (1989) 7417.

10 O. A. Evers, J. M. H. M. Scheutjens and G. J. Fleer, Macromolecules, 23 (1990) 5221.

11 Flory, Principles of Polymer Chemistry, Cornell University Press, Ithaca, NY, 1953.

12 B. van Lent and J. M. H. M. Scheutjens, Macromolecules, 22 (1989) 1931.

13 The effects of polyoxyethylene chain length distribution on the interface properties of polyoxyethylenated n-dodecyl alcohols, X. Jiding and H. Zhenyn (Ed.), (1986).

14 F. A. M. Leermakers and J. M. H. M. Scheutjens, J. Chem. Phys., 89 (1988) 3264.

15 I. Szleifer, D. Kramer, A. Ben-Shaul, D. Roux and W. M. Gelbart, Phys. Rev. Lett., 60 (1988) 1966.

CHAPTER 5

Bending Moduli and Spontaneous Curvature II. Bilayers and Monolayers of Pure and Mixed Ionic Surfactants

Abstract

Bending elasticity moduli of equilibrium bilayers and monolayers of surfactants are calculated using a self-consistent field lattice model. The model is extended by incorporating ionic interactions at curved interfaces, so that ionic surfactants can be treated as well. The interfaces are formed by self-assembling of the surfactants. It is found that the size of the counter ions is an important parameter in determining to the bending moduli of charged interfaces. Screening the electric double layer by salt has two opposing effects on the rigidity of monolayers and bilayers of ionic surfactants. The contribution of the double layer diminishes but, more importantly, the surfactant layer becomes thicker. Hence, the surfactant layers are more rigid in higher salt concentrations. In the case that salt ions decrease the solvent quality, as salting-out ions do, the rigidity of the layer passes through a maximum in high salt concentrations (c. 1 kmole/m^3).

Introduction

A fluid interface is the seat of an elastic free energy of bending A^c, for which Helfrich wrote [1]:

$$A^c/A_s = \tfrac{1}{2}k_c\left(J - J_{sp}\right)^2 + \bar{k}_c K \qquad (1)$$

In this equation, A_s is the area of the interface, J and K are the mean and Gaußian curvature defined through the principal curvatures c_1 and c_2 as $c_1 + c_2$ and $c_1 c_2$, respectively. Similarly, k_c is called the mean bending modulus and $\bar{k}_c$ the Gaußian bending modulus. The spontaneous curvature J_{sp} defines the situation where the elastic free energy of bending is minimal. In Helfrich's approach the contribution of a spontaneous Gaußian curvature, K_{sp}, is neglected.

The parameters k_c, $\bar{k}_c$ and J_{sp} play important roles in the physics of curved surfactant layers, which occur, for example, in vesicles and microemulsions. Also in planar layers, bending elasticity parameters can be important due to their role in thermally induced undulations of the interface [2]. Examples of such systems are a surfactant monolayer in a Langmuir trough and macroscopic free liquid films. Hence it is desirable to know the bending parameters for various systems.

Experimentally, the bending elasticity parameters are hard to determine. Nevertheless, several techniques have been applied to a variety of systems. Without being complete, we mention an ESR study on microemulsions by di Meglio et al. [3], an ellipsometry study on surfactant monolayers by Meunier [4] and an X-ray study on lamellar phases by Safinya et al. [5].

Theoretically, statistical thermodynamic approaches have been used to predict the rigidity of interfaces. The bending elasticity parameters can be related to the curvature dependence of the interfacial tension [6, 7]. Szleifer et al. investigated the influence of the length of short uncharged end-grafted chain molecules, also in the

presence of shorter chains (alcohols), using the statistical thermodynamic model of Ben-Shaul [8]. Milner and Witten have developed an analytical self-consistent field lattice model valid for high densities of end grafted long chains [9]. Both groups disregarded the head groups of the surfactants. Barneveld used the self-consistent field lattice lattice approach of Scheutjens and Fleer to study curvature elasticity parameters of full equilibrium bilayers and monolayers of poly (oxyethylene) surfactants [7].

Systems containing ionic surfactants, however, involve electrical double layer phenomena. Wintherhalter and Helfrich [10] and Lekkerkerker [11] investigated the influence of the double layer on the bending parameters k_c and $\bar{k}_c$ using the Debye-Hückel and Poisson-Boltzmann equations, respectively. They considered solid particles at different radii with constant surface charge density. The excluded volumes of surfactant and ions were neglected.

It is the aim of the present study to calculate the bending elasticity parameters for a more realistic situation, i.e., in which all molecules, including the small ions, have finite volumes and where self-assembling ionic surfactants form monolayers or bilayers in equilibrium with free surfactants in the solution. Consequently, the charge of the surfactant layer is not fixed but depends on parameters such as the ionic strength of the system. The results are compared with those for uncharged surfactants of the same size and for charged layers without surfactant.

In the following section we briefly review the relations between bending parameters and thermodynamic quantities. We proceed with a section on the self-consistent field lattice model that we use to

calculate the thermodynamic quantities and that we extend to charged interfaces with curvature. Following a discussion on the parameters used, the section on Results and Discussion presents calculations on charged solid interfaces, surfactant bilayers and monolayers.

Bending elasticity parameters

Aggregation of ionic surfactants introduces an inhomogeneous charge density distribution in and around the aggregate. Since no charges are introduced from the surroundings, no electrostatic work is performed by the system. Hence, the change in the interfacial grand potential (interfacial grand canonical characteristic function), Ω^s, as given in reference [7], can also be used to find expressions for the bending elasticity parameters in the case of systems with charged interfaces:

$$d\Omega^s = S^s dT - \sum_i n_i^s d\mu_i + \gamma dA_s + A_s C_1 dJ + A_s C_2 dK \qquad (2)$$

where T is the temperature, S the entropy, μ the chemical potential and n the number of molecules. The subscript i denotes any component in the system and the superscript s refers to the interfacial part of the quantity. The coefficients A_sC_1 and A_sC_2 are referred to as the first and second bending moment, respectively [12].

The curvature elasticity energy, A^c, per surface area, as given in eqn (1), is essentially the excess interfacial tension due to bending with respect to the spontaneous curvature J_{sp}, i.e.,

$A^c/A_s = \gamma(J,K) - \gamma(J_{sp},K_{sp})$, where in Helfrich's equation, eqn (1), $K_{sp} = 0$.

The interfacial tension can be expanded in the same way as in our previous work [7], where ionic surfactants were not considered. Combining eqn (2) and the integrated form of this equation, $\Omega^s = \gamma A_s$, we arrive at the following Gibbs-Duhem type relation:

$$d\gamma = -s^s\,dT - \sum_i \Gamma_i\,d\mu_i + C_1\,dJ + C_2\,dK \tag{3}$$

where s^s is the interfacial entropy per unit area and Γ_i is the adsorbed amount per unit area. At constant T and $\{\mu_i\}$, γ is a function of J and K and can be expanded, e.g., in a Taylor series around the point where the interfacial tension is at a minimum, i.e., where the interface is in the spontaneous state (J_{sp},K_{sp}). Retaining terms up to second order, we obtain:

$$\begin{aligned}&\gamma(J,K) - \gamma(J_{sp},K_{sp}) = \\ &\tfrac{1}{2}E_{JJ}\left(J - J_{sp}\right)^2 + \tfrac{1}{2}E_{KK}\left(K - K_{sp}\right)^2 + E_{JK}\left(J - J_{sp}\right)\left(K - K_{sp}\right)\end{aligned} \tag{4}$$

The elasticity parameters, $E_{ab} \equiv \dfrac{\partial^2\gamma}{\partial a\,\partial b}$, are given by:

$$\begin{aligned}E_{JJ} &= \frac{\partial C_1}{\partial J} \\ E_{KK} &= \frac{\partial C_2}{\partial K} \\ E_{JK} &= \frac{\partial C_1}{\partial K} = \frac{\partial C_2}{\partial J}\end{aligned} \tag{5}$$

For a cylindrical system ($K=0$) of which the interfacial tension as a function of curvature J is known, E_{JJ} can be calculated using eqn (4). If for that system E_{JK} can be neglected, the spontaneous mean curvature J_{sp} can also be calculated. The elasticity E_{JJ} coincides with Helfrich's k_c, occurring in eqn (1). With the results of a spherical interface ($K=J^2/4$), E_{KK} and K_{sp} can be retrieved. Note that Helfrich's parameter $\bar{k}_c$, which equals $C_2(0,0)=-\left(E_{KK}K_{sp}+E_{JK}J_{sp}\right)$ (cf. eqn 1, 3 and 4) can be obtained from a planar interface (see ref. [12], eqn 40).

In the next section, a lattice model is presented which allows for the calculation of the interfacial tension of ionic monolayers and bilayers. Essentially, we extend the self-consistent field lattice theory of curved nonionic monolayers and bilayers as described in our previous paper [7] by incorporating electrostatic interactions, using the method developed by Böhmer et al. [13] but modified for curved surfaces. The equations are solved by a newer and simpler iteration scheme, see the Appendix.

Self-consistent field lattice theory

The model is based on a lattice. The lattice can be either flat, cylindrical or spherical. Each chain segment, solvent molecule or (hydrated) ion occupies one lattice site. All sites have equal volume. Inhomogeneities are allowed in only one dimension z, which leads to the concept of lattice layers of constant segment volume fraction. A

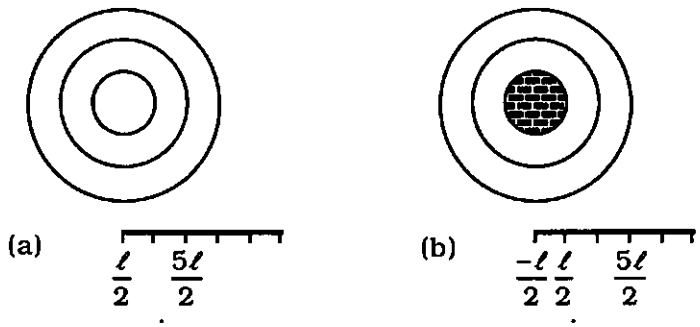

Figure 1. Definition of the lattice layers. The first available layer is layer ℓ. In situation (a) all layers are available for molecules ($z_0 = \ell/2$). In situation (b) a solid core of radius ℓ is inaccessible for molecules ($z_0 = -\ell/2$).

lattice layer extends from $z-\ell/2$ to $z+\ell/2$, where ℓ is the thickness of a layer. For convenience, the layers are numbered from $z=\ell$ up to M, where conventionally layer ℓ is the innermost layer and layer M is in bulk solution. The centre of the lattice, z_0, is located at $z_0 = \ell/2 - R$, where R is the radius of an optional solid core. This is illustrated in figure 1. The area and volume of the lattice up to layer z are given by:

$$A_s(z+\frac{\ell}{2}) = \begin{cases} L/\ell & \text{planar} \\ 2\pi h\left(z+\frac{\ell}{2}-z_0\right) & \text{cylindrical} \\ 4\pi\left(z+\frac{\ell}{2}-z_0\right)^2 & \text{spherical} \end{cases} \qquad (6)$$

and

$$V(z+\frac{\ell}{2})=\begin{cases} L\left(z+\frac{\ell}{2}-z_0\right)\Big/\ell & \text{planar} \\ \pi h\left(z+\frac{\ell}{2}-z_0\right)^2 & \text{cylindrical} \\ \frac{4}{3}\pi\left(z+\frac{\ell}{2}-z_0\right)^3 & \text{spherical} \end{cases} \tag{7}$$

respectively. In these equations, h is the length of the cylinder and L the volume of layer z. The latter quantity simply given by:

$$L(z)=V(z+\ell/2)-V(z-\ell/2) \tag{8}$$

The a priory probability to go from a given layer z to an adjoining layer z' is given by $\lambda_{z'-z}(z)$ and is dictated by the geometry of the lattice. In the case of a curved lattice these probabilities can be calculated from the planar ones [14], i.e. the λ's at $z\to\infty$:

$$\begin{aligned} \lambda_{-\ell}(z)&=\frac{\ell A_s(z-\ell/2)}{L(z)}\lambda_{-\ell}(\infty), \\ \lambda_{+\ell}(z)&=\frac{\ell A_s(z+\ell/2)}{L(z)}\lambda_{+\ell}(\infty), \\ \lambda_0(z)&=1-\lambda_{-\ell}(z)-\lambda_{+\ell}(z) \end{aligned} \tag{9}$$

Chain statistics

We consider linear molecules as chains of segments. Each segment has the same size, but can be of different chemical nature. For a segment of type x, irrespective to which chain it belongs, the potential energy in layer z relative to bulk solution (phase β) is $u_x(z)$. The distribution of a free (detached) segment x, e.g., a solvent molecule or small ion, is given by its Boltzmann factor $G_x(z)$, defined as

$$G_x(z) = e^{-u_x(z)/kT} \tag{10}$$

where k is Boltzmann's constant. Generally, $u_x(z)$ depends on all possible interactions of segment x with its environment. Here, we take into account the excluded volume effect, nearest neighbour interactions and electrostatic interactions:

$$u_x(z) = u'(z) + kT\sum_y \chi_{xy}\left[<\varphi_y(z)> - \varphi_y^\beta\right] + ev_x\left(\psi(z) - \psi^\beta\right) \tag{11}$$

where φ is the volume fraction, χ the Flory-Huggins parameter, v the valency of a segment, ψ the electrostatic potential and e the elementary charge. The subscripts x and y refer to any segment type A,B,C,... in the system and the superscript β indicates the bulk solution. The angular brackets, <>, indicate averaging of φ over the neighbouring cells of a site in layer z. This involves three consecutive layers, $z-\ell$, z and $z+\ell$:

$$<\varphi(z)> = \lambda_{-\ell}(z)\varphi(z-\ell) + \lambda_0(z)\varphi(z) + \lambda_{+\ell}(z)\varphi(z+\ell) \tag{12}$$

The excluded volume term in eqn (11), $u'(z)$, is a Lagrange parameter which is chosen such that $\sum_x \varphi_x(z)=1$ for all z.

To find the volume fraction profile $\varphi_i(z,s)$ of a particular segment s in chains of type i, we define end segment distribution functions $G_i(z,s|1)$. These functions describe the average Boltzmann weight of all conformations of a chain of s segments long with segment s in layer z. The functions are evaluated by step-weighted walks along the contour of chains i, starting with the distribution of a (detached) segment 1 and finishing after s-1 steps at segment s in layer z. Each step generates the distribution of the end segment of a chain from that of a chain which is one segment shorter, according to the recurrence equation.

$$G_i(z,s|1)=G_i(z,s|s)<G_i(z,s-1|1)> \tag{13}$$

In this equation, the angular brackets represent an average of $G_i(z,s-1|1)$ over three layers, in the same fashion as φ in eqn (12). The weight of segment s in layer z, $G_i(z,s|s)$, equals $G_x(z)$ when segment s is of type x. The sequence starts with $G_i(z,1|1)$. A similar end segment distribution function, $G_i(z,s|r)$, is calculated by starting the sequence at the other end of the chain (segment r). Now, $\varphi_i(z,s)$ can be evaluated from

$$\varphi_i(z,s)=C_i\frac{G_i(z,s|1)G_i(z,s|r)}{G_i(z,s|s)} \tag{14}$$

which combines the two chain ends at segment s in layer z. The division by $G_i(z,s|s)$ corrects for double counting of the statistical weight of segment s. The normalization factor C_i can be achieved from the equilibrium volume fraction φ_i^β in the bulk solution. Since in bulk solution all end segment distribution functions are unity, $\varphi_i^\beta = \sum_s \varphi_i^\beta(s) = r_i C_i$, or:

$$C_i = \varphi_i^\beta / r_i \tag{15}$$

Alternatively, C_i can be related to the total number of chains n_i in the system:

$$C_i = \frac{n_i}{\sum_z L(z) G_i(z,r|1)} \tag{16}$$

because the number of any segment s of chains i equals n_i and the total statistical weight of end segment r in chains i is $\sum_z L(z) G_i(z,r|1)$.

For a given initial guess of $\{u_x(z)\}$ we calculate $\varphi_i(z,s)$ and hence the volume fraction profile of each moiety in the system from eqn (10) and (13)-(16). With the volume fraction profiles we check $u_x(z)$ using eqn (11) and the boundary condition $\sum_x \varphi_x(z) = 1$ for all z. The values of $\{u_x(z)\}$ are changed and the calculation is repeated until a self-consistent solution is found. In the Appendix more details on the numerical method is given. When evaluating eqn (11) the electrostatic potential profile should be known. Its evaluation from the volume fraction profiles is discussed below.

Electrostatic potential profile

The electrostatic potential $\psi(z)$ in eqn (11) can be calculated from the volume fraction profiles of the charged species. Each segment of type x has a valency v_x and a dielectric constant ε_x. The charge distribution $q(z)$ and the permittivity profile $\varepsilon(z)$ can readily be obtained from the volume fraction profile:

$$q(z) = eL(z)\sum_x v_x \varphi_x(z) \tag{17}$$

and

$$\varepsilon(z) = \sum_x \varepsilon_x \varphi_x(z) \tag{18}$$

respectively. In this model, the charge $q(z)$ is assumed to be located on the planes in the centre of each layer z, forming a multi-plate capacitor of the same geometry as the lattice.

The contribution of any charged plate in the system to the electrostatic field $E(z)$, can be obtained from Gauß' law $\oint E dA_s = q/\varepsilon$. Since $E = -\nabla\psi$, this enables us to express the electrostatic potential in layer z in terms of the local charge and the electric potentials in the adjacent layers:

$$\psi(z) = \frac{C(z-\ell,z)\psi(z-\ell) + q(z) + C(z,z+\ell)\psi(z+\ell)}{C(z-\ell,z) + C(z,z+\ell)} \tag{19}$$

where $C(z,z+\ell)$ is the capacity of the system formed by the plates at z and $z+\ell$, while the dielectric permittivity changes at $z+\ell/2$ and is given by:

$$C^{-1}(z,z+\ell)=\frac{D(z,z+\ell/2)}{A_s(z)\varepsilon(z)}+\frac{D(z+\ell/2,z+\ell)}{A_s(z+\ell/2)\varepsilon(z+\ell)} \tag{20}$$

In this equation, the equivalent planar thickness $D(z,z+\ell/2)$ of the dielectric of half a lattice layer is defined by the integral $A_s(z)\int_z^{z+\ell/2} dz'/A_s(z')$, i.e.,

$$D(z,z+\ell/2)=\begin{cases}\ell/2 & \text{planar}\\ (z-z_0)\ln\left(\dfrac{z+\ell/2-z_0}{z-z_0}\right) & \text{cylindrical}\\ \dfrac{(z-z_0)\ell/2}{z-z_0+\ell/2} & \text{spherical}\end{cases} \tag{21}$$

With proper boundary conditions, e.g., $\psi(0)=\psi(1)$, $\psi^{\beta}=0$ and the electroneutrality condition $\sum_z q(z)=0$, the potential profile is obtained from eqn (19). During the iterations of the potential energy profile $u(z)$, the neutrality condition is hard to obey. Böhmer et al. have developed an iteration scheme to satisfy electroneutrality [13]. In the Appendix, we propose a simpler method which does not require that the neutrality condition is continually met during the

iterations but nevertheless guaranties that in the final numerical solution the system is neutral.

Thermodynamic parameters

Expressions for the chemical potential μ_i of component i:

$$\left(\mu_i - \mu_i^*\right)/kT = \ln\phi_i^b + 1 - r_i\sum_j \frac{\phi_j^b}{r_j} + \tfrac{1}{2}r_i\sum_x\sum_y \chi_{xy}\left(\phi_{xi}^* - \phi_x^b\right)\left(\phi_y^b - \phi_{yi}^*\right) + r_i p^b/kT + ev_i\psi^b/kT \qquad (22)$$

and the interfacial tension γ:

$$\begin{aligned}\gamma A_s &= p^\alpha V^\alpha + p^\beta V^\beta \\ &-kT\sum_z L(z)\sum_x \varphi_x(z)u_x(z) - kT\sum_z L(z)\sum_i \frac{\varphi_i(z)-\varphi_i^\beta}{r_i} \\ &+\tfrac{1}{2}kT\sum_z L(z)\sum_x\sum_y \chi_{xy}\left[\varphi_x(z)\left(<\varphi_y(z)> - \varphi_y^\beta\right) - \varphi_x^\beta\left(\varphi_y(z)-\varphi_y^\beta\right)\right] \\ &+\tfrac{1}{2}kT\sum_z q(z)\left(\psi(z)-\psi^\beta\right)\end{aligned} \qquad (23)$$

have been derived by Evers [15], Leermakers [14] and Böhmer [13]. In eqn (22), the superscript * denotes the reference state of unmixed components. The quantity φ_{xi}^* is the volume fraction of segments x in pure amorphous component i, which equals the fraction of x segments in the chain.

As the volume fractions and the electric potentials are known everywhere in the system, the Laplace pressure $p^\beta - p^\alpha$ can be calculated by applying eqn (22) twice, i.e., substitute for b first phase α and then β and taking the difference. Eqn (23) is then used to obtain γ, which is needed to calculate the bending elasticity parameters

(eqn 4). Some caution has to be exercised to avoid artificial influences of the lattice on the results [7].

Parameters

We represent a dodecyl sulfate molecule by the segment sequence $C_{12}B_3$, where C stands for either a -CH_2- or the terminal -CH_3 group and B_3 represents the large sulfate head group. The B segments have a valency ν_B of −1/3, i.e., the total valency of a surfactant molecule is −1.

The nonionic surfactant $C_{12}E_7$ is represented by the segment sequence $C_{12}(OCC)_7O$, where O stands either for an -O- or the terminal -OH group.

The solvent consists of monomers W (water). The following Flory-Huggins interaction parameters are used: $\chi_{CW} = \chi_{CO} = 2.0$, $\chi_{WO} = -1.6$ [7] and $\chi_{CB} = 2.0$, $\chi_{BO} = \chi_{WB} = 0$ [16].

The ionic strength of the solution is determined by two monomer types with valency +1 and −1, respectively. Except for their charge, the electrolyte ions are identical to the solvent monomers W, i.e., they have the same size and the same chemical interactions (χ-parameters) with the surfactant moieties as water (W).

In all calculations we have used a hexagonal lattice, for which $\lambda_{-\ell}(\infty) = \lambda_{-\ell}(\infty) = 1/4$ and $\lambda_{0\ell}(\infty) = 1/2$.

Results and Discussion

I. *Charged Particles*

We start with a very simple system consisting of hard cylindrical rods of various radii in an 1-1 electrolyte solution. All three types of molecules (solvent and the two ions) have the volume of one lattice site. In addition, all χ-parameters are zero. The cylinders have a fixed surface charge density of 0.15 Cm^{-2} (arbitrary chosen). In figure 2 the quantity $(\gamma(J,0)-\gamma(0,0))/J$ versus J is shown for three

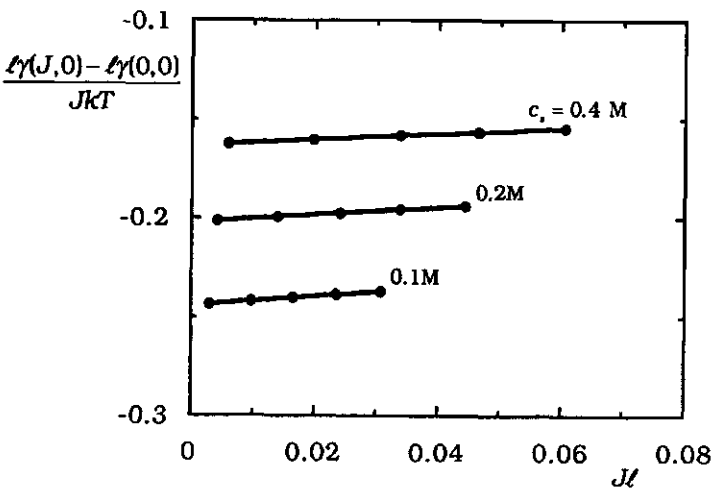

Figure 2. The contribution of the liquid to the interfacial tension of cylindrical solid rods as a function of the surface curvature J. The slope of each curve equals $\frac{1}{2}k_c/kT$ (cf. eqn 4). The surface charge density is 0.15 Cm^{-2}. The diameter of the small molecules is 0.3 nm. All χ-parameters are zero. The ionic strength of the solution is indicated.

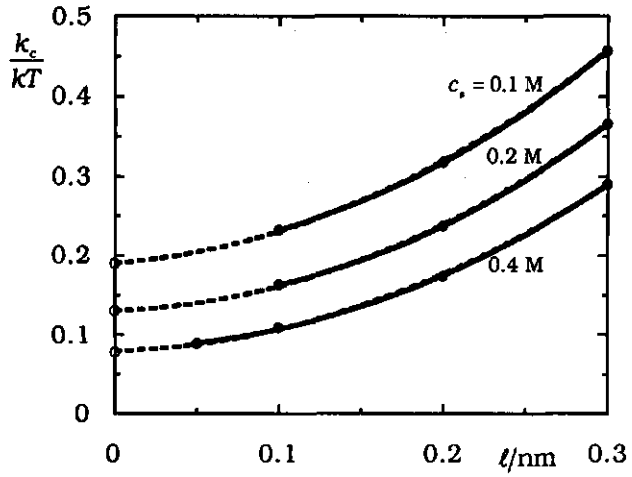

Figure 3. The mean bending modulus, k_c, of a charged surface in various electrolyte solutions as a function of the diameter of the ions, represented by the lattice layer thickness ℓ. The surface charge density is 0.15 Cm^{-2} and all χ-parameters are zero. The curves are extrapolated (dashed parts) to the Poisson Boltzmann limit (open circles), where the ions are point charges.

different electrolyte concentrations. Here, the diameter of the ions is the same as ℓ and equal to 0.3 nm. By applying eqn (4), k_c/kT is easily obtained from the slope of the curves. This amounts to 0.457, 0.366 and 0.290 in 0.1 M, 0.2 M and 0.4 M electrolyte solutions, respectively ($k_c = E_{JJ}$).

In figure 3, k_c is plotted versus the diameter of the ions (i.e., the lattice spacing ℓ) for three different electrolyte concentrations. The limiting values of k_c for $\ell \to 0$ must equal the values, which are indicated by open symbols on the k_c axis, as obtained by Lekkerkerker

[11] using the Poisson-Boltzmann approach. The bending elasticity modulus increases strongly with ℓ. For ions with a diameter of 0.3 nm, k_c is more than a factor of 2 larger than for point charges.

II. Bilayers

In this section, we show the dependence of the bending parameters k_c and $\bar{k}_c$ of ionic surfactant bilayers on the ionic strength of the solution. Effects of chain length and Flory-Huggins interaction parameters of nonionic surfactants have been extensively discussed in our previous paper [7]. Here, we focus on one ionic surfactant, sodium dodecyl sulfate (SDS), mixed with the nonionic surfactant $C_{12}E_7$.

The procedure to obtain the bending parameters from a plot of $\gamma\ell/JkT$ vs. $J\ell$ (cf. eqn 4) is the same as in our previous work [7] and is therefore not repeated here. Like in the nonionic case, bilayers of ionic surfactants are symmetrical and consequently, their spontaneous mean curvature is zero.

The stability of monolayers and bilayers depends on the values of k_c and $\bar{k}_c$. The total elastic free energy of bending (eqn 1) should be positive. If $\bar{k}_c$ is negative, as in most cases, k_c has to be positive. For spheres ($K = J^2/4$), the relevant parameter is $k_c + \bar{k}_c/2$. Negative values for this parameter characterize unstable aggregates, whereas positive values pertain to stable aggregates.

Figure 4 shows the bending moduli k_c and $\bar{k}_c$ of SDS bilayers mixed with 0, 10 or 20% $C_{12}E_7$ in the bilayer. In figure 4a, the mean bending modulus k_c appears to increase with increasing electrolyte

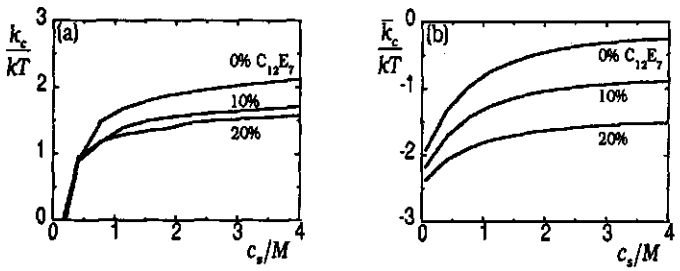

Figure 4. Mean (a) and Gaußian (b) bending elasticity moduli of bilayers of ionic surfactant $C_{12}B_3$ and 0, 10 or 20% nonionic surfactant $C_{12}E_7$ in the bilayer as a function of salt concentration. Parameters: see text.

concentration. This is in contrast to what is to be expected from the Poisson-Boltzmann analysis of Lekkerkerker [11]. The explanation must be sought in the difference in assumptions made in the two models. Lekkerkerker neglects the thickness of the interface. In our model, a bilayer of finite thickness is built spontaneously by *self*-assembling of surfactants. When the ionic strength of the solution increases, electric repulsion decreases, which allows the membrane to become thicker. As was emphasized in our previous paper [7], thicker bilayers are harder to bend, hence the larger k_c. Also the effect of the salt concentration on $\bar{k}_c$ indicates a more stable bilayer at higher ionic strength, see figure 4b. It is easy to observe that incorporating nonionic surfactant in the bilayer destabilizes the bilayer, since both k_c and $\bar{k}_c$ decrease.

The monotonous increase of the stability of the mixed bilayer with increasing salt concentration is not observed in practice [17], where it has been found that bilayers of mixed surfactants are only stable

over a distinct range of electrolyte concentrations, which often is in the order of kmole/m^3. The reason for this discrepancy is that in the experiments salting-out electrolytes were used.

In figure 5 the situation of figure 4 is given for the case that the ions have unfavourable interactions with the solvent. A Flory-Huggins parameter of 1.0 is assumed for the interactions between the electrolyte ions and water (instead of zero), as well as between the ions and the carbon segments (instead of 2.0). These values cause the quality of the solvent to decrease with increasing electrolyte concentration, as is the case with salting-out electrolytes like NaCl and KCl. In this situation, the mean bending modulus k_c passes through a maximum (figure 5a). The effect of increasing bilayer thickness, which increases k_c, is now opposed by a decreasing solvent quality, as explained in our previous paper [7]. Combining the results for k_c with those for $\bar{k}_c$ (figure 5b), a stable bilayer could be expected in a salt concentration of around 1 M electrolyte, in agreement with the experiments [17].

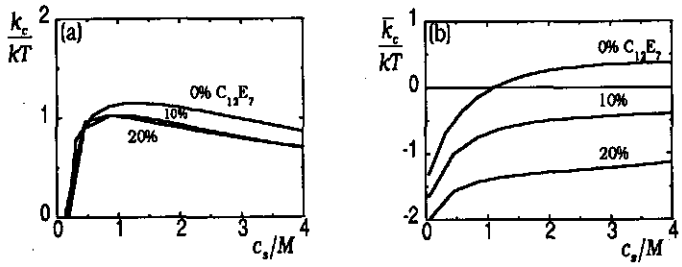

Figure 5. The same graphs as in figure 4, but for salt ions having unfavourable interactions with solvent and surfactant tails, representing salting-out electrolytes. Parameters: see text.

III. Monolayers

Here, we discuss the bending elasticity parameters of a monolayer of SDS on an oil-water interface. The oil is dodecane, C_{12}. As monolayers are asymmetrical, a nonzero spontaneous curvature is expected, which is anticipated to be strongly dependent on salt concentration. In practice, phase inversion may occur when the salt concentration is increased. This phenomenon is usually attributed to a changing effective head group area.

Figure 6 shows the effect of the concentration of indifferent electrolyte on the bending moduli k_c and $\bar{k}_c$, and the spontaneous curvature J_{sp}. The salt concentration has an dramatic effect on k_c. At low ionic strength, k_c is strongly negative, indicating that a cylindrical monolayer would be unstable. Adding salt increases k_c considerably; this is a consequence of the higher surfactant adsorption when the electrical double layer is screened. In this case, a positive k_c is found for salt concentrations larger than 0.4 M. The influence on $\bar{k}_c$ is just the opposite, like in the case of pure non-ionics [7].

Figure 6c presents the dependency of the spontaneous curvature of a SDS monolayer on the ionic strength. The most striking result is that the sign of J_{sp} changes near a salt concentration of 0.4 M and again at about 1.0 M. The curve below 0.4 M applies to unstable monolayers. Beyond 1 M, the spontaneous curvature increases with increasing ionic strength. This result is not consistent with current ideas in the literature. It is generally expected that the suppression of the double layer and ensuing decrease of the head group area,

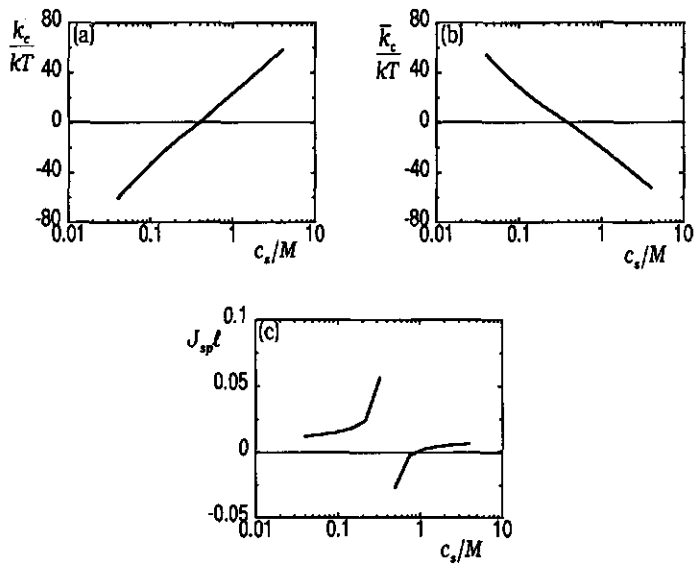

Figure 6. Bending elasticity parameters k_c (a) and (b), and spontaneous curvature (c) of a monolayer of SDS (modelled as $C_{12}B_3$) on a dodecane (C_{12})-water interface as a function of salt concentration. Parameters: see text.

giving the surfactant molecule a less conical shape, would lead to flatter layers. Indeed the head group area is decreased quite considerably. However, this leads also to more adsorption and hence to a thicker monolayer. Thus, in this way not only the increase of the mean bending modulus can be understood but also the characteristic shape of J_{sp} versus salt concentration. The curve in figure 6c is very similar to that of the spontaneous curvature of nonionic surfactants as a function of the surfactant concentration (Figure 6 of ref. [7]). Also in that case the concomitant increase of the monolayer thickness explains the observed behaviour.

Conclusions

In our self-consistent field lattice model, the contribution of the electric double layer to the mean bending elasticity modulus k_c increases significantly with the diameter of the electrolyte ions. Extrapolated to zero diameter, our values agree with those found with Poisson-Boltzmann theory [11].

However, screening the electric double layer by an increasing ionic strength does not diminish the rigidity of ionic surfactant mono- and bilayer systems. Instead, k_c increases because suppressing the electric double layer promotes a thicker surfactant layer. In bilayers, the Gaußian elasticity modulus $\bar{k}_c$ becomes larger with increasing ionic strength, whereas in monolayers it becomes smaller. In bilayers, addition of nonionic surfactant decreases both k_c and $\bar{k}_c$. In monolayers, additional electrolyte increases the spontaneous curvature, promoting the formation of small oil droplets in water which are, however, unstable because of a negative k_c. At a certain salt concentration J_{sp} changes sign and k_c becomes positive, leading to small water droplets in oil that become larger when the ionic strength increases. Eventually, J_{sp} changes sign again, so that the water in oil system is inverted into an oil in water system with big oil droplets becoming smaller in still higher salt concentrations.

Appendix

Numerical Method. The procedure to find a numerical solution consistent with eqn (10,11,13-16) is as follows. We define the potentials $u_x(z)$ as iteration variables.

Using eqn (11) we can write $u_x(z)$ as:

$$u_x(z) = u'(z) + u_x^{int}(z) + ev_x\left(\psi(z) - \psi^\beta\right) \tag{A1}$$

where $u_x^{int} = kT\sum_y \chi_{xy}\left[<\varphi_y(z)> - \varphi_y^\beta\right]$, which can be calculated from the iteration variables $\{u_x(z)\}$, using eqn (10,13-16) for the calculation of $\{\varphi_x(z)\}$. The electrical potential profile $\left(\psi(z) - \psi^\beta\right)$, can be deduced from $\{u_x(z)\}$ by combining eqn (A1) for each charged species x into two independent equations for each layer z, containing the contributions of the positive and negative charges (segments and salt ions), respectively:

$$\begin{cases} u_+(z) = u'(z) + u_+^{int}(z) + e\left(\psi(z) - \psi^\beta\right)v_+ \\ u_-(z) = u'(z) + u_-^{int}(z) + e\left(\psi(z) - \psi^\beta\right)v_- \end{cases} \tag{A2}$$

In this equation, the subscript + (-) means that only the positive (negative) charges are involved; e.g., $u_+(z)$ is the average value of $u_x(z)$ where x represents all types of positively charged segments and salt ions in the system. Eqn (A2) is a set of two equations per layer with $u'(z)$ and $\left(\psi(z) - \psi^\beta\right)$ as unknown. Therefore:

$$\psi(z)-\psi^{\beta}=\frac{\left(u_{+}(z)-u_{+}^{int}(z)\right)-\left(u_{-}(z)-u_{-}^{int}(z)\right)}{e\left(v_{+}-v_{-}\right)} \qquad \text{(A3)}$$

Note that v_+ is positive and v_- is negative, so that $(v_+ - v_-) > 0$.

For a segment x in layer z we define the hard-core potential $u'_x(z)$, which must become independent of x, as (cf. eqn 11):

$$u'_x(z)=u_x(z)-kT\sum_y \chi_{xy}\left[\frac{<\varphi_y(z)>}{\sum_x \varphi_x(z)}-\varphi_y^{\beta}\right]- ev_x\frac{C(z-\ell,z)\psi(z-\ell)+q(z)+C(z,z+\ell)\psi(z+\ell)}{C(z-\ell,z)+C(z,z+\ell)} \qquad \text{(A4)}$$

where eqn (19) is used to implement the correct interdependence between the electric potentials that are based on the current iteration variables. The division by $\sum_x \varphi_x(z)$ in eqn (A4) is introduced to stabilize the numerical iterations.

A self-consistent solution is guarantied when the sum of the volume fractions of all segment types in each layer, $\sum_x \varphi_x(z)$, equals unity and when $u'_x(z)$ is independent of the segment type, i.e., when $u'_x(z)=\sum_y u'_y(z)/\sum_y 1 \;\forall x$. We define functions $f_x(z)$, which are only zero in the self-consistent situation:

$$f_x(z)=1-1/\sum_y \varphi_y(z)-u'_x(z)+\sum_y u'_y(z)/\sum_y 1 \qquad \text{(A5)}$$

The point of zero of these simultaneous equations in $\{u_x(z)\}$ can be obtained by standard numerical methods. From the self-consistent set $\{u_x(z)\}$ all needed quantities can be calculated to find γA_s from

eqn (23). The bending elasticity moduli are obtained from the dependence of γA_s on the curvatures J and K.

References

1 W. Helfrich, Z. Naturforsch., 28c (1973) 693.

2 W. Helfrich, Z. Naturforsch., 33a (1978) 305.

3 J. M. di Meglio, M. Dvolaitzky, R. Ober and C. Taupin, J. Phys. Lett., 44 (1983) L-229.

4 J. Meunier, J. Phys. Lett., 46 (1985) L-1005.

5 C. R. Safinya, D. Roux, G. S. Smith, S. K. Sinha, P. Dimon, N. A. Clark and A. M. Bellocq, Phys. Rev. Lett., 57 (1986) 2718.

6 M. M. Kozlov, S. L. Leikin and V. S. Markin, J. Chem. Soc., Faraday Trans. 2, 85 (1989) 277.

7 P. A. Barneveld, This thesis, Ch. 4 (1991)

8 I. Szleifer, D. Kramer, A. Ben-Shaul, D. Roux and W. M. Gelbart, Phys. Rev. Lett., 60 (1988) 1966.

9 S. T. Milner and T. A. Witten, J. Phys., 49 (1988) 1951.

10 N. Wintherhalter and W. Helfrich, J. Phys. Chem., 92 (1988) 6865.

11 H. N. W. Lekkerkerker, Physica A, 159 (1989) 319.

12 V. S. Markin, M. M. Kozlov and S. L. Leikin, J. Chem. Soc., Faraday Trans. 2, 84 (1988) 1149.

13 M. R. Böhmer, O. A. Evers and J. M. H. M. Scheutjens, Macromolecules, 23 (1990) 2288.

14 F. A. M. Leermakers and J. M. H. M. Scheutjens, J. Phys. Chem., 93 (1989) 7417.

15 O. A. Evers, J. M. H. M. Scheutjens and G. J. Fleer, Macromolecules, 23 (1990) 5221.

16 M. R. Böhmer, Personal Communication (1990).

17 J. C. Van de Pas, Tenside Surf. Det., (1991) Accepted.

CHAPTER 6

The Role of Helfrich Repulsion in Free Liquid Films of Nonionic Surfactants

Abstract

Upon the addition of salt, the thickness of free liquid films stabilized by nonionic surfactant passes through a maximum at 0.5-2 kmole/m^3, depending on the nature of the salt used. We show that Helfrich repulsion, i.e., repulsion caused by undulation of the interacting monolayers, is responsible for this phenomenon. Undulations depend on the rigidity and the surface tension of the monolayers, which in turn depend on the packing of the surfactant molecules. The packing can be changed by incorporating, e.g., salt or linear alcohol in the film. Experimental data and theoretical calculations of the thickness of alcohol-containing films are in good agreement. Although the surface tension is high (≈ 30 mN/m), the monolayers remain so flexible that undulations are strong enough to affect the film thickness significantly.

Introduction

In recent years, the unexpected influence of high concentrations of electrolytes on the thickness of macroscopic thin liquid films stabilized by nonionic surfactant (figure 1) became apparent [1, 2, 3]. As a function of electrolyte concentration the film thickness of these systems shows a characteristic maximum around 0.5-2 kmole/m^3,

far above the ionic strength where electric double layers play a role in hydrophobic sols. The film thickness at this maximum appears to exceed twice the length of the stretched surfactant molecules. To explain this interesting feature, one needs insight into the interactions occuring in the film.

Unlike ionic surfactant films, pure nonionic films (e.g., stabilized by hepta-ethylene-glycol mono n-dodecyl ether, $C_{12}E_7$) are not stabilized by electrostatic repulsion. An obvious candidate to provide the observed stabilization is steric repulsion, resulting from repulsion between the large surfactant head groups. A possible effect of electrolyte is the dehydration of these head groups. This could lead to a diminished repulsion in very high salt concentrations. In addition, electrolytes could increase the osmotic pressure of the solution relative to that in the film. Both effects may be responsible for a decreasing film thickness with increasing ionic strength.

In order to explain the increase in film thickness at relatively low electrolyte concentrations (up to 1 kmole/m^3), we have suggested that Helfrich repulsion may be important in macroscopic thin liquid films [3]. Helfrich repulsion originates from the steric interaction between the two undulating surfactant monolayers of the film. The

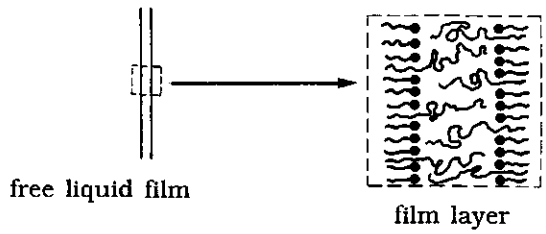

Figure 1. Schematic representation of a free liquid film stabilized by surfactant.

undulations are thermally induced and their amplitudes are restrained by the rigidity and surface tension of the monolayers. For two approaching monolayers, reduction of the amplitudes may also occur, leading to repulsion. For systems of high surface tension (20-30 mN/m), Helfrich repulsion is generally considered to be unimportant. Helfrich only gave an equation for tension-free layers [4]. However, it should be realized that surfactant monolayers on air-water interfaces are much thinner and hence, much more flexible than the lipid bilayers, considered by Helfrich.

The first issue of this paper is to show that, despite of the non-zero surface tension, Helfrich repulsion does play an important role in macroscopic thin liquid films. We expect the film thickness to increase when the rigidity and surface tension of the monolayers decrease. The film thickness and the surface tension can be measured, but the rigidity has to be calculated from molecular properties [5], since experimental determination is very cumbersome [6]. The effects of the rigidity and surface tension on the repulsion are also calculated. To that end, Helfrich's equation is extended with a surface tension term [6]. In order to obtain discriminating experimental data, such substances should be added to the system that mainly lead to changes in rigidity and surface tension, but not in the Hamaker constant, head group repulsion, electric double layer phenomena and the refractive index of the film. Molecules that to a large extent satisfy these requirements are (linear) alcohols, in particular those for which the alkyl length of the

alcohol matches that of the surfactant. Electrostatic features are not involved, which simplifies the calculation of the rigidity.

Another approach to get more insight into the forces acting in films stabilized by nonionics is to extend the previous study of the electrolyte effect. In ref. [3] only salting-out electrolytes were considered (for instance, NaCl and Na_2SO_4). Such electrolytes could reduce the thickness and hence, be responsible for the descending branch beyond the maximum. In order to verify this possibility some experiments have been done with the salting-in electrolytes NaI and NaSCN.

Below, we first discuss the implications of a non-zero surface tension on Helfrich repulsion. Thereafter, we present the results of thickness measurements of films stabilized by $C_{12}E_7$ in the presence of NaI, NaSCN, pentanol (C_5OH), octanol (C_8OH) and dodecanol ($C_{12}OH$). Then we give a quantitative interpretation of the thickness of the films with alcohol followed by a qualitative discussion of the results with films containing electrolytes.

Helfrich Repulsion in Macroscopic Free Liquid Films

Surfactant layers are subject to out-of-plane undulations due to thermal motion. When, as in thin films, two undulating layers approach one another, some of these undulation modes become restricted, which manifests itself in a repulsive interaction energy, G_H, for which Helfrich derived [4]:

$$\frac{G_H}{A_s} = \frac{3\pi^2}{128}\frac{(kT)^2}{k_c d^2} \qquad (1)$$

In this equation, k is Boltzmann's constant, T the temperature, A_s the surface area per layer and d the mean layer separation. The quantity k_c is the rigidity or the mean bending modulus of the layer. Layers that bend easily (small k_c), undulate strongly and hence, the interaction energy is high when two such layers approach. The numerical coefficient in eqn (1) is subject to some uncertainty and may well be twice as large [4]. Undulations are not only inhibited by the rigidity of the layer, but also by the contractile action of its surface tension [6]. Eqn (1) holds for tension-free layers only. As surface tensions can be moderately high in our systems (20-30 mN/m), we need to reconsider the derivations made by Helfrich.

Formally, the deformation u of a layer can be expressed by a Fourier series:

$$u(\mathbf{r}_0) = \sum_{\mathbf{q}} u_{\mathbf{q}} e^{i\mathbf{qr}} = \sum_{\mathbf{q}} u_{\mathbf{q}} e^{i(\mathbf{q}_{//}\mathbf{r}_{//} + \mathbf{q}_{\perp}\mathbf{r}_{\perp})} \qquad (2)$$

where $\mathbf{q}$ is the wave vector and $\mathbf{r}$ is a spatial vector. Both $\mathbf{q}$ and $\mathbf{r}$ can be divided into components parallel (//) and perpendicular ($\perp$) to the normal of the film. The parameter $u_{\mathbf{q}}$ is the amplitude of the wave of which the wave vector is $\mathbf{q}$. For $\mathbf{q}_{//}$ the upper cut-off value is π/d [4]. For $\mathbf{q}_{\perp}$ the lower cut-off is determined by the area of the film, A_s and is very small: $\pi/A_s^{\frac{1}{2}} \cong 0$, whilst the existence of an upper cut-off is ignored [7]. The elastic energy G_e of the film can be approximated by:

$$\frac{G_e}{A_s d} = \tfrac{1}{2} B\left(\nabla \mathbf{u}_{//}\right)^2 + \tfrac{1}{2}\frac{k_c}{d}\left(\nabla^2 \mathbf{u}_{\perp}\right)^2 + \tfrac{1}{2}\frac{\gamma}{d}\left(\nabla \mathbf{u}_{\perp}\right)^2 \qquad (3)$$

where γ is the surface tension and B is the compressibility modulus of the film, which will be defined below. In combination with eqn (2) the energy G_q of a single mode $\mathbf{q}$ can be obtained, with must equal the thermal energy $\frac{1}{2}kT$:

$$G_q = \frac{A_s d}{2}\left[B q_{//}^2 + \frac{k_c}{d} q_{\perp}^4 + \frac{\gamma}{d} q_{\perp}^2\right] < u_q^2 > = \tfrac{1}{2} kT \qquad (4)$$

The term $k_c q^4$ is the curvature energy and γq^2 is the capillary energy.

Hence, the mean square amplitude of mode $\mathbf{q}$ is given by

$$< u_q^2(B) > = \frac{kT}{A_s d} \; \frac{1}{B q_{//}^2 + \left(\frac{k_c}{d} q_{\perp}^2 + \frac{\gamma}{d}\right) q_{\perp}^2} \qquad (5)$$

When the layers are far apart, the compressibility modulus B, defined by :

$$B = d^2 \frac{\partial^2 \left(G/(A_s d)\right)}{\partial d^2} \qquad (6)$$

is zero. Formally, G contains not only the Helfrich repulsion energy, but all possible interactions between the two monolayers of the film.

When the layers approach, B becomes large since the concomitant decrease in amplitude of mode $\mathbf{q}$ implies a loss of entropy and hence, an increase $G_H(\mathbf{q})$ in the Gibbs energy G:

$$G_H(\mathbf{q}) = -kT \ln \frac{\sqrt{< u_{\mathbf{q}}^2(B) >}}{\sqrt{< u_{\mathbf{q}}^2(0) >}} \tag{7}$$

Integrating over all modes $\mathbf{q}$ yields the Helfrich repulsion energy:

$$\frac{G_H}{A_s} = \frac{kT}{(2\pi d)^2} \int_0^{\infty} \int_0^{\pi} x \ln \left\{ \frac{Bd^3 y^2}{(k_c x^2 + \gamma d^2) x^2} + 1 \right\} dy dx \tag{8}$$

which can be computed when B is known. In eqn (8) the dimensionless parameters x and y are defined by $x = q_{\perp} d$ and $y = q_{//} d$, respectively. Helfrich repulsion can now be obtained from the implicit differential equation which results when eqn (6) is substituted in eqn (8):

Unfortunately, this differential equation has no analytical solution. Also numerically this equation behaves very badly. Since the integral is slowly convergent, solutions are inaccurate. We therefore introduce a very rough approximation. We write for the denominator in eqn (8):

$$(k_c x^2 + \gamma d^2) x^2 \equiv k_c' x^4 \tag{9}$$

The quantity k_c' is a function of x. In first order, only the cut-off wave

is relevant. If we consider only one wave number, k_c' is essentially constant and hence, the form of Helfrich's equation is preserved:

$$G_H \cong \frac{3\pi^2}{128}\,\frac{(kT)^2}{k_c' d^2} A_s = \frac{3\pi^2}{128}\,\frac{(kT)^2}{k_c d^2 + \gamma d^4 / x_0^2} A_s \qquad (10)$$

Here, x_0 is a characteristic dimensionless wave number, which must be fitted to experimental data.

Materials and Methods

The experiments have been carried out with 98% pure $C_{12}E_7$, purchased from Nikko Chemicals, Japan. The NaI used was supra high quality from Merck. Water was purified by filtration through a Millipore Milli RD60 combined with a Super Q system. All other chemicals were at least of P.A. quality.

The details of the film thickness measurement apparatus have been described elsewhere [1]. The principal is that the thickness of a macroscopic vertical film in a frame of 1 by 1 cm is measured by laser light reflection. First, the equivalent solution thickness is calculated assuming the film to consist entirely of homogeneous bulk solution. This is not the case since the film consists of distinct alkane, ethylene oxide and aqueous layers. Along the lines of ref. [3] we calculate the real film thickness from the equivalent solution thickness. In order to apply this method, the thicknesses and refractive indices of the alkane and ethylene oxide layers must be

known. The thicknesses we use are based on the amount of $C_{12}E_7$ adsorbed at the solution-air interface [3]. We arrive at 0.6 nm for the alkane layer and 1.09 nm for the ethylene oxide layer. The refractive indices for these layers are 1.42 and 1.47, respectively. In the present study, films are drawn from a $C_{12}E_7$ solution which contains a mole fraction X of alcohol C_nOH. For the thickness of the alkane layer we use $0.6(1-X+nX/12)$ nm and for the ethylene oxide layer we use $1.09(1-X)$ nm. The optical corrections are estimated assuming that the electrolyte concentration in the film is the same as in the solution.

For each system studied, the solution refractive index is measured with a thermostatted refractometer. The surface tension at the solution-air interface is measured using the Wilhelmy plate method.

Experimental Results and Discussion

Effect of alcohols

We first investigate the effects of three linear alcohols, i.e., pentanol (C_5OH), octanol (C_8OH) and dodecanol ($C_{12}OH$), on the thickness of liquid films stabilized by $C_{12}EO_7$. Figure 2 summarizes the results. The film thickness is plotted as a function of the mole fraction of added alcohol. The total concentration of alcohol and surfactant in the solution is 0.8 mole/m^3. The most striking observation is that the thickness of the film is increasing over the whole range of C_5OH fractions, whereas the curve for $C_{12}OH$ shows a dip at $X_{C_{12}OH} \cong 0.5$. The curve for C_8OH has an intermediate shape.

Qualitatively, these features may be interpreted as follows. In the absence of alcohol, lateral head group repulsion forces the alkane regions to be below their optimal density. Short chain alcohols act as cosurfactants, which means that they dilute the film, both the head regions as well as the alkane regions. Their presence causes the film rigidity to decrease, which increases the amplitude of thermal undulation. The result is a thicker film. This explains the curves for pentanol and octanol.

When long chain alcohols are incorporated into the film, the alkane regions become denser, because the head groups are diluted and the alkane regions are not. For those systems, the rigidity will increase at low alcohol fractions, but eventually, when the alkane regions reach their optimal density, rigidity decreases, again since the head groups are still being diluted. This explains the curve for dodecanol starting from $X \cong 0.3$. The increase at $C_{12}OH$ concentrations below $X \cong 0.3$ is due to the effect of surface tension. From figure 2b we learn that the surface tension is decreasing quite

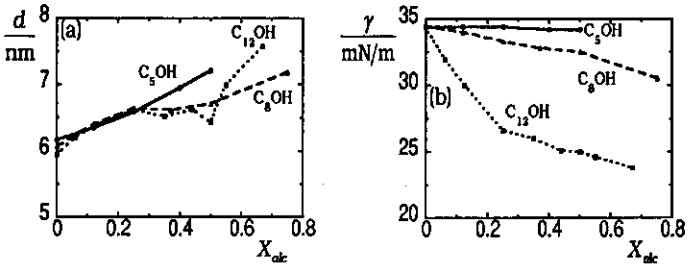

Figure 2. Experimental film thickness (a) and monolayer surface tension (b) as a function of alcohol in the surfactant layers. The surfactant is $C_{12}E_7$. The alcohols are indicated. The solution concentration of alcohol plus surfactant is 0.8 mM.

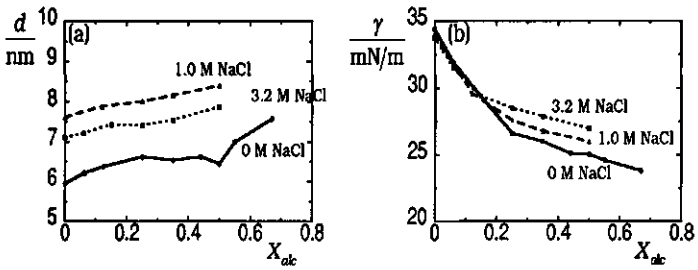

Figure 3. Experimental film thickness (a) and monolayer surface tension (b) as a function of the mole fraction of dodecanol in the surfactant layers. The surfactant is $C_{12}E_7$. The solution concentration contains 0.8 mM dodecanol and 0, 1 or 3.2 M NaCl.

strongly in this region, which allows for more thermal undulations, leading to thicker films. Note that the surface tension effect is completely absent in the case of pentanol.

In figure 3a, the curve in the presence of dodecanol is redrawn and compared with those where NaCl (1.0 and 3.2 M) is also present. All curves have about the same slope. The thickness of the films with 1.0 M NaCl is the highest of the three, which is in agreement with the results shown in figure 4a below. For completeness, figure 3b gives the corresponding surface tensions, showing that extra NaCl has only a minor influence. The main effect of NaCl in figure 3a is the induced decrease of the rigidity of the monolayers.

Effect of electrolytes

In figure 4a thicknesses of free liquid films stabilized by $C_{12}E_7$ are presented as a function of the ionic strength. The electrolytes used are NaI and NaSCN, which are both salting-in electrolytes for the EO

moiety. For comparison purposes, the curve for NaCl, which shows the characteristic maximum in film thickness, is redrawn from ref. [3]. As discussed there, this maximum is well-established although it does not seem very pronounced on the scale used. For the salting-in electrolytes, the maximum is however absent or almost absent. This is consistent with the idea that the decreasing part of the curve for NaCl is due to salting-out of the ethylene oxide head groups with the ensuing increase in rigidity of the monolayers. For salting-in electrolytes, the increase of the film thickness at low salt concentrations is still present. Such electrolytes increase the solubility for tails [8], which leads to thinner monolayers and hence, lower film rigidity. A lower film rigidity promotes thermal undulations, which lead to thicker films. Note that a thinner surfactant (mono)layer does not automatically lead to a thinner film. The influence of the film rigidity might in part be compensated by the effect of changes in surface

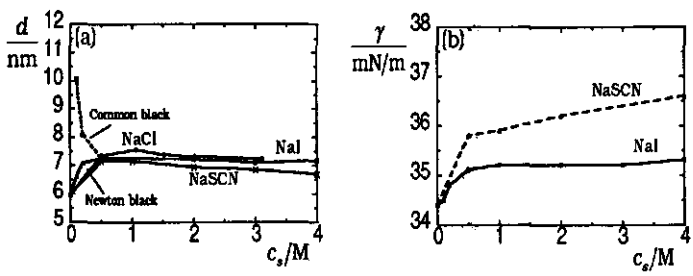

Figure 4. Experimental thickness of films stabilized by $C_{12}E_7$ (a) and surface tension of a monolayer of $C_{12}E_7$ on an air-water interface (b) as a function of salt concentration. The nature of the salt is indicated. The dashed curve represents a metastable film at low concentrations of NaI, stabilized by adsorption of iodide on the surfactant.

tension. The surface tension increases with salt concentration, as is shown in figure 4b, thereby reducing the thermal undulations.

The drainage of $C_{12}E_7$ films at low NaI concentrations shows an interesting feature; there appeared additional, metastable films of higher thickness (dashed curve in figure 4a). This phenomenon may perhaps be attributed to the specific adsorption of iodide on the surfactant tails [9], which creates a common black film stabilized by electrostatic repulsion. The strong decrease in film thickness with increasing salt concentration is due to vanishing electrostatic repulsion, showing the DLVO type of screening by electrolytes.

Quantitative interpretation of the alcohol-containing systems

The equilibrium thickness of thin liquid films is the result of a delicate balance between forces. Interactions leading to film thinning are the Van der Waals attraction and the hydrostatic pressure. Interactions promoting thicker films are steric repulsion, Helfrich repulsion, electrostatic repulsion and hydration forces. All these interactions are a function of the film thickness and the equilibrium thickness is found at the minimum of the total free energy. The minimum free energy per unit area equals the difference in the surface tension of the solution-air interface and that of the film-air interface and may be calculated from the contact angle that the film has with the solution.

In this section, we will calculate the equilibrium thickness for the all-nonionic systems, *i.e.*, the films with $C_{12}E_7$ surfactant and alcohol and compare them with the experimental results. For such systems there is no need to consider electrostatics. In addition, for the present purpose we neglect the softness of steric repulsion arising from interactions of the nonionic head groups. Steric repulsion is very strong, decaying exponentially with increasing film thickness [10]. As the incorporation of alcohols will not affect this repulsion very much, we assume that a hard wall potential defines the lower limit of the thickness. As all films considered in this section are thicker than this lower limit, we do not need to include these interactions. Hydration forces are also neglected since they have a very limited range of action.

Consequently, for the present case we only consider Van der Waals compression, hydrostatic attraction and Helfrich repulsion only.

Van der Waals attraction

For two semi-infinite phases separated by a flat uniform gap of thickness d the Van der Waals interaction energy, G_{vdW}, is given by:

$$G_{vdW} = -\frac{A}{12\pi d^2} A_s \qquad (11)$$

where A is the Hamaker constant of the medium and A_s is the area of the gap. Duyvis pointed out that this equation also holds for systems that consist of two layers of surfactants, separated by an aqueous phase[11]. For our nonionic system we use for the Hamaker constant the value $A = 2 \bullet 10^{-20}$ J ($\cong 2.5\ kT$) [12].

Hydrostatic pressure

The potential energy of the film, G_{hydr}, at height h is given by:

$$G_{hydr} = \Delta\rho g h d A_s \qquad (12)$$

where $\Delta\rho$ is the difference in mass density between the film and air, g is the acceleration due to gravity. For our 1 by 1 cm aqueous film, observed 5 mm above the meniscus, we use $\Delta\rho gh = 50 N/m^2$.

Helfrich repulsion

Eqn (10) represents the Helfrich repulsion energy, G_H, for free liquid films:

$$G_H \cong \frac{3\pi^2}{128} \frac{(kT)^2}{k_c d^2 + \gamma d^4 / x_0^2} A_s \qquad (13)$$

In this equation k_c and γ are the rigidity and the surface tension of the film, respectively. As the rigidity is very hard to measure, we have calculated it using the method described in ref. [5], based upon the self-consistent field lattice theory of Scheutjens and Fleer. The results are summarized in figure 5a. The surface tensions are taken from figure 2b.

The alcohol-free systems ($X_{alc} = 0$) are chosen to fit the parameter x_0. For $x_0 = 7.2$ the appropriate film thickness is obtained at the minimum of the total interaction Gibbs energy. This value for x_0 is used throughout the calculations.

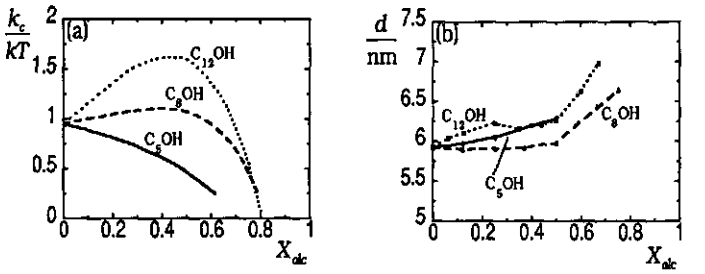

Figure 5. Theoretical plots of the mean bending elasticity modulus k_c of a bilayer of $C_{12}E_7$ (a) and the thickness of films stabilized by $C_{12}E_7$ (b), as a function of the mole fraction of alcohol in the surfactant layers. The alcohols are pentanol, octanol and dodecanol, respectively. The symbols are calculated from theoretical k_c values and experimental surface tension data.

The total interaction Gibbs energy

By adding all contributions, the total interaction Gibbs energy is obtained:

$$G = G_{vdW} + G_{hydr} + G_H \qquad (14)$$

For the $C_{12}E_7$ systems with alcohol, G_{vdW} and G_{hydr}, depend only on the film thickness d. The Helfrich term also depends on the rigidity moduli and the surface tension.

Minimizing G as a function of d gives the equilibrium thickness of the thin liquid films. The results are collected in figure 5b. The correspondence between this figure and the measured data in figure 2a is quite satisfactory and, in our opinion, a convincing indication that Helfrich repulsion plays a central role in explaining film thickness effects in these nonionic systems. For the pentanol system,

there is virtually no variation of the surface tension (*cf.* figure 2b) and hence, k_c is the sole parameter determining the influence of X_{alc} on d. As k_c decreases (figure 5a), d increases over the whole range of alcohol fractions. Judging only the shape of the k_c curve for dodecanol, a minimum in d as a function of the dodecanol content could be expected. However, at low dodecanol fractions the effect of an increasing k_c is outweighted by the decrease of the surface tension. The net effect is that the dodecanol curve has a characteristic shape with a local minimum and a minimum, in agreement of the experimental curve in figure 2a..

Qualitative interpretation of the electrolyte-containing systems

Although at present we are not yet able to explain quantitatively the behaviour of the $C_{12}E_7$ - electrolyte systems, we can give a qualitative interpretation of the results presented in figure 4a.

To explain the increase in film thickness with increasing ionic strength, we consider the solubility of head groups and tails of the surfactant in electrolyte solutions. Salting-out electrolytes reduce the solvent quality for the head groups by means of dehydration. This effect may be best illustrated by the ability of those electrolytes to decrease the cloud-points of nonionic surfactant or PEO solutions [13, 14]. As was shown in Ref. [5], a decreasing solvent quality leads to lower film rigidity, which accounts for the increase in film thickness. The decrease in film thickness at high salt concentrations, is

due to an osmotic effect: dehydration causes a concentration difference of salt between the film and the solution below the film.

For salting-in electrolytes the situation is slightly different. Since these electrolytes dehydrate the surfactant head group to a much smaller extent, the decrease in film thickness at high salinity is also much less, or completely absent. In this case, the initial increase is due to tails becoming better soluble, rather than head groups becoming less soluble. According to Ref. [5], this promotes thinner surfactant layers, thus lower rigidity and thicker films. As iodide adsorbs specifically onto the tails, this effect is stronger for NaI then for NaSCN.

Conclusion

The thickness of macroscopic thin liquid films stabilized by nonionic surfactant $C_{12}E_7$ depends non-linearly on the amount of electrolyte or alcohol in the film. For salting-in electrolytes like NaI and NaSCN an increase in film thickness is observed up to ca. 1 M, which can be attributed to a diminished film rigidity. Films mixed with relatively short chain alcohols like pentanol show an increase in film thickness over the whole range of pentanol fractions, which is also interpreted as the result of a decreasing film rigidity. Films to which relatively long chain alcohols like dodecanol are added become thicker at low alcohol fractions, due to a decreasing film tension, thinner at intermediate fractions and again thicker at high

alcohol fractions. The decrease and eventual increase in film thickness are due to changes in film rigidity.

Thicknesses of purely nonionic films can be explained quantitatively in terms of Van der Waals attraction, hydrostatic attraction and Helfrich repulsion. The main conclusion is that the properties of films can only be interpreted by invoking and quantitatively accounting for undulation repulsion. These films have surface tensions of 25-30 mN/m. Hence it is concluded that tensions of this magnitude are not large enough to inhibit the effect of undulations on the film thickness.

References

1 T. v. d. Boomgaard and J. Lyklema, Langmuir, 5 (1989) 245.

2 H.-J. Müller, G. Kretzschmar and R. Holzbauer, Abh. Akad. Wiss. DDR, Abt. Math., Naturwiss., Tech., 1N (1987) 331.

3 P. A. Barneveld, J. M. H. M. Scheutjens and J. Lyklema, Colloids Surfaces, 52 (1991) 107. *This thesis, Ch. 3.*

4 W. Helfrich, Z. Naturforsch., 33a (1978) 305.

5 P. A. Barneveld, This thesis, Ch. 4 (1991)

6 J. Meunier, J. Phys. Lett., 46 (1985) L-1005.

7 D. Sornette and N. Ostrowsky, J. Physique, 45 (1984) 265.

8 N. Nishikido and R. Matuura, Bull. Chem. Soc. Jpn., 50 (1977) 1690.

9 T. Van Voorthuysen, Unpublished conductivity measurements (1989).

10 F. T. Hesselink, A. Vrij and J. T. G. Overbeek, J. Phys. Chem., 75 (1971) 2094.

11 E. M. Duyvis, Thesis, Utrecht 1962.

12 J. Visser, Advan. Colloid Interface Sci., 3 (1972) 331.

13 F. E. Bailey Jr. and R. W. Callard, Appl. Polymer Sci., 1 (1959) 56.

14 E. Florin, R. Kjellander and J. C. Eriksson, J. Chem. Soc. Faraday Trans. I, 80 (1984) 2889.

SUMMARY

General

The present study was carried out to obtain more insight into the unusual swelling behaviour of surfactant layers. Here, swelling means that the thickness of the water layer between two surfactant layers increases. It was shown recently that high salt concentrations can bring about swelling in aqueous multilayer vesicles and free liquid films of nonionic surfactants (polyoxyethylenated n-dodecyl alcohols). By this so-called salt-induced swelling the water layer becomes thicker up to relatively high salt concentrations (1-2 kmole/m^3), reaches a maximum and, beyond these concentrations, shrinks again. In multilayer vesicles, the maximum swelling can be substantial (extreme swelling): the water layer thickness can easily be 10 times the surfactant layer thickness

Until now, an explanation for salt-induced swelling in terms of interaction forces between the surfactant layers was not available. The Van der Waals force is relatively unaffected by the ionic strength of the water layer. On the basis of steric repulsion, shrinking is expected due to salting-out of the ethylene oxide head groups of the nonionic surfactant. This could explain the decreasing part of the swelling curve. A problem with this explanation is that the bilayers in the vesicles are too far apart for the head groups to interact. When

pushed to extremes, electrostatic repulsion could lead to some swelling if salt ions adsorb specifically onto the surfactants. In that case, as a function of salt concentration two regimes can be distinguished: in low concentrations the electrostatic double layer is built up by an increasing surface charge, leading to swelling, whereas in high salt concentrations the double layer is compressed, leading to shrinking. In chapter 3 this mechanism is shown to be quantitatively insufficient to account for the thickness variation of free liquid films, let alone for the extreme swelling in multilayer vesicles.

Helfrich has suggested that thermal undulations of nearby surfactant layers provide an additional steric repulsion between the layers. Since this is a long range force, it could be responsible for the extreme swelling in multilayer vesicles. Quantitative analyses are required to test this suggestion. A parameter that dominates the magnitude of the Helfrich force is the mean bending elasticity modulus of the surfactant layer involved: a small modulus implies strong undulations and hence, large repulsions. The presence of a surface tension restricts the undulations. The surface tension of vesicles is negligible, but that of a film is significant. However, monolayers are thinner than bilayers and hence may be less rigid so that undulations can still be large enough to affect the film thickness.

A major part of the present study is the modelling of surfactant monolayers and bilayers, with the aim to calculate bending moduli from the solution properties of the surfactants (see chapters four and five). Based on these calculations, it was predicted that the thickness of free liquid films containing n-alcohol instead of salt would show qualitatively the same trends if Helfrich repulsion is responsible for

the salt-induced swelling. The experimental verification of this prediction is described in chapter six. The results agree very well with the proposed influence of undulations.

About the Chapters

In chapter one, the context of the study is outlined. The situation at the start of the present study is described.

In chapter two, upper and lower critical solution temperatures (i.e., solubility gaps) are calculated for solutions of poly(ethylene oxide) (PEO) in water. The behaviour of PEO in water is relevant since PEO constitutes the head groups of the nonionic surfactants. The model used is a simple extension of the well-known Flory-Huggins theory for linear homopolymers, in that with the PEO molecule considered as a copolymer with alternating polar and non-polar segments. The effect of temperature is incorporated by letting the Flory-Huggins χ-parameters decrease with increasing temperature. Upper and lower critical temperatures are calculated as a function of the degree of polymerization of the PEO. The results are compared with experimental data. In addition, upper and lower critical temperatures are calculated as a function of the non-polar fraction in the polymer. With this model, the insolubility of poly(propylene oxide) is recovered. However, the insolubility of poly(methylene oxide) is not reproduced.

In chapter three the thickness of thin liquid films stabilized by hepta-ethylene-glycol mono n-dodecyl ether ($C_{12}E_7$), measured as a

function of NaCl concentration, is reported. This thickness passes through a maximum at around 1 M, similar to what has been found with other non-ionic surfactants. The maximum is much less pronounced in films stabilized by a mixture of $C_{12}E_7$ and sodium dodecyl sulfate (SDS) or cetyl trimethyl ammonium chloride (CTAC) and there is an enhanced thickness at lower NaCl concentration in these films. We have extended the self-consistent field lattice theory of Böhmer et al. for the adsorption of polyelectrolytes to liquid films stabilized by a mixture of non-ionic and ionic surfactants. This theory accounts for the presence of electric fields and for the excluded volumes of surfactant segments and ions. For mixed films, the enhanced thickness at low salt concentration can indeed be explained by electrostatic repulsion. When the thickness of the mixed film is corrected for this repulsion the result of pure $C_{12}E_7$ films is retrieved, re-establishing the effect of electrolytes on non-ionic surfactants. For non-ionic films, in the absence of ionic surfactants, the maximum at high salt concentration cannot be explained by the model. We suggest an explanation for this maximum in terms of contributions of monolayer fluctuations leading to an additional repulsion, which depends on the salt concentration.

In chapter four, the mean and Gaußian bending elasticity moduli of monolayers and bilayers of nonionic surfactants are computed from the solution properties of the surfactant, without adjustable parameters. To that end, the grand potential Ω (the grand canonical characteristic function) is calculated as a function of the surface curvature using a modification of the the self-consistent field lattice model of Scheutjens and Fleer. The interfaces are formed by self-assembling

of the surfactants. It is found that with increasing tail length of the surfactant the bending modulus k_c of a bilayer rises linearly, whereas the Gaußian bending modulus $\bar{k}_c$ shows a maximum. The addition of short linear alcohols considerably decreases k_c and $\bar{k}_c$, whereas the presence of long chain alcohols can increase the rigidity of the bilayer. The spontaneous curvature of a monolayer at an oil-water interface strongly depends on the concentration of the surfactant.

In chapter five, the model is extended by incorporating ionic interactions at curved interfaces, so that bending elasticity moduli can also be calculated if ionic surfactants are involved. It is found that the size of the counter ions is an important parameter in determining the bending moduli of charged interfaces. Screening the electric double layer by salt has two opposing effects on the rigidity of monolayers and bilayers of ionic surfactants. The contribution of the double layer diminishes but, more importantly, the surfactant layer becomes thicker. Hence, the surfactant layers are more rigid in higher salt concentrations. In the case that salt ions decrease the solvent quality, as salting-out ions do, the rigidity of the layer passes through a maximum in high salt concentrations (c.a. 1 kmole/m^3).

In chapter six, the theoretical predictions of the mean bending elasticity modulus given in chapters four and five and the experimental film thicknesses described in chapter one are linked together. Upon the addition of salt, the thickness of free liquid films stabilized by nonionic surfactant passes through a maximum at 0.5-2 kmole/m^3, depending on the nature of the salt used. We show that Helfrich repulsion, i.e., repulsion caused by undulation of the interacting monolayers, is quantitatively responsible for this phenomenon.

Undulations depend on the rigidity and the surface tension of the monolayers, which in turn depend on the packing of the surfactant molecules. The packing can be changed by incorporating, e.g., salt or linear alcohol in the film. Experimental data and theoretical calculations of the thickness of alcohol-containing films are in good agreement. Although the surface tension is high (≈ 30 mN/m), the monolayers remain so flexible that undulations are strong enough to affect the film thickness significantly.

SAMENVATTING

Algemeen

Onlangs werd aangetoond dat hoge zoutconcentraties ertoe kunnen leiden dat er zwelling optreedt in multilaag vesicles en vrije vloeistoffilms van niet-ionogene zepen (surfactants). Door deze zogenaamde zoutgeïnduceerde zwelling neemt de dikte van de waterlaag toe en bereikt een maximum bij relatief hoge zoutconcentraties (1-2 molair). Bij nog hogere concentraties neemt de dikte weer af. Bij multilaag vesicles kan de zwelling erg groot zijn: de waterlaagdikte kan gemakkelijk het tienvoudige van de dikte van een surfactantlaag bedragen (men noemt dit verschijnsel *extreme zwelling*).

Dit proefschrift beschrijft een onderzoek dat werd uitgevoerd om meer inzicht te krijgen in dit zwelgedrag van surfactantlagen. Een verklaring voor de zoutgeïnduceerde zwelling in termen van interactiekrachten was niet beschikbaar. De Van der Waalskracht wordt niet beïnvloed door de ionsterkte van de waterlaag. Op grond van het uitzouten van de ethyleenoxidekopgroepen van de niet-ionogene zepen wordt een dunnere waterlaag verwacht, omdat de sterische repulsie tussen de surfactantlagen afneemt. Dit effect kan het dalende gedeelte van de curve verklaren. Het is echter zo dat de surfactantlagen te ver van elkaar verwijderd zijn om elkaar te kunnen

raken. In het uiterste geval zou electrostatische repulsie tot enige zwelling kunnen leiden indien de zoutionen op het surfactant zouden adsorberen. Men zou dan twee gebieden kunnen onderscheiden: bij lage zoutconcentraties wordt de electrische dubbellaag opgebouwd door een toenemende oppervlaktelading, terwijl bij hoge concentraties de dubbellaag wordt ingedrukt met als gevolg een afname van de waterlaagdikte. In hoofdstuk 3 wordt aangetoond dat dit effect onvoldoende sterk is om de diktevariaties in films, laat staan in multilaag vesicles, te verklaren.

Helfrich heeft laten zien dat de termische fluctuaties, die van nature in surfactantlagen optreden, een repulsieve kracht tot gevolg hebben. Vereenvoudigd weergegeven komt het er op neer dat lagen die fluctueren (flapperen) elkaar sneller in de weg gaan zitten dan op grond van hun gemiddelde afstand verwacht mag worden. De fluctuaties dragen dus bij tot een grotere waterlaagdikte. Omdat Helfrich tevens heeft afgeleid dat deze repulsie een lange dracht heeft kunnen de fluctuaties van belang zijn voor het eerder geschetste probleem. De grote van deze zogenaamde Helfrichrepulsie wordt voor een belangrijk deel bepaald door de gemiddelde buigingselasticiteit van de surfactantlaag. Een kleine buigingselasticiteit betekent sterke fluctuaties en derhalve een grote repulsie. De aanwezigheid van een grensvlakspanning beperkt de fluctuaties. Voor vesicles is dit nauwelijks een factor om rekening mee te houden, omdat daar de grensvlakspanning erg laag is, maar bij surfactantmonolagen (zoals die in vrije vloeistoffims voorkomen) kan dit de Helfrichrepulsie aanmerkelijk remmen. Daar staat tegenover dat monolagen (vloeistoffilms) dunner en dus flexibeler

zijn dan bilagen (vesicles), waardoor de fluctuaties toch van belang kunnen zijn voor de dikte van de waterlaag.

Een groot deel van dit onderzoek gaat over de modellering van surfactantmonolagen en -bilagen met als doel de buigingsmoduli van die lagen te berekenen (zie de hoofdstukken 4 en 5). De berekeningen gaven aan dat het toevoegen van n-alcohol aan een vrije vloeistoffilm een overeenkomstig zwelgedrag zou moeten opwekken als het toevoegen van zout, mits de Helfrichrepulsie werkelijk een rol speelt. In hoofdstuk 6 wordt experimenteel aangetoond dat dit inderdaad het geval is.

LEVENSLOOP

De schrijver is geboren op 29 mei 1960 te Rotterdam. In 1979 is hij aan de Landbouwuniversiteit Wageningen begonnen met de studie Moleculaire Wetenschappen, die hij in 1986 afrondde met als hoofdvakken *de kolloïdchemie* en *de natuurkunde* en als bijvak *de wiskunde*. In datzelfde jaar is hij aan dezelfde universiteit begonnen met het onderzoek dat tot dit proefschrift heeft geleid.

NAWOORD

Vooral in de afrondingsfase van het werk werd het mij steeds duidelijker dat het aandeel van Hans Lyklema en vooral Jan Scheutjens aan dit proefschrift niet onaanzienlijk is. De onvermoeibaarheid van deze mensen is spreekwoordelijk (wie kent niet het gezegde *die is zo onvermoeibaar als Scheutjens?*). Het klinkt afgezaagd, maar ik weet zeker dat het gereedmaken van dit werkje zonder hen een nog zwaardere bevalling geweest zou zijn.

Natuurlijk zijn zij niet de enigen die het werk verlicht hebben. Chris Wijmans, Tijmen van Voorthuysen en Lilian Hesselink hebben in het kader van hun afstudeervak kolloïdchemie aan mijn project meegewerkt. Discussies over o.a. de grensvlakspanning van oliebollen, en de invloed van de Van der Waalswisselwerking op de Helfrichrepulsie waren zeer waardevol. Een deel van Tijmens werk is beschreven in hoofdstuk 3. A major part of the experimental results described in chapter 6 was obtained by Emil Manev from Sofia University, who stayed in Wageningen for a period of 9 months. The tenacity of that man is beyond imagination.

Een speciale plaats wordt ingenomen door de mensen die vanuit het Unilever Research Laboratory Vlaardingen het project bijgestaan hebben. Het was goed samenwerken met Albert Jurgens en Freek Schepers. Het was uitstekend samenwerken met John van de Pas, vooral tijdens de bezoekjes die georganiseerd werden om nog "even" wat dieper op de zaak in te gaan.

peter